Atomic Force Microscopy on domains in biological model membranes

Atomic Force Microscopie aan domeinen in biologische model membranen.

(met een samenvatting in het Nederlands)

Proefschrift ter verkrijging van de graad van doctor aan de Universiteit Utrecht op gezag van de Rector Magnificus, Prof. dr. W. H. Gispen, ingevolge het besluit van het College voor Promoties in het openbaar te verdedigen op woensdag 5 september des middags te 12.45 uur.

door

Hilde Anna Rinia

geboren op 9 juni 1971, te Franeker

promotoren:

Prof. dr. B. de Kruijff

verbonden aan het Centrum voor Biomembranen en Lipide Enzymologie,
Faculteit Scheikunde der Universiteit Utrecht

Prof. dr. J. P. J. M. van der Eerden

verbonden aan het Debye Instituut,
Faculteit Scheikunde der Universiteit Utrecht

Voor Mick

This work was financed by the Division of Chemical Sciences of
The Netherlands Organization for Scientific Research (NWO)
and financially supported by **Thermo**Scientific, Breda, the Netherlands.

Rinia, Hilde Anna
Atomic Force Microscopy on domains in biological model membranes
Proefschrift, Universiteit Utrecht
Atomic Force Microscopie aan domeinen in biologische model membranen
Met een samenvatting in het Nederlands
ISBN: 90-393-2790-4

Reproductie:  Offsetdrukkerij Ridderprint B.V., Ridderkerk

CONTENTS

CHAPTER 1

General Introduction

Biological membranes envelop all cells, providing a barrier between the interior and the exterior of a cell, and they divide the cell in compartments. This compartmentalization makes it possible to separate different cellular processes. Membranes consist of proteins and lipids. The lipids, which are amphipatic molecules, are self assembled in two monolayers, with their hydrophobic acyl chains directed towards each other, and their hydrophilic headgroups directed outward, facing the inside or the outside of a cell or a cell organelle. Integral membrane proteins, also called intrinsic or transmembrane proteins, traverse the membrane, while peripheral, or extrinsic membrane proteins are adsorbed on, or partially inserted in the membrane. Membrane proteins fulfill important functions like transporting nutrients, waste products and signals. Lipids provide for a stable bilayer, fulfilling the barrier function, and for an environment in which proteins can function. Apart from this, many lipids are directly involved in important processes like blood coagulation and signal transduction. Lately they are also suspected to be involved in programmed cell death.

1.1 Transmembrane proteins and peptides

Integral membrane proteins span the hydrophobic core of the membrane with a hydrophobic transmembrane domain (TMD), consisting of α-helices or β-strands. The latter forms a so-called β-barrel, and is mainly found in outer membranes of bacteria and evolutionary related cell organelles. In α-helical proteins, the TMD is formed by one or more α-helices, traversing the membrane. Well-known examples are bacteriorhodopsin and the photosynthetic reaction centers. TMD's are usually flanked by specific amino acids which are found to preferentially locate at the hydrophobic-hydrophilic interface of bilayers (Killian and von Heijne, 2000). Such amino acids consist of aromatic residues like tryptophan and tyrosine, or positively charged residues like lysine, and are thought to stably anchor transmembrane proteins in the membrane.

In order to systematically study the molecular interactions between TMD's and membrane lipids, model peptides have been designed and synthesized. Examples of such model peptides are the so-called WALP peptides. They consist of an alternating alanine-leucine (AL) stretch of varying length, flanked by tryptophans (W). These peptides form a hydrophobic,

transmembrane α-helix, which renders them excellent models for α-helical proteins. They are used to study hydrophobic mismatch, which occurs when the length of a TMD does not match with the hydrophobic thickness of the surrounding membrane, by incorporating peptides with different lengths in bilayers of varying hydrophobic thickness (de Planque et al., 1998). Mismatch is believed to be important for protein insertion, activity, stability and protein sorting and aggregation (Killian, 1998; Dumas et al., 1999) Also, by using peptides with different flanking residues, interfacial anchoring of different amino acids has been investigated (de Planque et al., 1999; 2000).

1.2 Lipids and their phase behavior

Since, next to proteins, lipids are the main constituents of membranes, much effort has been undertaken to elucidate the properties of these molecules. Three main groups of membrane lipids are phospholipids, sphingolipids and sterols. Fig. 1.1 *A* depicts the molecular structures of examples of these different lipid classes (Gennis, 1989).

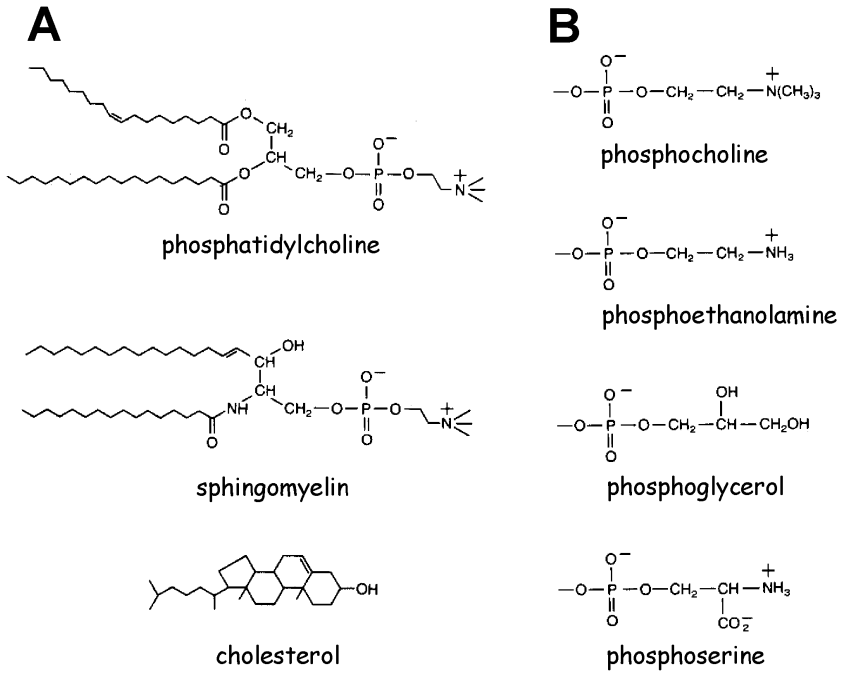

FIGURE 1.1 (A) Molecular structures of a phospholipid (phosphatidylcholine), a sphingolipid (sphingomyelin) and a sterol (cholesterol). (B) A few examples of phospholipid headgroups, found in (from top to bottom) phosphatidylcholine, phosphatidylethanolamine, phosphatidylglycerol and phosphatidylserine.

Phospholipids are derived from glycerol. They can contain different headgroups. The phospholipid depicted in Fig. 1.1 *A* is a phosphatidylcholine (PC), containing a phosphocholine headgroup. This headgroup is zwitterionic and net uncharged, as is phosphoethanolamine, the headgroup found in phosphatidylethanolamine (PE). Phosphatidylglycerol (PG) and phosphatidylserine (PS) both contain anionic headgroups and are net negatively charged. Fig. 1.1 *B* depicts the molecular structures of these headgroups. Other phospholipids are phosphatidic acid (PA) and phosphatidylinositol (PI) which are also both negatively charged. Sphingolipids are derived from sphingosine linked with an amide bond to an acyl chain. In glycosphingolipids, the headgroup consists of one or more sugar groups, and in sphingomyelin, depicted in Fig. 1.1 *A*, it consists of a phosphocholine moiety. Cholesterol, the most common sterol in mammalian cells is also depicted in Fig. 1.1 *A*. Apart from the headgroups, membrane lipids can also differ in acyl chain composition. Acyl chains of membrane lipids can be saturated or unsaturated and differ in length from C_{10} to C_{28} (Jones and Chapman, 1995).

The headgroup composition, and the length and the saturation of the acyl chains influence the phase behavior of lipids in bulk (Gennis, 1989). Lipids can self assemble in different aggregate structures, with different morphologies. Biological membranes are organized as the most common structure, the bilayer. Bilayers consisting of one lipid component are, above the chain melting temperature (T_m) of the lipid, in the fluid phase, also called liquid-disordered or liquid-crystalline phase, abbreviated to l_α phase. Below T_m they are in a solid phase. Examples of solid phases are the crystalline, gel, ripple and interdigitated phase. The organization of lipids in bilayers in different phases are depicted in Fig. 1.2.

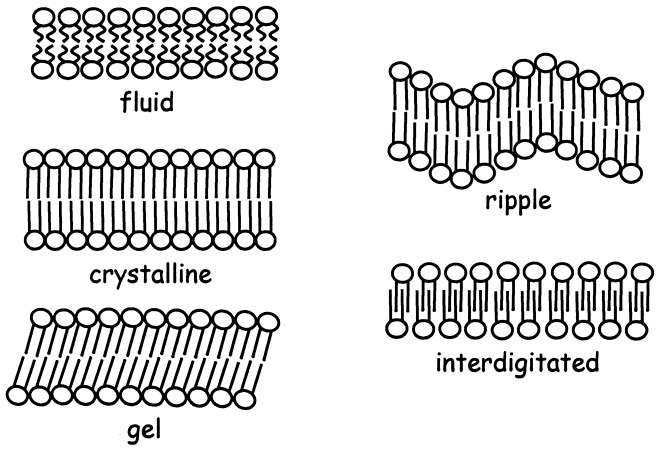

FIGURE 1.2 Molecular organization of bilayers in different phases.

In the fluid phase, the lipids have a high mobility, and their acyl chains are disordered, while in the solid phase, lipids have a low mobility and their acyl chains are stretched and more ordered. Lipids with long and/or saturated acyl chains have a higher T_m than lipids with short and/or unsaturated acyl chains. For example, distearoylphosphatidylcholine (DSPC) contains two saturated C_{18} acyl chains and has a T_m of 54°C, while dioleoylphosphatidylcholine (DOPC) contains two unsaturated C_{18} acyl chains and has a T_m of -15°C. Dipalmitoyl-phosphatidylcholine (DPPC), which contains shorter saturated chains, namely two C_{16} acyl chains, has a T_m of 41°C. Not only the acyl chain composition of a lipid, also headgroup hydration, size and the possibility of headgroups to form hydrogen bonds have their effects on the T_m. For instance dipalmitoylphosphatidyl-ethanolamine (DPPE) and DPPC have the same acyl chains, but DPPE has a higher T_m (60°C).

In bilayers in the crystalline phase, the lipids are laterally ordered, with their (saturated) acyl chains fully extended, i.e. in an all-*trans* configuration. The mobility and the hydration of the lipids are nearly zero. In the gel (l_β) phase, the headgroups are more hydrated, the lipids are more mobile, while the saturated acyl chains are still extended. Although gel phase bilayers are laterally less ordered than in the crystalline phase, a certain amount of order can still be present. For example in DPPC bilayers, the acyl chains display hexagonal order.

Certain lipids, like PC's, contain headgroups that are rather bulky and occupy a larger area than two saturated acyl chains, which, due to van der Waals interactions, prefer a close packing. As a compromise, such lipids adopt a tilted conformation, in the solid phase. Phase diagrams of PC's generally show a phase between the fluid and the gel phase. This phase is known as the P_β' phase or the ripple phase, because the surface of bilayers in this phase are rippled, as was shown by freeze-fracture Electron Microscopy (Verkleij and Ververgaert, 1975). The thermotropic phase transition from the P_β' to the fluid phase is called the main transition, while the transition from the solid to the P_β' phase is called the pre-transition. Another phase that can be formed by saturated PC's, induced by alcohol (Simons and McIntosh, 1984) or glycerol (O'Leary and Levin, 1984), is a solid phase in which the acyl chains of opposing monolayers are interdigitated. Apart from the discussed lamellar bilayer structures, lipids can also form nonbilayer phases (Cullis and de Kruijff, 1979), e.g. the hexagonal or cubic phase.

The phase behavior of lipids can be influenced by the presence of incorporated molecules. Proteins and peptides are known to be able to shift the phase transition of lipid bilayers (Papahadjopoulos et al., 1975), and can even induce non-bilayer phases (Killian et al., 1996). When cholesterol is incorporated in bilayers, it can abolish the phase transition. In this case, the bilayers are said to be in the liquid-ordered phase, in which the lipids have a lateral mobility almost as high as in the fluid phase, but the acyl chains are extended.

In bilayers containing lipids in different phases, phase separation can occur, leading to the formation of domains. Also protein-lipid interactions can lead to segregation. Indeed domains have been found to occur in membranes (Welti and Glaser, 1994), the most well known one being the separation of apical and basolateral sides of plasma membranes of epithelial cells. Another example is the transmembrane asymmetry of most cell membranes. A vexed question lately is whether specific cholesterol containing lipid domains, which are also referred to as rafts, exist. All domains discussed so far, are found to be biological functional, thus it is important to gain more insight in the mechanisms behind the formation of domains. Domain formation in model membranes has been studied by Electron Microscopy and Fluorescence Microscopy. A relatively new method is Atomic Force Microscopy (AFM, Binnig et al., 1986) which can image biological samples under aqueous conditions with a high resolution.

1.3 Atomic Force Microscopy

With AFM, the sample surface is scanned by a sharp tip (radius 1-10 nm, depending on the conditions, see Sheng et al., 1999), which is integrated at the end of a very flexible cantilever. On this cantilever a laser beam is directed which is deflected in a detector, consisting of a split diode. As the tip encounters height differences at the surface, it moves up and down, which in turn causes the cantilever to deflect up and down. This deflection is monitored, via the laser beam, by the detector (Fig. 1.3). In this way, a profile of the scanned surface is obtained with a height resolution of 1-2 Å, and a lateral resolution of less than 1 nm (Engel et al., 1997), depending on the sample.

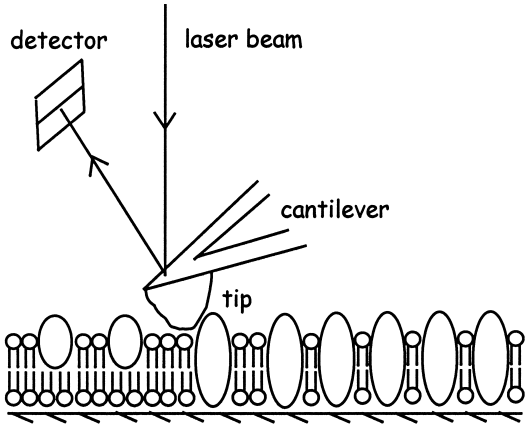

FIGURE 1.3 Principle of Atomic Force Microscopy. The movement of the tip is followed, via the deflection of the cantilever and the laser beam, by the detector. The tip is scanning the sample, in this case a supported lipid bilayer containing peripheral (left) and integral (right) proteins, in the x and y direction.

In air, most surfaces are covered with a nanoscopic layer of water, and the tip is pulled toward the surface by the surface tension of this water layer. Due to these hydration forces, the tip is exerting a relatively large force (10 nN) on the scanned sample, when operating in air. This large force can easily damage biological samples, fragile as they are. This problem can be circumvented by scanning in water, where no hydration forces are present, and forces exerted by the tip are much smaller: several hundreds of pico Newtons (Butt et al., 1991a). Scanning in water holds an extra benefit of AFM for biologists, since the natural environment of biomolecules is usually an aqueous solution. Another advantage is that buffers with variable pH or salt concentration, or with biological relevant components like ATP can be used. Also, the liquid above the sample can be replaced, so that certain molecules can be added or removed.

The thickness and length of a cantilever determine the spring constant of that cantilever, and thus the force exerted on the sample during scanning. Chips are commercially available, with four integrated cantilevers, each with their own spring constant. Since biological samples are fragile, usually the cantilever with the lowest spring constant (0.06 N/m) is chosen. Chip, cantilever and tip are made of Si_3N_4, which is hydrophilic and negatively charged. With AFM, strictly spoken, one measures the forces between the tip and the underlying molecules of the scanned sample. It is useful to distinguish hydration forces (discussed above), electrostatic forces, van der Waals forces (Butt, 1991b) and contact forces. Electrostatic forces can be repulsive or attractive and have a range of one to several tens of nm, depending on the ionic strength of the solution above the sample. Van der Waals forces are attractive and have a range of 0.1-10 nm (Meyer and Heinzelmann, 1995). When the tip closely approaches the sample, electron orbitals of tip atoms and sample atoms repel each other, and it is at this point where tip and sample are said to be in contact. When scanning an uncharged sample, only contact forces and van der Waals forces play a role. However, many biological molecules, like DNA and anionic lipids, are negatively charged. In this case, the longer ranged electrostatic interactions would cause to repel the, also negatively charged, tip and give rise to artifacts in the measured heights (Butt, 1991a; Müller and Engel, 1997). This can be overcome, and even be used to obtain a higher resolution, by adjusting the ionic strength of the buffer solution above the scanned sample (Müller et al., 1999). Another artifact in height images obtained by AFM stems from the tip geometry, which is called tip convolution. Due to the finite tip size, protrusions on the sample appear wider, and depressions appear narrower than they are. The influence of tip charge and tip geometry on height images is clarified in Fig. 1.4.

An Atomic Force Microscope can operate in different modes. The mode mostly used is Contact Mode (CM), in which the tip is in constant contact with the sample during scanning. The advantage of this mode is that in principle, when used on sturdy, ordered samples, high

resolution can be achieved. The disadvantage is that it can damage the sample, since the tip is "dragging" along the surface, and possibly removes molecules from the sample. This ability to remove molecules has also been used to modify thin layers on purpose (ten Grotenhuis et al., 1995; Beckmann et al., 1998). In these cases, the applied force was increased, to let the tip scratch a line or a square in these layers.

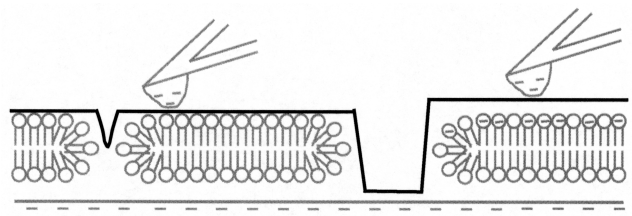

FIGURE 1.4 Artifacts in morphology induced by tip charge and geometry in height images of samples, in this case a supported bilayer. Due to the tip convolution the defects (holes) in the bilayer appear too narrow. The defect on the left is too narrow for the tip to reach the substrate, and appears also too shallow. The negative charges present on the tip, substrate and the bilayer also influence the measured height.

To avoid damaging, the Tapping Mode (TM) was developed (Hansma et al., 1993). In Tapping Mode, the cantilever is oscillating in the z-direction, causing the tip to bounce up and down, all the time touching the surface briefly during scanning. In this way, no lateral force is exerted, so that scanned samples are less easily damaged. However this mode requires a much lower scan speed (1 Hz) compared to Contact Mode (6 Hz). All images presented in this thesis are obtained in Contact Mode.

The resolution of AFM images highly depends on the sample. For instance, adsorbed proteins, scanned in Contact Mode appear hazy, mostly due to damage caused by the tip, as explained above (Tapping Mode in this case yields better images). However, proteins present in a 2 dimensional (2-D) crystal scanned in Contact Mode, yield images with a high resolution (<1 nm, Scheuring et al., 1999a; Czajkowsky et al., 1999; Müller et al., 2000). Membranes when present around whole cells give low resolution images (Hoh and Schoenenberger, 1994), due to the presence of the underlying cytoskeleton, cytoplasm and organelles. The latter three are a soft foundation under the scanned membrane. As a contrast, in some model membranes deposited directly on a solid support, the lipid headgroups could be directly resolved (Zasadzinski et al., 1991; Hui et al., 1995). As in the case of 2-D crystals of proteins, the lipids in these bilayers were ordered in a lattice. The regularity of samples increases the obtained resolution.

In order to image biological samples like proteins (Czajkowsky and Shao, 1998; Kasas et al., 1997), DNA (Hansma et al., 1993), lipid bilayers (Dufrêne and Lee, 2000) or 2-D crystals of

proteins, with AFM, they have to be deposited onto a solid support (Müller et al., 1997a). Such a substrate should be flat on the molecular level, otherwise height differences arising from the sample can not be distinguished from height differences arising from the substrate. Substrates that meet this condition are highly orientated pyrolytic graphite (HOPG), which is hydrophobic, and mica and hydrophilized silicon wafer (silica), which are both hydrophilic and negatively charged. The samples described in this thesis are deposited on either silicon wafers or mica.

1.4 Supported lipid bilayers

Supported lipid bilayers, also called planar lipid bilayers, can be made by the Langmuir-Blodgett method, by vesicle fusion or a combination of these two (Shao et al., 1996). With the Langmuir-Blodgett (LB) method (Blodgett, 1935), a lipid monolayer is spread on an aqueous solution present in a Langmuir trough and compressed to the desired surface pressure with a moveable barrier. Subsequently a clean, hydrophilic substrate is pulled from the aqueous phase, through the interface, in the air. In this way, a lipid monolayer is deposited on the substrate, with the lipid headgroups facing the substrate and the acyl chains facing the air. A second monolayer is deposited by pushing the substrate, coated with one monolayer, through the interface into the aqueous phase. The lipid acyl chains in the second monolayer, or leaflet, face the acyl chains of the lipids in the first monolayer, while their headgroups face the aqueous phase (Fig. 1.5).

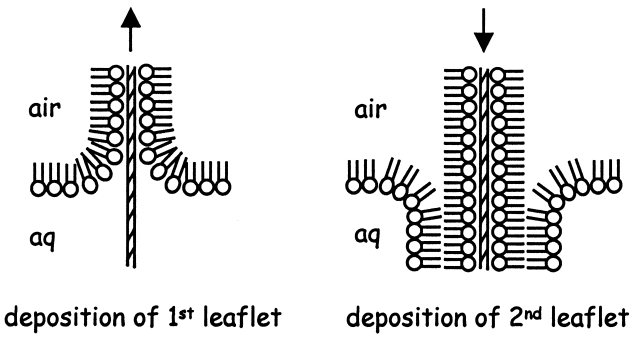

FIGURE 1.5 Preparation of a phospholipid bilayer with the Langmuir-Blodgett technique.

Bilayers prepared with this technique usually contain holes, often referred to as defects (see below). These defects probably stem from a process that occurs as the second leaflet is deposited. During this process, lipids from the first leaflet jump to the monolayer on the trough, leaving vacancies in the deposited bilayer (Bassereau and Pincet, 1997). The amount

of defects can be regulated by changing the surface pressure of the deposited monolayer and the speed of deposition.

A different way of depositing the second leaflet is by using the Langmuir-Schaeffer (LS) method. With this method the substrate, coated with a monolayer, is pushed horizontally through the air-water interface. With the LB method it is not possible to prepare bilayers with a first leaflet of phospholipids in the fluid phase, since these, upon deposition of the second leaflet, would all jump to the monolayer on the trough, leaving a bare substrate. Preparation of bilayers with a first leaflet of anionic phospholipids should be possible, when divalent cations are present in the subphase. However, by using an LS-like procedure, bilayers with a fluid first leaflet have been made (Czajkowsky et al., 1998; 1999). Native biological membranes are often asymmetric (Op den Kamp, 1979), and both LB and LS offer the possibility to prepare asymmetric model bilayers.

With the vesicle fusion method (Brian and McConnell, 1984), a vesicle suspension is deposited on a hydrophilic substrate. The vesicles then adsorb to the substrate, burst open and fuse with neighboring opened vesicles to form a bilayer (Fig.1.6). This process has been studied extensively by Reviakine (Reviakine and Brisson, 2000a) using AFM.

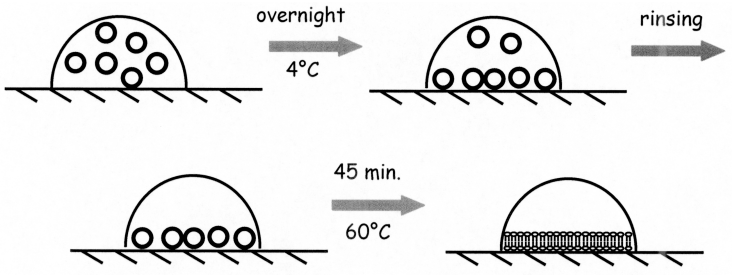

FIGURE 1.6 Principle of vesicle fusion.

Vesicle fusion occurs readily with vesicles of lipids in the fluid phase, leaving a smooth bilayer without defects. When using vesicles of lipids in the solid phase, heating of the sample to above the phase transition temperature is recommended, to obtain a clean bilayer. Bilayers in the solid phase, made by vesicle fusion often contain defects. In this case, defects stem from the fact that there are not enough lipids present to cover the whole substrate, since the bilayer shrinks during cooling after the heating mentioned above. Lipids in the solid phase occupy less space than lipids in the fluid phase. The amount and size of the defects can be regulated by changing the adsorption time, the concentration of the used vesicle suspension, or by letting the bilayer cool down in the presence of vesicles (Beckmann et al., 1998), although this usually yields bilayers with contamination on top.

The defects present in the bilayers can be used to verify if a bilayer is indeed present, since it takes a practiced eye to see the difference between a perfectly smooth bilayer and a bare substrate. In addition, large defects can be used to measure the height of the prepared bilayer. Also, when scanning in Contact Mode, defects can be created by increasing the force applied by the tip, which results in removal of the scanned part of the bilayer. It is generally assumed that between the bilayer and the substrate a layer of water is present, with a thickness of 1-2 nm (Tamm and Shao, 1998). When imaging supported bilayers with AFM, this water layer manifests itself in an increased height difference between the bilayer and the support. For example, a DPPC bilayer has a thickness of 4.7 nm, as measured by X-ray diffraction (Marsh, 1990), but the height as determined by AFM is found to be around 5.8 nm (Mou et al., 1995; Beckmann et al., 1998; Rinia et al., 1999).

1.5 Imaging model membranes by AFM

Since AFM offers the possibility to image model membranes under aqueous conditions, with a high resolution, much effort has been made to image supported bilayers, with or without associated proteins or peptides (Dufrêne and Lee, 2000). Single component phospholipid bilayers consisting of PC (Mou et al., 1994a; 1994b; 1995; Czajkowsky et al., 1995; Beckmann et al., 1998), PE (Zasadsinski et al., 1991, Hui et al., 1995) and a polymerizable PC (Yang, 1993) have been imaged. As mentioned above, these look flat with some defects, and when the lipids are ordered, molecular resolution can be obtained. Upon treatment of such bilayers, the morphology could be changed dramatically. Fang and Yang (1997) found that prolonged heating of DPPC bilayers resulted in lipid-loss, visible as an increase in amount and size of defects, and the appearance of lower areas in the bilayer (2 nm lower than the intact bilayer). Such lower areas are generally believed to consist of interdigitated lipids (Mou et al., 1994b; Fang and Yang, 1997; Janshoff et al., 1999). Also interdigitated domains in DPPC bilayers induced by alcohols have been imaged (Mou et al., 1994b). Constituents of often used buffers, like Trishydroxymethylaminomethane (Tris) and phosphate buffered saline (PBS), were shown to be able to induce ripple phases in several phospholipid bilayers (Czajkowsky et al., 1995; Mou et al., 1994a). Ripple phases are usually observed in second bilayers, present on top of a bilayer on a solid support (Fang and Yang, 1996; Mou et al., 1996). Upon addition of Phospholipase A_2, DPPC bilayers were degraded in a specific way (Grandbois et al., 1998). Degradation always started at the edges of defects, in the shape of thin line type defects, which only branched at angles of 120°, presumably reflecting the organization of the lipid molecules.

The fact that bilayers in the solid phase are thicker than bilayers in the fluid phase implies that fluid-solid phase separation can be visualized by AFM. Indeed, DPPC/POPC bilayers

showed higher domains, consisting of DPPC in the solid phase surrounded by lower areas, consisting of POPC in the fluid phase (Mou et al., 1995). Fig. 1.7 shows an AFM image of such a bilayer, which we prepared using the vesicle fusion method. Defects were seen only in the solid phase domains.

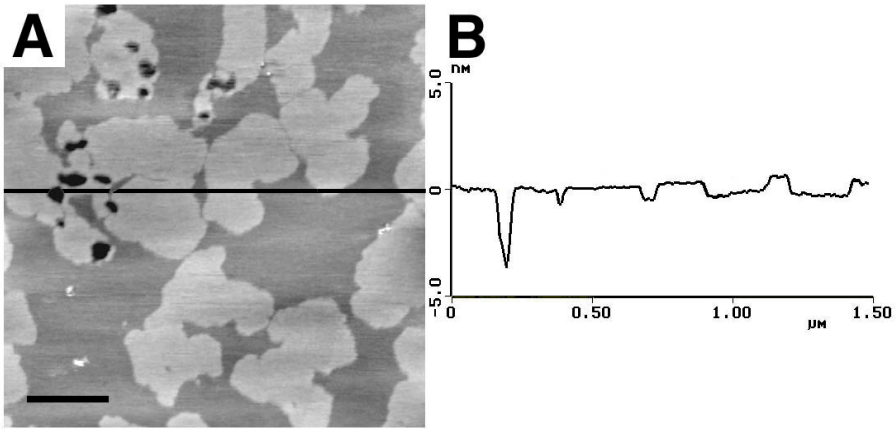

FIGURE 1.7 (A) AFM topographic image of a DPPC/POPC (1:1) phase separated bilayer. High areas appear light, and low areas dark. DPPC is visible as high domains surrounded by lower POPC. Defects are visible as black spots. Scale bar 0.3 mm, z-scale 10 nm. (B) Height profile of the line drawn in A, showing the height difference between the fluid and solid phase of nearly 1 nm. The defect appears only 4 nm deep, since it is too narrow for the tip to reach the bottom.

In order to prepare membrane protein samples that allow imaging with AFM, often 2-D crystals of proteins are used. The close packing of the proteins in such samples provides the rigidity needed to stand scanning forces, and the high degree of order facilitates high resolution imaging. One of the first samples imaged with AFM were naturally occurring densely packed membranes, like the purple membrane, a 2-D crystal of Bacteriorhodopsin (see for a review Müller et al., 2000), Hexagonally Packed Intermediate (HPI) layer (Wiegrabe et al., 1991; Müller et al., 1996) and gap junctions (Hoh et al., 1991; 1993). Also 2-D crystals of pores have been imaged, such as the outer membrane porin OMPF from *Escherichia coli* (Lal et al., 1993; Schabert et al., 1995), Aquaporin 1 (Walz et al., 1996) and Aquaporin Z (Scheuring et al., 1999a; 2000) and Aquaporins from spinach leaf (Fotiadis et al., 2001). The topography of the c-subunits of ATP-synthase has been revealed only recently (Seelert et al., 2000). Apart from just yielding high-resolution images, it was also possible to see conformational changes using AFM (Müller et al., 1997b).

The 2-D crystals discussed so far were made in solution, and subsequently adsorbed on a solid substrate. They consisted of integral membrane proteins. Another method is to prepare a monolayer on a Langmuir-trough and let proteins bind to the lipid headgroups and form a 2-D crystal. This monolayer with proteins attached can then be deposited on a hydrophobic substrate, such as HOPG or a hydrophilic substrate coated with a lipid monolayer. This has been done for the vacuolating toxin VacA (Czajkowsky et al., 1999), Staphylococcal α-Hemolysin (Czajkowsky et al., 1998) and for bacterial cell surface layer (S-layer) proteins (Wetzer et al., 1997), which have a natural affinity for (anionic) lipids. For Streptavidin (Scheuring et al., 1999b) biotinylated lipids were used to ensure protein binding to the monolayer.
When the protein of interest is a water-soluble protein, able to insert in membranes containing specific lipids, another method can be used. For this method, first a bilayer containing these specific lipids is made and imaged, and subsequently the protein is added to the solution above this bilayer and allowed to insert. When using lipids in the fluid phase, and an optimum amount of ligand-lipids, it is possible to obtain at least densely packed protein layers, and even 2-D protein crystals. This has been shown for pore-forming proteins as the cholera toxin β-oligomer in bilayers containing 10% ganglioside (Mou et al., 1995). Annexin A5, a protein that participates in cell processes involving membrane fusion and trafficking, binds to membranes containing anionic phospholipids. This binding is known to be dependent on Ca^{2+}. This system was used to obtain high resolution images of this protein, as well as to study the growth of Annexin A5 crystals on PS containing bilayers (Reviakine et al., 1998; 2000b).

1.6 Outline of this thesis

Since AFM has proven to be such a powerful tool to image biological samples under aqueous conditions, this technique was used to study domains in model membranes. Many biological membranes are asymmetric, and several membrane proteins associate with anionic lipids. Hence asymmetric bilayers were prepared, with a first leaflet of zwitterionic, and a second leaflet of anionic phospholipids. Chapter 2 reports on the morphology of such bilayers. The defects present in these bilayers were surrounded by elevations. The formation of these elevations was found to arise from electrostatic interactions, and was called bilayer blistering. Chapter 3 and 4 deal with domain formation due to peptide-lipid interactions. In order to study the lateral organization of lipid bilayers mixed with transmembrane peptides, DPPC bilayers with transmembrane model peptides incorporated were imaged. Chapter 3 describes how WALP peptides induced the formation of domains with an unusual, highly ordered pattern and it describes the effect of the length of WALP peptides on these striated domains.

Chapter 4 deals with the influence of flanking residues other than tryptophans on the formation of striated domains. In Chapter 5 domain formation due to lipid-lipid interaction is studied. Bilayers containing sphingolipids and cholesterol were chosen because these lipids are known to preferentially associate, and in certain cell membranes they are suspected to form functional domains which are assumed to correspond to certain parts of cell membranes that are resistant to non-ionic detergents. The formation of such domains as well as their resistance to a non-ionic detergent was imaged. In Chapter 6 all the results presented in this thesis are summarized and discussed.

CHAPTER 2

Blistering of Langmuir-Blodgett bilayers containing anionic phospholipids observed by Atomic Force Microscopy.

(Biophysical Journal, 1999, 77:1683-1693)

ABSTRACT

Asymmetric bilayers of different phospholipid compositions have been prepared by the Langmuir-Blodgett (LB) method, and imaged by Atomic Force Microscopy (AFM). Such bilayers can function as models for biological membranes. The first leaflet consisted of zwitterionic phospholipids: phosphatidylcholine (PC) or phosphatidylethanolamine (PE). The second leaflet consisted of the anionic phospholipid phosphatidylglycerol (PG), in either the condensed or fluid phase or, for comparison, of PC. Different bilayers showed different morphology. In all bilayers defects in the form of holes were present. In some bilayers with a first leaflet consisting of PC, polygonal line-shaped defects were observed, whereas when the first leaflet consisted of PE, mainly round defects were seen. Not only the shape, also the amount of defects varied, depending on the condition and the composition of the second leaflet. In most of the PG containing systems, the defects were surrounded by elevations, which reversibly disappeared in the presence of divalent cations. This is the first time that such elevations have been observed on phospholipid bilayers. We propose that they are induced by phospholipid exchange between the two leaflets around the defects, leading to the presence of negatively charged phospholipids in the first leaflet. Because the substrate is also negatively charged, the bilayer around the edges is repelled and lifted up. Since it was found that the elevations are indeed detached from the substrate, we refer to this effect as bilayer blistering.

2.1 INTRODUCTION

Phospholipid bilayers are commonly used as models for biological membranes. They have been extensively studied by a broad range of techniques, leading to detailed information on both their structure and the molecular orientation of their constituents. The last decade, Atomic Force Microscopy (AFM) (Binnig et al., 1986) has proven to be a useful additional method to elucidate the structure of supported phospholipid bilayers (Shao et al., 1996). The main advantage of AFM is that it can provide high resolution information on the surface of samples under aqueous and physiological conditions (Engel, 1991; Bustamante et al., 1994; Hansma and Hoh, 1994; Lal and John, 1994).

Images have been made of phospholipid bilayers in the condensed phase (Hui et al., 1995; Mou et al., 1995), fluid phase (Rädler et al., 1994) and of phase-separated bilayers (Mou et al., 1995). Also, ripple phases (Mou et al., 1994a; Czajkowsky et al., 1995) and domains of interdigitated phospholipids (Mou et al., 1994b) have been observed by AFM. A common feature of supported phospholipid bilayers is the presence of defects, in the form of holes in the bilayer. These defects can be used to measure the bilayer thickness, which is typically in the order of 5 to 6 nm (Mou et al., 1994a; 1994b; 1995; Czajkowsky et al., 1995; Hui et al., 1995; Beckmann et al., 1998).

Molecular resolution has been obtained on layers of phosphatidylglycerol (PG) on alkylated mica (Egger et al., 1990; Weisenhorn et al., 1991), phosphatidylethanolamine (PE) on alkylated mica (Weisenhorn et al., 1991) and on PE bilayers (Zasadzinski et al., 1991; Hui et al., 1995). On phosphatidylcholine (PC), high resolution was achieved after manipulating the bilayer by scanning the same area at least four times at a force of 1nN. Ridges appeared perpendicular to the scan direction with a spacing of 0.63-0.68 nm (Beckmann et al., 1998).

AFM offers prospects to reveal the surface organization of membrane associated proteins. For membrane embedded proteins the first promising results have been published already (Hoh et al., 1993; Karrasch et al., 1994; Yang et al., 1993; Mou et al., 1995; Müller et al., 1995; Sommer et al., 1997; for a review see Engel et al., 1997). However, many proteins associate with membranes via interactions with anionic phospholipids (for a recent review see van Klompenburg and de Kruijff, 1998). In order to study such proteins, it is important to be able to prepare and analyze supported bilayers containing anionic phospholipids.

There are two established methods to prepare a supported phospholipid bilayer (Shao et al., 1996). One is vesicle fusion and has been described previously (Brian and McConnell 1984, Mou et al., 1994a). With this method, a droplet of suspension of phospholipid vesicles is deposited on substrates like glass, mica or silicon wafer. After adsorption of the vesicles on the substrate, they spontaneously form a bilayer. Then, excess vesicles are washed away,

leaving a symmetric phospholipid bilayer. Due to electrostatic repulsive forces it will be difficult, if not, impossible to prepare bilayers of negatively charged lipids, by vesicle fusion in the absence of divalent cations.

Another method to prepare supported bilayers is the Langmuir-Blodgett (LB) method, developed by Katharine Blodgett (Blodgett, 1935). After spreading a monolayer on a subphase in a Langmuir trough, the monolayer can be deposited on a substrate by pulling this substrate up through the air-water interface, from the aqueous phase into the air. A second layer can be deposited by dipping the substrate, coated with a monolayer, through the air-water interface again, from the air into the aqueous phase (Roberts, 1990).

With the LB method, asymmetric bilayers can be prepared, of which the first leaflet is formed by zwitterionic phospholipids and the second by anionic phospholipids, potentially available for interaction with proteins. The aim of this study was to prepare such asymmetric bilayers and analyse them by AFM. We selected PG as anionic phospholipid because it is a common anionic membrane lipid, known to anchor proteins such as the translocation motor protein SecA (Breukink et al., 1992). The lipid composition of both leaflets was varied as well as the ionic strength of the solution.

2.2 MATERIALS AND METHODS

2.2.1 Materials

1,2-Dipalmitoyl-*sn*-glycero-3-phosphocholine (DPPC), 1,2-Dimyristoyl-*sn*-glycero-3-phosphoethanolamine (DMPE), 1,2-Dimyristoyl-*sn*-glycero-3-[phospho-*rac*-(1-glycerol)] (DMPG), 1,2-Dipalmitoyl-*sn*-glycero-3-[phospho-*rac*-(1-glycerol)] (DPPG), 1,2-Dioleoyl-*sn*-glycero-3-[phospho-*rac*-(1-glycerol)] (DOPG), 1,2-Dimyristoyl-*sn*-glycero-3-[phospho-L-serine] (DMPS), 1,2-Dipalmitoyl-*sn*-glycero-3-[phospho-L-serine] (DPPS) were purchased from Avanti Polar Lipids (Alabaster, Alabama) and were used without further purification. For all experiments MilliQ water (18.2 MΩ) was used.

Silicon (100) p-type wafers (Wacker-chemitronic GMBH, Germany) were cut in squares of 1x1 cm^2 and cleaned in a mixture of 95-97% H_2SO_4 and 35% H_2O_2 (1:1; v/v). The surface was hydrophylized by boiling for 5 min in a mixture of 25% NH_4OH and 35% H_2O_2 (1:1; v/v), and rinsed with water.

2.2.2 Langmuir-Blodgett transfer

For the Langmuir-Blodgett experiments, a homebuilt trough with a volume of 65 ml and an operational area of 5x13 cm^2 was used, with a well to collect the substrates on which a bilayer

was transferred. The surface tension of the spread monolayer on the trough was measured with a platinum Wilhelmy plate, connected to a Cahn microbalance (Demel, 1994).
The first leaflet of the bilayer (headgroups towards the substrate) was deposited by transferring a monolayer of DPPC or DMPE with a surface pressure of 35 mN/m from a pure water subphase, onto a silicon substrate, on the upstroke. Before deposition of a second leaflet, some of these monolayers were investigated by AFM in contact mode, in air.
The second leaflet of the bilayer (headgroups towards the aqueous phase) was deposited by transferring a monolayer of either DPPC, DPPG or DOPG at a surface pressure of 26 mN/m from a subphase of 10 mM Tris and 100 mM NaCl, pH 7.4, on the downstroke. A concentration of 10 mM Tris is too small to cause a ripple phase (Mou et al., 1994a). DMPG was deposited at a surface pressure of 22 mN/m or 35 mN/m. DPPS and DMPS were transferred at a surface pressure of 26 mN/m and 35 mN/m respectively. The monolayers used to form second leaflet were left to equilibrate on the trough for 1 hr before deposition. The transfer speed was 4.7 mm/min. With a moveable barrier, surface pressures were kept constant during transfer. The transfer ratios (the transfer of the second layer relative to the transfer of the first layer) varied between 0.5 and 1. After deposition of the second leaflet, the samples were vertically lowered in a well in the trough. After removal of the phospholipid monolayer from the surface, the substrate with the bilayer was kept under water and positioned horizontally on the bottom of the trough with the bilayer side up. Then an O-ring was put on the substrate, kept in place with some vacuum grease. After this, the substrates could easily be taken out of the trough and transferred to the AFM whilst the bilayer area within the O-ring remained covered with buffer. All bilayers were made at room temperature and, unless stated otherwise, imaged within 4 hrs after deposition.

2.2.3 AFM measurements

The bilayer bearing silicon substrate was affixed to a metal disc and mounted on the E-scanner, which was calibrated on a standard grid of 1x1 μm, of a Nanoscope III (Digital Instruments, Santa Barbara, California). The AFM head with a quartz flow cell was placed over the sample such that the circular slit in the flow cell fell over the O-ring. Sometimes the O-ring was removed, because we found that it can give rise to distorted images. Care was taken that the bilayer was not exposed to air. After removal of the O-ring the surface-tension of the buffer usually kept a droplet on the bilayer in its place. Undistorted measurements with the O-ring gave identical results compared to the measurements without the O-ring.
Oxide-sharpened tips with a spring constant of 0.06 N/m, as estimated by the manufacturer, were used (Digital Instruments, Santa Barbara, California). Images were obtained while scanning with a scan speed of 4 lines/sec, in Contact Mode. We found that scanning in

Tapping Mode did not give better images, compared to Contact Mode. During scanning the force was set such that it was as small as possible while the image was stable and clear, which was usually at a force smaller than 0.5 nN. Scanning at larger forces damaged the scanned area of the bilayer. Tip-induced defects were created by scanning a part of the bilayer at high speed (60 lines/sec), using a force of 10 nN.
The Nanoscope software offers the possibility to study vertical linear cross sections and height distributions of images. Vertical linear cross sections gave estimations for the height of a bilayer, using the largest defects, already present in the bilayer. The defects in the different bilayers varied in amount and size, leading to different fractions of uncovered substrate. These fractions were quantified using height distributions. The values given in the results section are the means ± the standard deviations.
In order to examine the influence of divalent cations and the ionic strength of the buffer on the bilayer, in some experiments the buffer above the sample, in the flow-cell was replaced by 10 mM Tris, 100 mM NaCl and 3 mM $MeCl_2$, pH 7.4 (Me^{2+} = Mg^{2+}, Ca^{2+}, Ba^{2+} or Sr^{2+}) or by 10 mM Tris, 300 mM NaCl, pH 7.4.

2.3 RESULTS

Phosphatidylcholine (PC) and phosphatidylethanolamine (PE) are common membrane lipids that can be anchored to hydrophilic substrates via their zwitterionic headgroups (Grandbois et al., 1998, Hui et al., 1995). The bilayers which we studied, always had a first leaflet (headgroups towards the substrate) consisting of DPPC or DMPE, both in the condensed phase. DPPC and DMPE monolayers were imaged with AFM in air (Figs. 2.1 *A* and 2.2 *A*, respectively) and in general they looked smooth with a few small defects. The second leaflet of the bilayers (headgroups towards the aqueous phase) consisted of DPPC (for control purposes), or the negatively charged phospholipids DPPG, DMPG or DOPG. At room temperature and at a surface pressure of 26 mN/m, a monolayer of DPPG is in the condensed phase and of DOPG in the fluid phase. At room temperature, and at a surface pressure of 35 mN/m, a monolayer of DMPG is in the condensed phase whereas, at a surface pressure of 22 mN/m, it is in the fluid phase. The phases of the monolayers were confirmed by π-A measurements. We selected these different PG's and different surface pressures to be able to examine the influence of the packing of the second leaflet on the morphology of the bilayer.
In the following text we refer to the phases of the leaflets of LB bilayers as those of the monolayer on the trough, before deposition on the substrate. Also, in this paper, we refer to an asymmetric bilayer with, for example, DPPC as the first leaflet and DPPG as the second, as DPPC/DPPG.

2.3.1 Bilayers with a first leaflet of DPPC

Fig. 2.1 *B* shows a typical AFM image of a DPPC/DPPC bilayer (both leaflets in the condensed phase). DPPC/DPPC bilayers in general looked smooth, with some defects (the fraction of uncovered substrate was 6±1%) and quite often, some debris was seen on top of the bilayer. The bilayer height was found to be 6.0±0.1 nm. These results are consistent with what has been found previously (Mou et al., 1994b; Fang and Yang, 1997; Grandbois et al., 1998).

Fig. 2.1 *C* is a representative image of a DPPC/DPPG bilayer. This image differs distinctively from those obtained on the symmetric DPPC/DPPC bilayer. There are both round and irregularly shaped defects in the DPPC/DPPG bilayer and these defects are always surrounded by elevations. The fraction of uncovered substrate was found to be 8±2%, which is slightly higher compared to the DPPC/DPPC bilayer. A mesh-like, polygonal structure can be seen on the bilayer, which seems to connect the irregularly shaped defects. The height of the DPPC/DPPG bilayers was found to be 5.9±0.3 nm. The height of the elevations around the defects varied between 1.5 and 2.5 nm, and the height of the mesh-like structure varied between 2 and 6 nm, taking the bilayer surface as the zero level. The precise heights of these elevations depended on the applied force during scanning. This also applies to the height of elevations on other investigated bilayers, discussed in the next sections.

Similar features were observed for a bilayer with a second leaflet of DMPG in the condensed phase, as is DPPG (Fig. 2.1 *D*). Again, irregularly shaped defects are present and elevations can be seen on the bilayer. These elevations usually surround the defects but not as explicitly as in the case of DPPC/DPPG bilayers. The height of these elevations on the bilayer varied between 2 and 3 nm, taking the bilayer surface as the zero level. The height of the DPPC/DMPG (condensed) bilayer was found to be 6.0±0.5 nm and 15±3% of the substrate was uncovered.

A typical image of a bilayer with DPPC as the first leaflet and DMPG in the fluid phase as the second leaflet, is depicted in Fig. 2.1 *E*. Unlike the DPPC/DMPG (condensed) bilayer, no elevations can be seen on the surface, apart from some debris. There are line-shaped, polygonal defects and some small irregularly shaped defects in these bilayers. The fraction of uncovered substrate was 21±4%, and the height of the DPPC/DMPG (fluid) bilayer was 6.0±0.3 nm.

DPPC/DOPG bilayers (DOPG in the fluid phase) gave similar results, as shown in Fig. 2.1 *F*. There are line-shaped polygonal and irregularly shaped defects in the bilayers, but the polygonal defects seem more irregular and branched compared to the ones in the DPPC/DMPG (fluid) bilayer. Again, some debris can be seen on the bilayer. DPPC/DOPG bilayers seemed soft under the AFM tip and sometimes it was difficult to get a stable image. The bilayer height was found to be 6.1±0.4 nm and 24±4% of the substrate was uncovered.

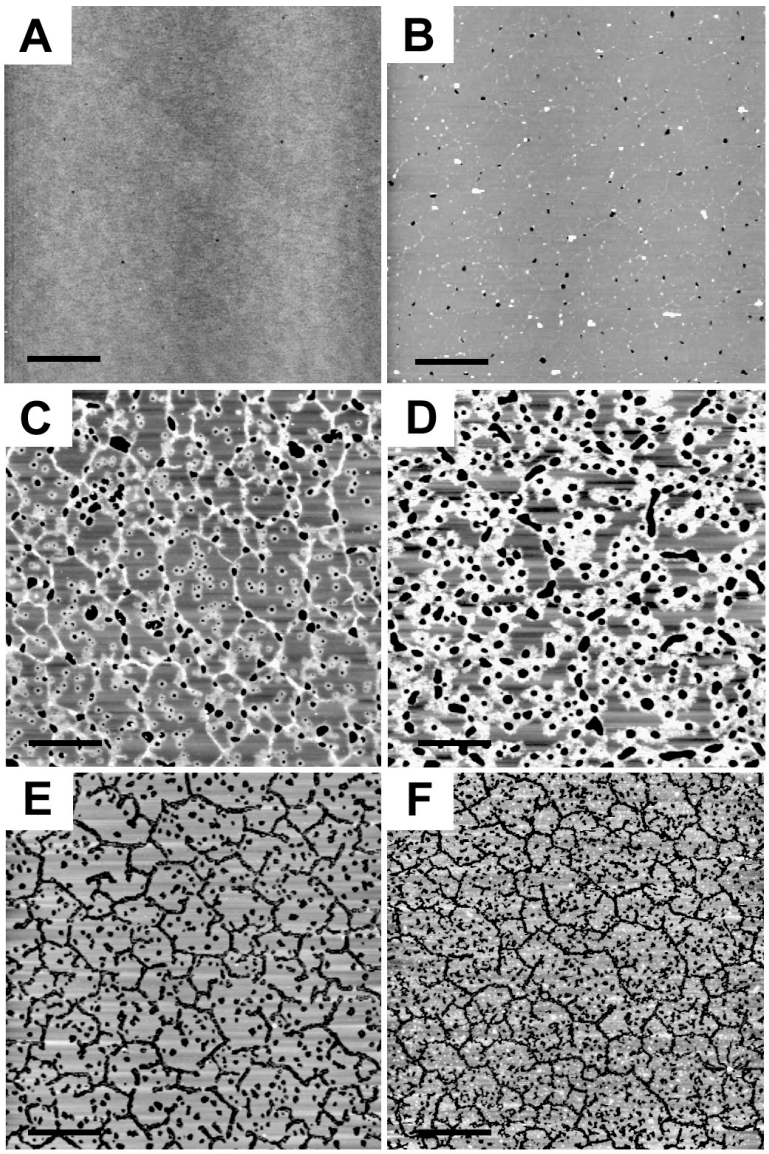

FIGURE 2.1 Morphology of LB phospholipid layers, (A) Monolayer of DPPC (condensed), transferred from water at a surface pressure of 35 mN/m. Such a monolayer was used as the first leaflet of the following bilayers, of which the second leaflet was transferred from 10 mM Tris buffer, with 100 mM NaCl, pH 7.4, and consisted of (B) DPPC deposited at a surface pressure π *of 26 mN/m (condensed); (C) DPPG deposited at* π*=26 mN/m (condensed); (D) DMPG deposited at* π*=35 mN/m (condensed); (E) DMPG deposited at* π*=22 mN/m (fluid) and (F) DOPG deposited at* π*=26 mN/m (fluid). All images are 10x10 mm; scale bars 2 mm; z-scales 10 nm.*

2.3.2 Bilayers with a first leaflet of DMPE

Fig. 2.2 *B* is an image of a DMPE/DPPC bilayer (both leaflets in the condensed phase). This asymmetric bilayer of zwitterionic lipids looks smooth with only a few defects (the fraction of uncovered substrate was 7±5%) and there is less debris on top than on the DPPC/DPPC bilayer (Fig. 2.1 *B*). The height of this bilayer was found to be 5.6± 0.3 nm.

When DPPG (in the condensed phase) was deposited as a second leaflet on a DMPE layer, some of the striking features of the DPPC/DPPG bilayer were observed again, but also some differences were noticed (Fig. 2.2 *C*). In the DMPE/DPPG bilayer many round defects can be seen, surrounded by elevations. Their height varied between 2 and 3 nm, the bilayer height was found to be 6.0±0.2 nm, and the fraction of uncovered substrate 7±2%. In contradiction to a DPPC/DPPG bilayer (Fig. 2.1 *C*), there are no mesh-like, polygonal elevations on, and no irregularly shaped defects in the DMPE/DPPG bilayer.

Similar images were obtained for the DMPE/DMPG (condensed) bilayer (Fig. 2.2 *D*). Here the elevations around the round defects are very wide-spread. Only at some places, indicated by an arrow, the darker gray level of the bilayer itself can be seen. Where the defects are not perfectly round, it seems like two round defects have coalesced. The bilayer was 6.4±0.5 nm high, the elevations were between 2 and 3 nm high and 10±1% of the substrate was uncovered. Compared to the DPPC/DMPG (condensed) bilayer (Fig. 2.1 *D*), the defects are rounder and the elevations are more wide-spread.

When the second leaflet of DMPG in the fluid phase is deposited on DMPE, again round defects are present in the bilayer surrounded by elevations of about 2.5 to 3.5 nm high, as can be seen in Fig. 2.2 *E*. The elevations are not as wide-spread, and there are more defects (17% uncovered substrate) in the bilayer compared to the bilayers with DMPG in the solid phase (Fig. 2.2 *D*). The thickness of the DMPE/DMPG (fluid) bilayer was found to be 5.3±0.1 nm.

Fig. 2.2 *F* depicts a DMPE/DOPG bilayer (DOPG in the fluid phase) which shows irregular defects in the bilayer and elevations randomly on the bilayer. Like in the case of DPPC/DOPG, the layer was easily damaged and it was hard to get a stable image. It appeared that under some elevations, defects were present which were only seen after scanning the bilayer surface two or three times or when the force was increased a bit (about 0.1 nN). This dual character of defects sometimes appearing as holes and sometimes as elevations made it difficult to determine the fraction of uncovered substrate, which was estimated to be 16±9%. The height of the elevations varied between 1.5 and 3 nm and the bilayer was 5.2±0.4 nm high. It is striking that when PG in the fluid phase is deposited on DMPE (Fig. 2.2, *E* and *F*), there are elevations present and no line-shaped, polygonal defects can be seen, whereas when PG is deposited on DPPC (Fig. 2.1, *E* and *F*), there are no elevations on the bilayer and the defects mainly have a line-shaped polygonal character.

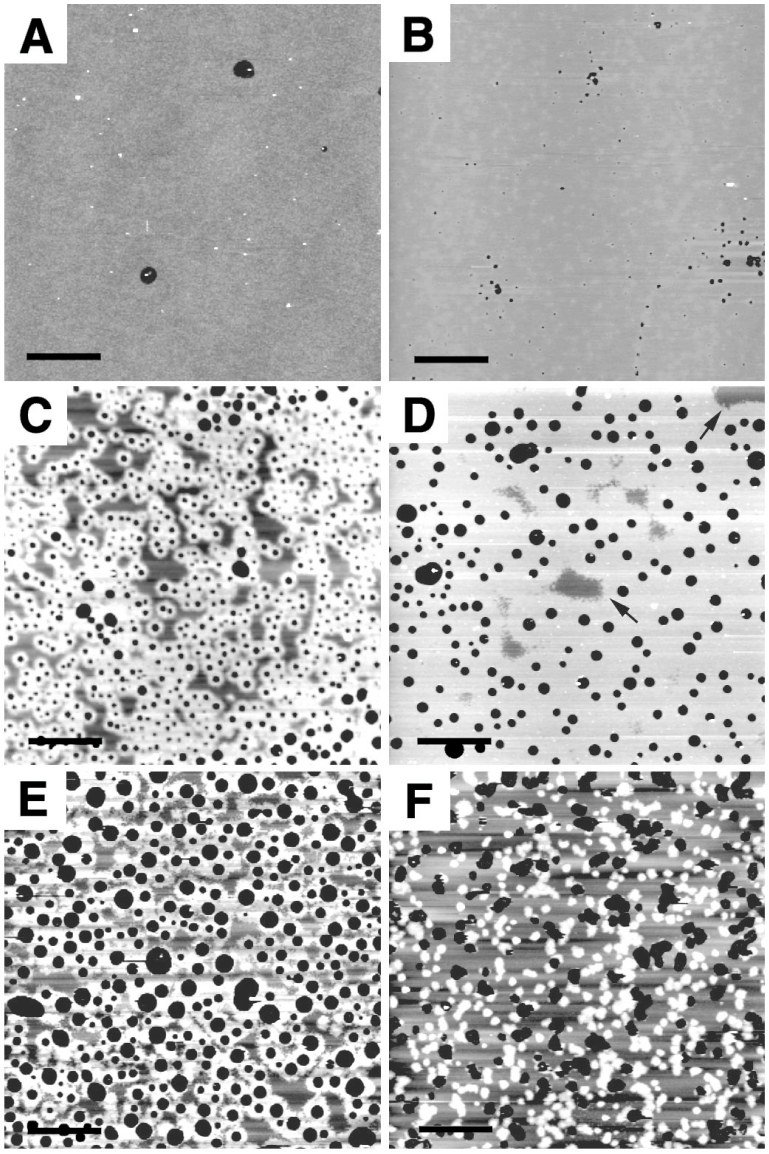

FIGURE 2.2 (A) Monolayer of DMPE, transferred from water at a surface pressure of 35 mN/m (condensed). Such a monolayer was used as the first leaflet of the following bilayers, of which the he second leaflet was transferred from 10 mM Tris buffer, with 100 mM NaCl, pH 7.4, and consisted of (B) DPPC deposited at a surface pressure π *of 26 mN/m (condensed), (C) DPPG deposited at* π*=26 mN/m (condensed), (D) DMPG deposited at* π*=35 mN/m (condensed), (E) DMPG deposited at* π*=22 mN/m (fluid) and (F) DOPG deposited at* π*=26 mN/m (fluid). All images are 10x10 mm; scale bars 2 mm; z-scales 10 nm.*

2.3.3 About the elevations

In order to acquire more information on the nature of the elevations present on most of the bilayers with a second leaflet consisting of PG, we studied the influence of the scanning force, time and the ionic composition of the buffer on the appearance of the bilayers and we introduced tip-induced defects. To determine whether the elevations are induced by the negatively charged headgroups of anionic phospholipids in general, or whether they are specific for PG, we also imaged bilayers with a second leaflet consisting of a different anionic phospholipid, phosphatidylserine (PS).

By increasing the force applied by the tip (to about 1.5 nN), whilst scanning a DPPC/DPPG bilayer, the height of the elevations could be reduced until almost zero. When afterwards the same area was scanned at minimal force, the elevations were again clearly visible, although their height was slightly reduced compared to the height in the initial scan (data not shown). Apparently the elevations can be pushed down reversibly.

After leaving a DPPC/DPPG bilayer overnight (20 hrs after deposition), both the polygonal elevations and the elevations around the defects had spread out, giving the bilayer an appearance comparable to that of a DPPC/DMPG (condensed) bilayer (Fig. 2.1 *D*). The elevations usually surround the defects already present in the bilayer. To examine the involvement of defects in the formation of elevations, defects were induced with the AFM tip in a DPPC/DPPG bilayer. After leaving the damaged bilayer overnight, these self made defects were almost completely surrounded by elevations (data not shown).

All images described so far were obtained by scanning under a 10 mM Tris buffer with 100 mM NaCl, pH 7.4. We also studied some of the systems in the presence of Mg^{2+} or an increased NaCl concentration. These conditions will lead to an increased screening of the surface charge on the bilayer and possibly direct electrostatic interactions.

We imaged the DPPC/DPPG and the DMPE/DMPG (condensed and fluid) bilayers in the presence of Mg^{2+} and found that under these conditions the elevations are absent. This is illustrated in Fig. 2.3, *A-C*, for a DPPC/DPPG bilayer. Fig. 2.3 *A* depicts the control situation.

After replacing the buffer in the flow cell by a 10 mM Tris buffer with 100 mM NaCl and 3 mM $MgCl_2$, pH 7.4, the elevations had completely disappeared (Fig. 2.3 *B*). This process is reversible since after replacing the Tris buffer with Mg^{2+} by Tris buffer without Mg^{2+}, the elevations reappeared in the same places (Fig. 2.3 *C*).

When the same DPPC/DPPG bilayer was scanned under 10 mM Tris buffer with 300 mM NaCl, pH 7.4, the elevations became somewhat hazy (Fig. 2.3 *D*). After replacing this buffer by 10 mM Tris with 100 mM NaCl and 3 mM $MgCl_2$, pH 7.4, the elevations had disappeared again (results not shown).

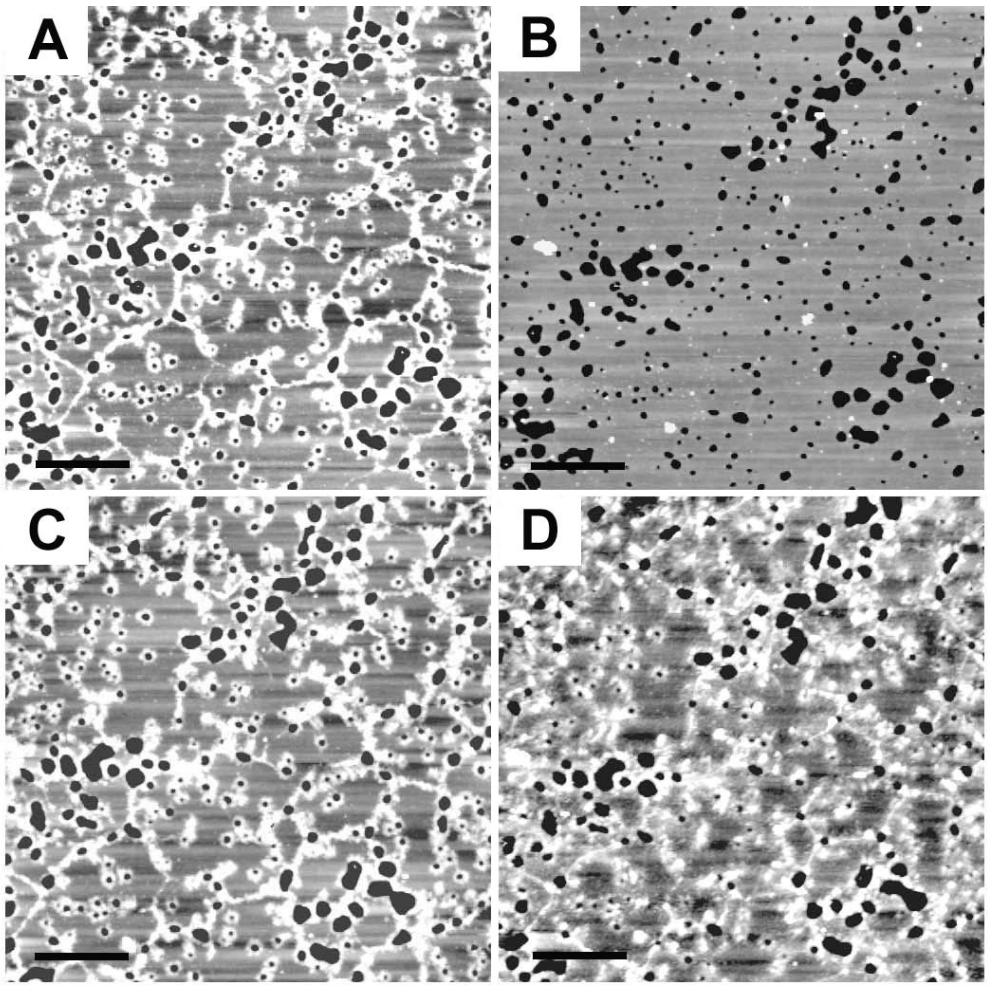

FIGURE 2.3 The effect of changes in ionic conditions on the morphology of a phospholipid bilayer. On a DPPC/DPPG bilayer (condensed) scanned under (A) 10 mM Tris, 100 mM NaCl, pH 7.4, elevations can be seen; (B) 10 mM Tris, 100 mM NaCl with 3 mM $MgCl_2$, the elevations have disappeared; (C) 10 mM Tris, 100 mM NaCl, pH 7.4, the elevations have reappeared and (D) 10 mM Tris, 300 mM NaCl, pH 7.4, the elevations have become somewhat hazy, but are still present. All images are 5x5 mm; scale bars 1 mm, z-scales 10 nm.

Note that all images in Fig. 2.3 are taken on the same area of the DPPC/DPPG bilayer. The pattern of defects remained stable, although due to the repeated scanning, the defects became slightly larger. Apparently the tip removed lipids from the edges of the defects. The haziness. of the elevations in Fig. 2.3 *D* is not due to replacing the fluid or scanning the same bilayer

several times, because on a different DPPC/DPPG bilayer, we determined the influence of 300 mM NaCl straight away and we found the same effect. After replacing the Tris buffer with 300 mM NaCl by Tris buffer with 100 mM NaCl, the elevations had lost their haziness (results not shown).
In order to determine if this effect is specific for Mg^{2+}, we imaged DPPC/DPPG and DMPE/DMPG bilayers under buffer (10 mM Tris, 100 mM NaCl, pH7.4) containing 3 mM Ca^{2+}, Ba^{2+} or Sr^{2+} and found qualitatively the same results, namely that in the presence of these divalent cations the elevations reversibly disappear. This suggests that the disappearance of the elevations is not the result of specific interactions of PG with Mg^{2+}. Also on DMPE/DPPS (condensed) and DMPE/DMPS (condensed) bilayers, defects were surrounded by elevations, which reversibly disappeared in the presence of divalent cations (data not shown). This implies that the presence of elevations is not PG specific, but is induced by the negative charges on the headgroups of anionic phospholipids. These results indicate that both the formation and the reversible disappearance of the elevations are governed by electrostatic interactions.

2.4 DISCUSSION

In this study, AFM images of asymmetric phospholipid bilayers, of which the second leaflet consists of anionic phospholipids, are presented. The results show that in all the systems in which the second leaflet consists of PG, defects in the shape of holes are present, often surrounded by elevations. Defects have been observed earlier, in phospholipid LB bilayers (Hui et al., 1995; Mou et al., 1995; Czajkowsky et al., 1995; Bassereau and Pincet, 1997; Grandbois et al., 1998). However, to our knowledge, the presence of elevations surrounding the defects has never been reported before.
Bilayers with a second leaflet of PG have been studied with respect to ripple phases, induced by the constituents of PBS buffer (Czajkowsky et al., 1995). We never observed a ripple phase in our systems which is probably due to the fact that we deposited the leaflets at a lower surface pressure and worked with different buffers.

2.4.1 Defects in supported bilayers

Defects perforating the bilayer are commonly observed in supported phospholipid bilayers (Shao et al., 1996; Bassereau and Pincet, 1997). Our study shows that, in agreement with previous results (Czajkowsky et al., 1995; Mou et al., 1995), also in LB-bilayers with a second leaflet of anionic phospholipids, defects tunneling both leaflets are present. The presence of

holes in phospholipid bilayers is surprising because the same lipid systems self assemble in aqueous solution into tightly sealed vesicular bilayers. The fact that supported phospholipid monolayers hardly contain any defects (Bassereau and Pincet, 1997 and Fig. 2.1 *A* and 2.2 *A*) makes the presence of defects in supported bilayers all the more peculiar. The reason why defects are stable and how the boundary between the lipid phase, and the aqueous phase in the defects looks like on molecular scale is not yet clear (Fang and Yang, 1997). Recently, Grandbois and coworkers (1998) found that Phospholipase A_2 starts degrading a DPPC bilayer at the boundary of the defects, which led them to propose a plausible model for the edge of defects, with the two leaflets curved towards each other forming a convex structure, such that only headgroups are exposed to the aqueous phase (see also Fig. 2.4).

An explanation for the origin of defects in LB bilayers has been proposed (Bassereau and Pincet, 1997). These authors suggest that during the deposition of the second monolayer on the first, some lipids of the first monolayer desorb from the substrate and move over to the monolayer on the trough. The same authors state, in agreement with Mou et al., that fewer defects appeared, when the second leaflet was transferred at higher surface pressures (Bassereau and Pincet, 1997; Mou et al., 1995). We also found that the percentage of uncovered substrate in bilayers with DMPG as a second leaflet, deposited at a high surface pressure (35 mN/m), is lower than in bilayers with DMPG deposited at a low surface pressure (22 mN/m). Moreover, the phase the second leaflet is in, also influences the amount of defects, since in the bilayers with PG in the condensed phase (Fig. 2.1, *C* and *D*; Fig 2.2, *C* and *D*), the fraction of uncovered substrate is lower than in bilayers with PG in the fluid phase (Fig. 2.1, *E* and *F*; Fig. 2.2, *E* and *F*). Even though the first leaflets of the bilayers depicted in Fig. 2.1, *B-F* are the same, the amount of uncovered substrate in these bilayers varies, which also counts for Fig. 2.2, *B-F*. Apparently the conditions of the second leaflet as it is on the trough determine how many lipids leave the substrate during deposition of the second leaflet, which eventually determines the amount of defects in the bilayer.

Not only the amount of the defects in the different bilayers varied, but also the shape of the defects differed, primarily related to the constituents of the first leaflet. In the case of DMPE as the first leaflet, the defects are nearly round, whereas for DPPC as the first leaflet a more irregular pattern was observed. This suggests that it is energetically favorable for DMPE layers to form defects with the lowest boundary to uncovered surface ratio possible. This might be related to the fact that PE headgroups strongly interact with one another (Hauser et al., 1981).

In all bilayers of which the first leaflet consists of DPPC and the second of PG (Fig. 2.1, *C-F*), a polygonal structure in the shape of elevations or defects can be seen, even though in the case of DMPG (condensed), it is merely vaguely visible. Interestingly, similar polygonal patterns

have been observed by AFM previously in DPPC containing bilayers or monolayers. They appeared in bilayers in which hydrophobic peptides were incorporated (Mou et al., 1996; von Nahmen et al., 1997) and as a phospholipase A_2 hexagonal degradation pattern (Grandbois et al., 1998). These authors suggest that the latter might be due to phospholipase A_2 sensing the hexagonal lattice of the DPPC molecules in the gel phase, or that the enzyme amplifies narrow polygonal defects that are already present in the bilayer.
Apparently, specific properties of PC cause these polygonal patterns in supported bilayers. PC is known to have a bulky headgroup with a larger cross sectional area than that occupied by two saturated acyl chains. In hydrated bilayers in the condensed phase, this causes packing constraints, resulting in tilted acyl chains (Hauser et al., 1981). We propose that supported DPPC monolayers exist of ordered domains with lipids in a tilted conformation. The direction of the tilt differs from one domain to another and on the borderlines between these domains, disordered line defects are formed which are beyond detection by AFM. From these weak line defects, DPPC molecules preferentially desorb upon passing through the second monolayer on the trough, resulting in a polygonal pattern of defects. In DPPC/DPPC (condensed) bilayers these defects are too narrow to detect, as in the case of DPPC/DPPG (condensed), except here, the elevations give away their presence. When the second leaflet consists of PG in the fluid phase, more lipids desorb from the substrate during deposition of the second leaflet, resulting in wider line defects, detectable by AFM.

2.4.2 The elevations

We found the most intriguing observation in this study, the presence of the elevations which appeared in most of our systems containing PG. Since these elevations are also observed on bilayers containing PS, but not on bilayers with zwitterionic phospholipids, we presume that they are anionic phospholipid specific. They formed circular structures surrounding the defects, but they also appeared as a polygonal mesh-like structure on the DPPC/DPPG bilayer. The height of most of the elevations on the PG leaflets varied between 1.5 and 3.5 nm, the meshlike elevations were somewhat higher, namely 2-6 nm. The former height suggests that the elevations may be formed by a phospholipid monolayer on top of the bilayer. However, the lipids in such a monolayer would have their tails exposed to either the aqueous phase or the headgroup phase of the underlying bilayer and both orientations are unstable. Also, the fact that the elevations disappear in the presence of divalent cations and that this process is reversible, makes it unlikely that the elevations are material, lying on the bilayer.
A possible explanation is that the elevations are artifacts caused by varying surface charge densities which are known to influence the distance between the negatively charged tip and the surface (Müller and Engel, 1997). Locally higher negative charge densities on a surface

would be registered by AFM as elevations, of which the height would decrease with increasing force applied by the tip. At higher ionic strength, surface charges are screened and thus the thickness of the electrical double layer around the charged surfaces is reduced, lowering the height of the charged surface, as observed by AFM (Müller and Engel, 1997). This could explain the reversible disappearance of the elevations in the presence of divalent cations. However, a higher negative charge density around the defects is impossible since the lipids around the defects cannot be more closely packed than in the bulk of the bilayer. Moreover, in the case of the high concentration of 300 mM NaCl, where the calculated electrical double layer thickness is lower than in the case of 100 mM NaCl with 3 mM $MgCl_2$ (Israelachvili, 1985; Verwey and Overbeek, 1948), the elevations are still visible. In conclusion, we regard it improbable that the nature of the elevations is a local higher negative charge density on the bilayer surface.

We propose that the elevations are induced by the lipid organization around the defects and that they are formed when the bilayer surrounding the defects is lifted up from the substrate, as illustrated in Fig. 2.4 *A*. We coin the term bilayer blistering for this novel type of bilayer morphology.

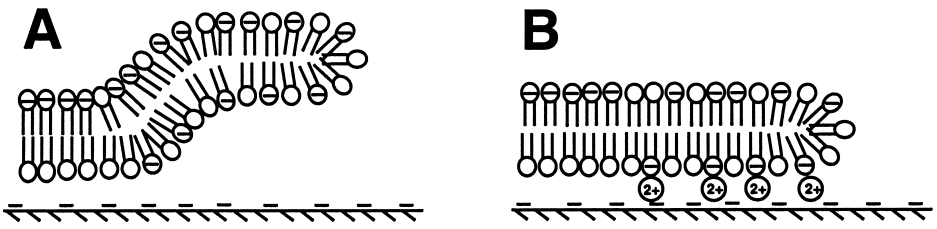

FIGURE 2.4 Possible molecular model of the elevations around the defects. (A) Due to electrostatic repulsion between the negatively charged substrate and anionic phospholipids, present in the first leaflet after lipid exchange, the bilayer edge is lifted up. (B) divalent cations screen the surface charges and act as a bridge between the substrate and the first leaflet, forcing the bilayer in a flat conformation.

According to the model of the lipids bordering the defects, the two leaflets of a bilayer are in contact via the convex curvature of the bilayer edge (see also Fig. 2.4). Normally, in sealed bilayers without defects, transbilayer movement occurs very slowly with halftimes in the order of days (De Kruijff and van Zoelen, 1978). However, in our system, the presence of a connection between the two leaflets at the edge of the defects, could locally allow lipid exchange between both leaflets. Due to this exchange, the first leaflet would contain some negatively charged lipids (PG or PS), around the defects. Since the substrate is negatively charged, repulsive forces between the first leaflet and the substrate would be present. As a

result of this electrical repulsion, the bilayer is lifted up around the defects (Fig. 2.4 *A*). In the presence of divalent cations, the edges lie flat on the substrate due to the screening effect of these ions and because a divalent cation might act as a bridge between a negative charge on the substrate and a negatively charged lipid (Fig. 2.4 *B*). The increased concentration of NaCl theoretically has a larger screening effect, but Na^+ ions cannot form bridges between two negative charges. Thus an increased Na^+ concentration merely results in a more hazy appearance of the elevations.Increasing the applied force during scanning, made it possible to reduce the height of the elevations to almost zero. In the light of the proposed model, the tip pushes, when the force is large enough, the elevated parts of the bilayer down to the surface of the substrate.

Our assumption that the elevations are caused by lipid exchange between the two leaflets, induced by the lipid organization around the defects, is supported by the observation that around tip-induced defects, also elevations were formed. Since lipid exchange is a dynamic process, the area of the first leaflet which contains phospholipids from the second leaflet should, according to our model, expand in time. Leaving a bilayer overnight showed that indeed the elevations spread in time.

If our proposed model holds true, the elevated parts of the bilayer would be repelled by, and therefore detached from the substrate, while in the presence of divalent cations the same parts would be attached to the support. To examine if this is the case, we prepared a DMPE/DPPG bilayer and left it for 24 hrs, yielding a bilayer that consisted almost completely of elevations around the defects (comparable to a DMPE/DMPG (condensed) bilayer (Fig. 2.2 *D*)). In the presence of Mg^{2+}, we isolated a triangular part of the bilayer from the main bilayer, by scratching three lines in the shape of the contours of a triangle (Fig. 2.5 *A*). This isolated part remained on the substrate in the presence of Mg^{2+}. However, after changing the buffer in the flow cell for Tris buffer without Mg^{2+}, the isolated triangle within the scratched lines had disappeared, as can be seen in Fig. 2.5 *B*. Also the isolated parts in the scratched lines and other defects (indicated with arrows) in Fig. 2.5 *A* have disappeared in Fig. 2.5 *B*. This means that the parts of the bilayer that consist of elevations are indeed detached from the support, and that divalent cations can attach these parts on the substrate.

A layer of paint can detach from the surface on which it is applied. This is called blistering and can be prevented by pre-treating the surface with a primer which is designed to improve the attachment of paint. From this point of view, an anionic phospholipid containing bilayer can also blister and in this case, divalent cations are acting as a primer. We introduce the phenomenon that the bilayer is locally detached and lifted up from the substrate, as bilayer blistering. This bilayer blistering, as we observed by AFM, offers interesting and new possibilities for analysis of lipid-protein interactions.

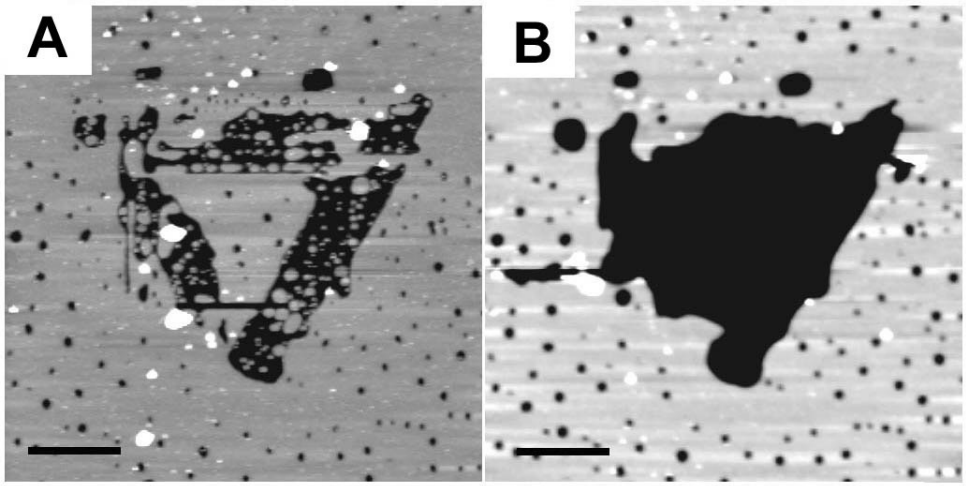

FIGURE 2.5 Isolation of an elevated part of the bilayer from the main bilayer. A DMPE/DPPG bilayer was left overnight (under 10 mM Tris, 100 mM NaCl, pH 7.4) until it consisted largely of elevations. (A) In this bilayer, after the buffer was replaced by 10 mM Tris, 100 mM NaCl, 3 mM $MgCl_2$, pH 7.4, three line defects, contouring a triangle were scratched with the AFM-tip. (B) In the absence of Mg^{2+}, the isolated part of the bilayer has disappeared. Both images are 7x7 mm, scale bars 1.4 mm, z-scales 10 nm.

2.5 CONCLUSIONS

In this paper we present AFM images of supported asymmetric bilayers, with a second leaflet consisting of anionic phospholipids (PG). Such systems are of potential interest with respect to studies of membrane associated proteins. Our results reveal that in our systems with a second leaflet of PG, defects in the form of holes are present. The shape of the defects is influenced primarily by the first leaflet: DPPC as a first leaflet gives rise to polygonal, line-shaped defects while DMPE tends form round defects. In the case of DPPC/DPPG and DPPC/DMPG (condensed) and DMPE/PG bilayers, elevations were observed, which disappeared reversibly in the presence of divalent cations. In order to explain the origin of these elevations and their behavior, we have described a model of the lipidic phase, bordering the defects. We propose that, after lipid exchange between the first and the second leaflet, the bilayer edges are lifted up due to repulsive forces between the negatively charged substrate and negatively charged lipids that would be present in the first leaflet, due to the lipid exchange. It was found that the elevations are indeed detached from the surface, which led us to call their formation bilayer blistering.

CHAPTER 3

Visualization of highly ordered striated domains induced by transmembrane peptides in supported phosphatidylcholine bilayers

(Biochemistry, 2000, 39:5852-5858)

ABSTRACT

We used Atomic Force Microscopy (AFM) to study the lateral organization of transmembrane WALP peptides incorporated in phospholipid bilayers. These well-studied model peptides consist of a hydrophobic alanine-leucine stretch of variable length, flanked on each side by two tryptophans. They were incorporated in saturated phosphatidylcholine (PC) vesicles, which were deposited on a solid substrate via the vesicle fusion method, yielding hydrated gel-state supported bilayers. At low concentrations (1 mol%) WALP peptides induced primarily line-type depressions in the bilayer. In addition, striated lateral domains were observed, which increased in amount and size (from 25 nm up to 10 μm) upon increasing peptide concentration. At high peptide concentration (10 mol%), the bilayer consisted mainly of striated domains. The striated domains consist of line-type depressions and elevations with a repeat distance of 8 nm, which form an extremely ordered, predominantly hexagonal pattern. Overall, this pattern was independent of the length of the peptides (19-27 amino acids) and the length of the lipid acyl chains (16-18 carbon atoms). The striated domains could be pushed down reversibly by the AFM tip and were found to be thermodynamically stable. This is the first direct visualization of α-helical transmembrane peptide-lipid domains in a bilayer. We propose that these striated domains consist of arrays of WALP peptides and fluid-like PC molecules, which appear as low lines. The presence of the peptides perturbs the bilayer organization, resulting in a decrease in the tilt of the lipids in between the peptide arrays. These lipids therefore appear as high lines.

3.1 INTRODUCTION

Lateral segregation of proteins and lipids in biological membranes is commonly assumed to give rise to biologically differentiated regions (Welti and Glaser, 1994; Mouritsen and Bloom, 1984; Vaz, 1994; Simons and Ikonen, 1997). Segregation processes would lead to the formation of domains and the length scales of these domains may be as small as 10-100 nm, which is difficult to detect with most experimental techniques (Mouritsen and Biltonen, 1993).
Fluorescence microscopy studies have already demonstrated the existence of lipid domains in cell membranes (Haverstick and Glaser, 1987). However, the resolution of this technique is relatively low and the presence of probes is required. The resolution of Electron Microscopy is much higher, and lateral phase separation yielding micro-domains has been observed in biomembranes and model membranes with freeze-fracturing techniques (Verkleij, 1989; Luna and McConnel, 1978). A drawback of this technique is that it demands quenching of the sample, which could lead to structural reorganization. Computer simulations can visualize the distribution of individual molecules in model bilayers (Mouritsen and Biltonen, 1993; Gil et al., 1998). Monte Carlo simulations have suggested that proteins can induce lipid sorting in binary lipid bilayers (Sperotto and Mouritsen, 1993; Dumas et al., 1997) and that lipids in turn, can cause clustering of proteins (Sperotto and Mouritsen, 1991; Sabra et al., 1998).
Atomic Force Microscopy (AFM) (Binnig et al., 1986) offers the possibility to directly image phospholipid bilayers on a solid support, under aqueous conditions (Tamm and Shao, 1998; Yang et al., 1993) while the resolution (0.5-1 nm) (Engel et al., 1997) is sufficient to directly visualize domains of mesoscopic size. Indeed, domains have been observed by AFM. In dipalmitoylphosphatidylcholine (DPPC) monolayers, intermixed liquid expanded and liquid crystalline lipid domains as small as 500 nm have been imaged (Hollars and Dunn, 1998). Also interdigitated domains, induced by alcohol (Mou et al., 1994) or heat (Fang and Yang, 1997) have been visualized in DPPC bilayers. From AFM images of binary mixtures of dipalmitoylphosphatidylethanolamine and the cholera toxin receptor ganglioside, it was concluded that such bilayers phase-separate, forming small domains (Yang et al., 1993). Also, protein aggregation in lipid monolayers (Amrein et al., 1997) has been observed. Amphipathic peptides were found to induce round domains and filaments in fluid phosphatidylcholine (PC) monolayers (Van Mau et al., 1999) and interdigitated domains in DPPC bilayers (Janshoff et al., 1999). In a thorough AFM study, Mou et al (Mou et al., 1996) have reported on the aggregation behavior of Gramicidin A (GA), which is known to span bilayers as a β-helical dimer. They were able to visualize line-type GA aggregates in supported gel-state PC bilayers, and these aggregates clustered together in ordered domains. These findings prove that AFM is indeed a powerful tool to study lateral segregation in

bilayers. Although the hydrophobic transmembrane domains of integral membrane proteins, interacting with the hydrophobic core of the surrounding lipid membrane, usually consist of α-helices, none of the above mentioned AFM studies concern proteins with an α-helical transmembrane domain.

In order to systematically study the interactions of such α-helices with the surrounding lipid membrane, synthetic transmembrane model peptides are commonly used (Killian, 1998). An example of such peptides are the WALP peptides (Killian et al., 1996), which consist of an alternating alanine-leucine stretch of variable length and form an hydrophobic α-helix. The peptides are flanked on both ends by two tryptophans. These residues are often found in membrane spanning proteins at the hydrophobic-hydrophilic interface of the bilayer (Reithmeier, 1995). WALP peptides have mainly been used to study the effect of mismatch between the hydrophobic transmembrane regions of integral membrane proteins and the hydrophobic core of the lipid bilayer. Such hydrophobic mismatch is thought to have an important effect on lateral segregation in membranes (Mouritsen and Bloom, 1984), on membrane protein activity and stability and on protein sorting (Killian, 1998; Dumas et al., 1999). It has been found that WALP peptides can induce the formation of the H_{II} phase in fluid PC bilayers (Killian et al., 1996) and alter the thickness of fluid PC bilayers (de Planque et al., 1998).

The aim of our study is to visualize possible lateral segregation of these α-helical, transmembrane model peptides in phospholipid bilayers. WALP peptides give us the opportunity to systematically vary the length of the peptides and to investigate possible effects of mismatch on the aggregation behavior of these peptides in gel-state bilayers. We found that WALP peptides in supported PC bilayers segregate in highly ordered striated domains and that they have a distinct influence on the organization of the surrounding lipids.

3.2 MATERIALS AND METHODS

3.2.1 Materials

1,2–Dipalmitoyl-*sn*-glycero-3-phosphocholine (DPPC) and 1,2–distearoyl-*sn*-glycero-3-phosphocholine (DSPC) were purchased from Avanti Polar Lipids (Alabaster, AL) and used without any further purification. WALP peptides consist of a hydrophobic alanine-leucine stretch of variable length flanked by tryptophans. To avoid complications due to electrostatics, the N-terminus and C-terminus are blocked with an acetyl group and an ethanolamine group respectively. Table 3.1 shows the amino acid sequences and the lengths of the different WALP peptides we used. All WALP peptides were synthesized essentially as

described (Killian et al., 1996) and were a kind gift of drs. Roger E. Koepe II and Denise V. Greathouse.
2,2,2-Trifluoroethanol (TFE) was from Sigma (St. Louis, MO). For all experiments MilliQ water was used.

Table 3.1 Amino acid sequences of the WALP peptides and their estimated total length, when present as an α-helix.

Peptide	Amino acid sequence	Total length [a] (nm)
WALP16	Ac-GWW(LA)$_5$WWA-NHCH$_2$CH$_2$OH	2.5
WALP19	Ac-GWWL(AL)$_6$WWA-NHCH$_2$CH$_2$OH	3.0
WALP23	Ac-GWWL(AL)$_8$WWA-NHCH$_2$CH$_2$OH	3.6
WALP27	Ac-GWWL(AL)$_{10}$WWA-NHCH$_2$CH$_2$OH	4.2

[a]*Assuming each amino acid has a length of 0.15 nm, with the C-terminal ethanolamine included as the length of one amino acid (Killian et al., 1996).*

3.2.2 Vesicle preparation

The peptides were dissolved in TFE and added to DPPC or DSPC dissolved in a mixture of chloroform and methanol (3:1; v/v). The obtained peptide/lipid mixtures contained 1, 2, 5 or 10 mol% peptide. These mixtures were dried in a rotary evaporator followed by overnight storage under high vacuum. To the dried mixed films, 1.25 ml of a 20 mM NaCl solution was added, resulting in a lipid concentration of 0.62 mM. After ten cycles of freeze-thawing, small unilamellar vesicles were made by sonicating the suspension in a bath sonicator (Branson, Danburry, Connecticut) at maximum power for at least 30 minutes, at 50°C (in the case of DPPC), or 65°C (in the case of DSPC). Possible remaining large vesicles were spun down at 20800 g for 1 hr, at 4°C. The resulting vesicle suspensions had a pH of 6, and were used within 10 days after preparation.

3.2.3 Preparation of supported bilayers

75 µl of vesicle suspension was applied onto freshly cleaved mica (∅ 10 mm), glued on a steel disc coated around the mica with hydrophobic silicone sealant (Sigma coatings, Uithoorn, Holland). The vesicles were allowed to adsorb to the mica for at least 10 hrs at 4°C, as described (Mou et al., 1996). After rinsing the sample with 5-10 times 75 µl of 20 mM NaCl, the sample was heated above the main transition temperature of the lipids present (to 60°C

for DPPC and 70°C for DSPC) for 45 min. Afterwards, the sample was left to cool down to room temperature at ambient conditions, which usually took less than 15 min, and rinsed again with 5-10 times 75 µl of 20 mM NaCl. In this way bilayers were obtained, usually containing defects and with some unopened vesicles on top. Occasionally, the bilayers were partly covered by a second bilayer, which, when imaged by AFM, appeared hazy and contaminated. The images presented in the results section are of the first bilayer. Care was taken that the samples remained hydrated. In order to investigate the thermodynamic stability of the bilayers, some samples of 2 mol% WALP23 in DPPC were, after they had been heated, either cooled down very quickly by immediately applying cold solution (4°C), or were left to cool down very slowly, at a rate of 10°C per hour. Unless stated otherwise, all samples were scanned a few hours after preparation.

3.2.4 AFM measurements

The sample was mounted on an E-scanner, which was calibrated on a standard grid, of a Nanoscope III (Digital Instruments, Santa Barbara, CA). A quartz flow cell was used without the O-ring. All samples were scanned with oxide-sharpened tips with a spring constant of 0.06 N/m, as estimated by the manufacturer (Digital Instruments, Santa Barbara, CA). Scans were recorded at a minimal force where the image was stable and clear, which was usually smaller than 500 pN, and with a scan speed of 6 lines/s. To investigate the compressibility of the samples, in some cases the scanning force was increased up to 1500 pN.
The AFM software was used to measure distances within an image and to perform Fourier Transformations. All images shown in this paper, except for Fig. 3.2 *B*, are flattened raw data.

3.3 RESULTS

3.3.1 WALP23 in DPPC

Pure DPPC (Fig. 3.1 *A*) bilayers have a smooth appearance with a few defects, in agreement with previous studies (Tamm and Shao, 1998; Mou et al., 1996). Occasionally shallow cracks can be seen in the bilayer surface, with a depth of less than 0.1 nm. Fig. 3.1 *B* depicts a bilayer of DPPC with 1 mol% WALP23 incorporated. Distinct line-type depressions appear which are flanked by slightly higher areas and, occasionally, small point-like depressions are present. Also small striated domains can be seen, usually where more than two line-type depressions meet. These domains consist of low (dark) and high (light) lines. Increasing the concentration of WALP23 to 2 mol% (Fig. 3.1 *C*), resulted in again point-like and line-type depressions, and in larger striated domains in which the lines curve at defined angles.

Upon incorporation of 5 mol% WALP23 (Fig. 3.1 *D*), even larger striated domains are formed in which small defects are present.

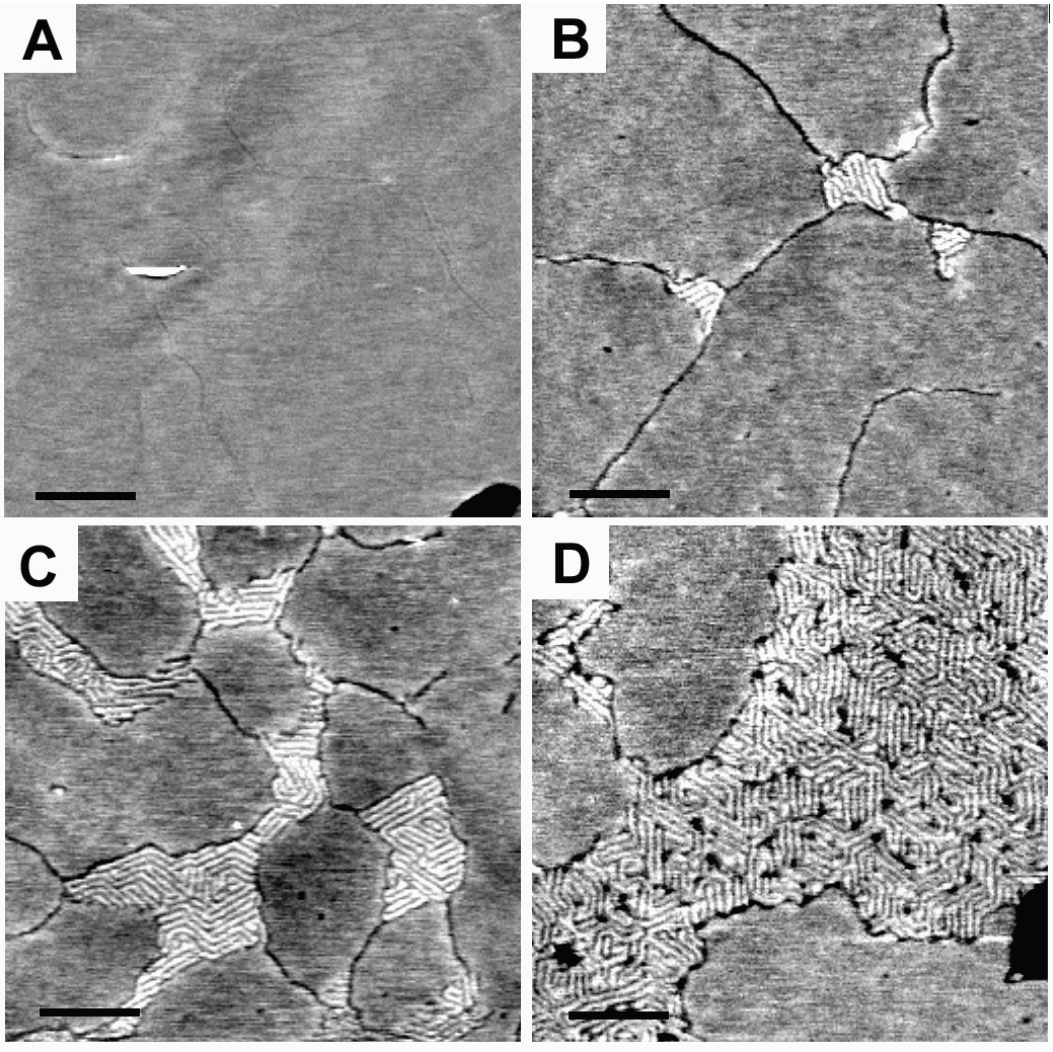

FIGURE 3.1 Formation of striated domains induced by WALP23 in DPPC bilayers. AFM images of (A) a pure DPPC gel-state bilayer, image size 1x1mm, scale bar 200 nm, (B) a bilayer of DPPC with 1 mol% WALP23 incorporated, (C) a bilayer of DPPC with 2 mol% WALP23 incorporated and (D) a bilayer of DPPC with 5 mol% WALP23. Image sizes of B-D are 500x500 nm, scale bars 100 nm.

Bilayers of DPPC with 10 mol% WALP23 incorporated, consisted almost completely of striated domains, which sometimes occupied areas as large as 100 μm^2. Fig. 3.2 *A* depicts an image at larger magnification of such a domain which clearly shows that in the striated domains the lines curve in angles of 120°, showing a three-fold symmetry. The Fourier Transformation of this domain is shown in Fig. 3.2 *B*. This power spectrum displays a hexagonal pattern, consistent with the angles of 120°, found in the original pattern. Fourier Transformations of large striated domains formed at 2 or 5 mol% gave the same results. The average repeat distance, as deduced from power spectra of the striated domains, and as determined directly from the images was found to be 7.5±0.4 nm (n=27).
The width and the depth of the isolated line-type depressions in WALP23 containing DPPC bilayers, were about 9 nm and 0.3 nm respectively, and the height of the higher areas along these depressions varied between 0.1 and 0.3 nm, taking the bilayer surface as the zero level.

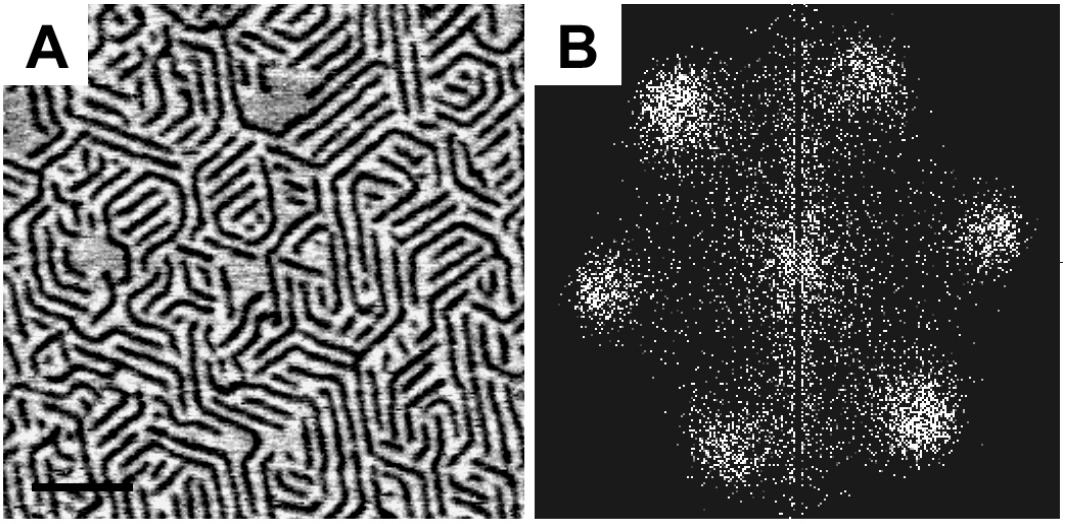

FIGURE 3.2 (A) AFM image at high magnification of a striated domain, formed in a bilayer of DPPC with 10 mol% WALP23. Image size 250x250 nm and scale bar 50 nm. (B) Power spectrum made of this domain, from which it is deduced that the average angle between the lines in the domains is 60°, and their average distance is 7.5 nm.

3.3.2 Other WALPs and lipids

To investigate the importance of the length of the peptide and lipid acyl chains for domain formation, bilayers of DPPC (C_{16}) with WALP16, WALP19 and WALP27 and of DSPC (C_{18}) with WALP23 were imaged. In all DPPC bilayers with WALP incorporated, point-like and

line-type depressions appear, the latter with a width and a depth of about 9 nm and 0.3 nm respectively, flanked by higher areas, varying between 0.1 and 0.3 nm (taking the bilayer surface as the zero level). Also in these systems striated domains are observed.

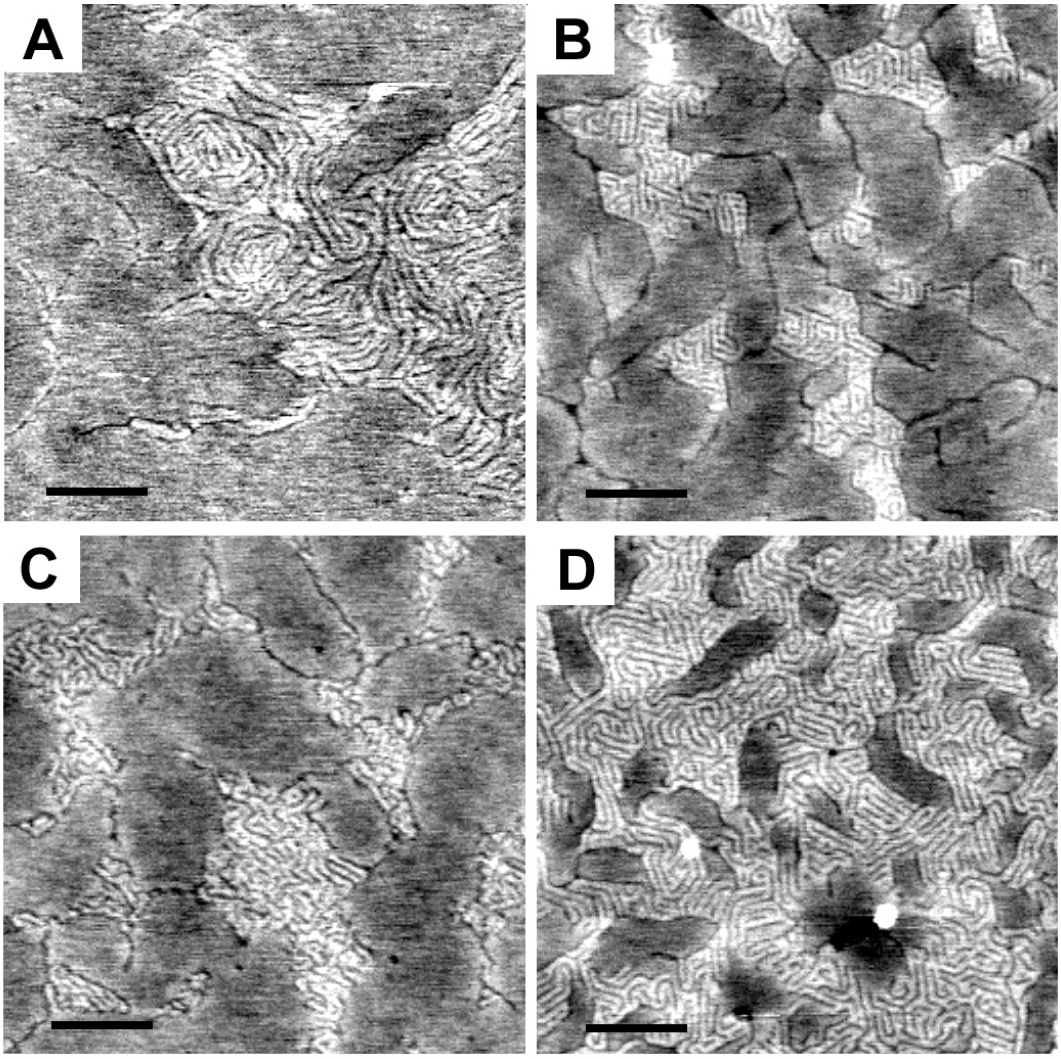

FIGURE 3.3 Domains induced by WALP peptides of varying lengths, in PC bilayers. (A) WALP16 (2 mol%) in DPPC, image size 1x1 mm, scale bar 200 nm. (B) WALP19 (2 mol%) in DPPC. (C) WALP27 (5 mol%) in DPPC. (D) WALP23 (5 mol%) in DSPC. Image sizes of B-D are 500x500 nm, scale bars 100 nm.

In the case of WALP16 incorporated in DPPC bilayers, the amount of line-type depressions increased with increasing peptide concentration. Often, but not always, striated domains could be seen. Fig. 3.3 *A* shows an example of such a domain formed in a bilayer of DPPC with 2 mol% WALP16 (note that the scale is larger compared to the WALP19, 23 and 27 images). These domains also consist of low lines separated by higher areas, but the distance between the line-type depressions is larger (23 nm±4 nm (n=26)) as compared to the repeat distance of the lines in the striated domains formed in bilayers containing WALP23. Also, the period is not as well defined as in the case of WALP23 in DPPC and the lines do not usually curve at specific angles.

When incorporating WALP19 or WALP27 in DPPC bilayers, striated domains were present of which the amount and size increased with increasing peptide concentration. Fig. 3.3 *B* shows an image of striated domains formed in a DPPC bilayer with WALP19 (2 mol%) incorporated. The period of the lines in such patterns is 8.2±0.5 nm (n=9), as measured directly from the images. The pattern of these striated domains has the same appearance as the pattern of the striated domains induced by WALP23, albeit that the lines look somewhat straighter and the curves sharper. When WALP27 was incorporated, striated domains were formed as depicted in Fig. 3.3 *C* (5 mol% WALP27 in DPPC). The period, as measured directly from the images, was 7.9±0.9 nm (n=10). The pattern differs merely slightly from the pattern of the striated domains in the bilayers containing WALP23, in that the lines seem less straight and curve at less defined angles. Also, for both WALP19 and WALP27, it was more difficult to obtain sharp images of the striated domains, hence we were not able to reliably determine the angle and period from Fourier Transformations.

The use of DSPC, with saturated acyl chains of 18 carbon atoms long, instead of DPPC, with saturated acyl chains of 16 carbon atoms, did not distinctly influence the pattern of the striated domains either. This can be seen in Fig. 3.3 *D* which shows striated domains in a bilayer of DSPC with 5 mol% WALP23 incorporated. The period of the lines in the pattern was found to be 8.1±0.7 nm (n=7).

The thickness of the bilayers was determined using the largest defects already present in the bilayer (Janshoff et al., 1999). The thickness of the DPPC bilayer outside the striated domains was 5.8-5.9 nm, independent of the length of the incorporated peptide. The bilayer thickness as measured by AFM is larger than the DPPC bilayer thickness given in Table 3.2, because presumably there is a layer of 1-2 nm of water between the supported bilayer and the substrate (Tamm and Shao, 1998).

Table 3.2 Total bilayer thickness and hydrophobic bilayer thickness of DPPC and DSPC in the gel and fluid phase, in excess water.

Lipid	Bilayer thickness (nm)	Hydrophobic bilayer thickness (nm)
DPPC (gel)	4.7 [a]	3.6 [b]
DPPC (fluid)	3.7 [c]	2.6 [c]
DSPC (gel)	4.7 [a]	3.6 [b]
DSPC (fluid)	4.1 [c]	3.0 [c]

[a]*Values for the total bilayer thickness of PC in the gel phase are adopted from Marsh (1990). The tilt angle of the acyl chains in a DPPC gel-state bilayer is 33°, and in a DSPC gel-state bilayer 40°.*

[b]*Value for the hydrophobic bilayer thickness of DPPC in the gel phase is adopted from Dumas et al. (1999), and for DSPC (following Dumas et al. (1999)), 1.1 nm is subtracted from the total measured length.*

[c]*Values for the total and hydrophobic bilayer thickness of PC in the fluid phase are adopted from Lewis and Engelman (1983).*

Imaging fluid bilayers with peptides incorporated, yielded images without contrast, which is in agreement with the findings of Mou et al. (1996). This could be attributed to the high compressibility of the fluid bilayers (Mou et al., 1996) or to the rapid movement of the molecules present in such systems.

3.3.3 Examining the striated domains

The height of the striated domains was depending on the force applied by the tip. When during scanning the force was low (<500 pN), the height of the striated domains varied between 0.2 and 0.4 nm, taking the bilayer surface as the zero level. This was found for WALP19, 23 and 27 in DPPC and for WALP23 in DSPC. Upon increasing the force, the striated domains could be pushed down. Fig. 3.4 *A* shows an example of striated domains in a system of WALP23 in DPPC, imaged at low force (<500 pN). When the scanning force was increased to 1500 pN, the striated domains appear below the surface of the bilayer (Fig. 3.4 *B*). When afterward the force was decreased again, the height and the pattern of the striated domains reappeared (Fig. 3.4 *C*). Note that also the higher areas along the line-type depressions disappear at higher force (Fig. 3.4 *B*) and reappear at low force (Fig. 3.4 *C*).

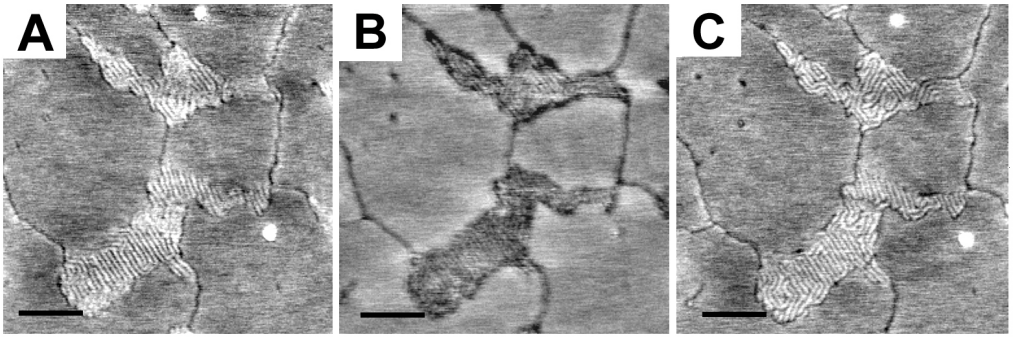

FIGURE 3.4 Striated domains (2mol% WALP23 in DPPC) imaged at different forces. (A) At low force (<500 pN), the domains appear higher than the surrounding bilayer. (B) Upon increasing the force to 1500 pN, the domains are pushed down. (C) At low force (<500 pN), the domains appear high again. Scale bars 100 nm.

To determine whether the striated domains are thermodynamically stable, some samples of 2 mol% WALP23 in DPPC were, after they had been heated to 60°C, cooled down quickly and some were left to cool down slowly. In the systems which had been cooled down quickly, domains were present (data not shown) with the same pattern as presented above (Fig. 3.1 *C*), although on the whole, the striated domains seemed somewhat smaller in the quenched sample. In the samples which were cooled down slowly (10°C per hour), again striated domains could be seen (data not shown) with the same pattern as the systems with WALP23, cooled down at ambient conditions. However, the domains seemed larger and had the appearance of the striated domains in 5 mol% WALP23 in DPPC (Fig. 3.1 *D*). Some samples of 2 mol% WALP23 in DPPC were imaged after they had cooled down at ambient conditions and subsequently had been left at room temperature for 2 days. The pattern of the domains in these systems was again the same (data not shown) as in the bilayers imaged within a few hours after cooling down.
These results indicate that the striated domains are flexible and thermodynamically stable.

3.4 DISCUSSION

3.4.1 Formation of line-type depressions

In the systems we studied with WALP peptides at low concentrations, mainly line-type depressions were observed (Fig. 3.1 *B*). All WALP peptides have a smaller length than the bilayer thickness of DPPC and DSPC in the gel phase (see Table 3.2). Moreover, tryptophans are known to preferentially locate at the interface of the lipid headgroups and acyl chains (De

Planque et al., 1999), which would keep the peptides below the surface of the bilayer. Hence we assume that in the line-type depressions, peptides are residing. The measured depth of the line-type depressions in the bilayers with WALP peptides of different length does not differ much from one WALP peptide to another (all about 0.3 nm). We suspect this to be due to the fact that the lines (measured width ± 9 nm) are too narrow for the tip (radius ± 10 nm) to reach "the bottom" of the depressions, and that therefore differences in depth due to differences in peptide length could not be detected.

We suggest the following explanation for the formation of the line-type depressions.

In pure DPPC bilayers, sometimes shallow line-type depressions or cracks can be seen in the surface (Fig. 3.1 *A*). We believe that these cracks are borders between different domains in the gel-state bilayers. In DPPC layers in the gel state, the lipid acyl chains are tilted at a 33° angle (Marsh, 1990) and are short range, hexagonally ordered. When the fluid bilayer is cooled down during the preparation (from above- to below the phase transition temperature), the lipids will start to solidify at different sites within the bilayer, leading to the formation of different domains. Within each domain the lipid acyl chains are tilted in the same direction, which might be different from the direction of the lipids in the neighboring domain. This would lead to disordered boundaries. We have discussed this principle for a DPPC monolayer in a previous study (Rinia et al., 1999).

When peptides are present in a solidifying PC bilayer, they might not be incorporated in the ordered lipid domains but rather be "squeezed out" of those domains, so that they end up in the disordered boundaries (this mechanism is comparable to surface enrichments of contaminations in a crystal). This would explain the line-type depressions in the PC bilayers with 1 or 2 mol% peptide incorporated, as shown in Fig. 3.1 *B*, *C* and Fig. 3.3 *A*-*C*.

Unlike in pure DPPC bilayers (Fig. 3.1 *A*), sometimes isolated small point-like depressions can be seen in the gel-state domains in the mixed bilayers (Figs. 3.1 *B*-*C* and 3.3 *C* and 3.4), wherein possibly also peptides are residing. It could be that not all the peptide is excluded from the DPPC gel-state domains into the line-type depressions, and that some peptide is present as small point-like aggregates in the bilayer.

The measured width of the line-type depressions is 9 nm, but due to the tip convolution the real width is probably even larger. This is larger than the diameter of an α-helix, which is estimated to be 1 nm (Reithmeier, 1995). Proteins and peptides are known to be able to change the state of the neighboring (annular) lipids from gel to more fluid-like (Sperotto and Mouritsen, 1991; Bloom and Smith, 1985). These fluid-like annular phospholipids would also appear lower than phospholipids in the gel state. Hence we expect that the line-type depressions consist of arrays of peptides (possibly more than one peptide wide), which are bordered by fluid-like, disordered PC lipids.

The line-type depressions are flanked by slightly higher areas (0.1-0.3 nm) (Fig. 3.1 *B*, *C*, 3.3 *A-C* and 3.4 *A*, *C*). These higher areas appeared usually along every line-type defect we observed, especially at low force. Theoretical studies have predicted a possible local larger bilayer thickness around inclusions, like proteins and peptides (Nielsen et al., 1998; Dan and Safran, 1998), even in case of hydrophobic matching (Dan and Safran, 1998). We speculate that these elevations are a result of packing constraints in the bilayer, caused by the presence of the peptides (see also below).

3.4.2 Formation and composition of the striated domains

We suggest that when there is more peptide present than can be accommodated in the boundaries, striated domains are formed, often at the intersection of three or more lines (Figs. 3.1 *B*, *C* and 3.3 *B*, *C*). It could be that the disordered boundaries serve as channels along which the peptides are transported to the growing striated domain, during solidification of the mixed bilayer.

The height difference between the striated domains and the bulk bilayer is too small for the Nanoscope software to quantify the percentage of area occupied by striated domains. However, from the images of the bilayers with 10 mol% WALP23, it is easy to see by eye that these bilayers consist almost completely of striated domains. In the striated domains themselves (Fig. 3.2), half of the area is low (dark lines) and the other half is high (white lines). This means that almost 50% of the area in the bilayers with 10 mol% WALP23 consists of low lines. Assuming one PC headgroup occupies 0.5 nm^2 (Marsh, 1990) and one α-helix 0.8 nm^2 (diameter is 1 nm, (Reithmeier, 1995)), in a DPPC bilayer containing 10 mol% WALP23, only 25% of the area would be occupied by protein. From this it follows that the area taken up by the low lines in the domains, cannot consist completely of peptide, simply because there is not enough peptide present. This implies, analogous to the isolated line-type depressions, the presence of phospholipids in a more fluid-like phase, which would also appear below the level of the gel-state bilayer.

We propose that the organization of the lipids and the peptides in the striated domains is comparable to the organization in the line-type depressions. The domains exist of arrays of peptide, flanked by phospholipids in a fluid-like state, observed as low lines. The width of these low lines in the domains is extremely constant, suggesting that the peptide lines consist of arrays of constant peptide units: either monomers or oligomers. Since the formation of WALP-oligomers is unlikely (De Planque et al., 1998) we think that the low lines in the striated domains consist of arrays of peptide monomers, flanked by fluid-like lipids.

In the striated domains the bilayer is perturbed by the presence of inclusions in the form of peptide arrays. These inclusions make it impossible for the surrounding lipids to pack in a

tilted conformation, as they prefer at gel-state temperature. Since these lipids appear in our AFM images as elevated lines, we assume that they are present with a decreased or no tilt.
Fig. 3.5 depicts a possible model of the molecular organization in the striated domains (on the right) and the neighboring gel-state bilayer (on the left). In the lipid phase between the peptide arrays, the lipids are more disordered, and thus have a higher compressibility compared to the lipids in the gel-state bilayer. This would explain the fact that the striated domains can be pushed down (reversibly) below the level of the bulk bilayer (Fig. 3.4).

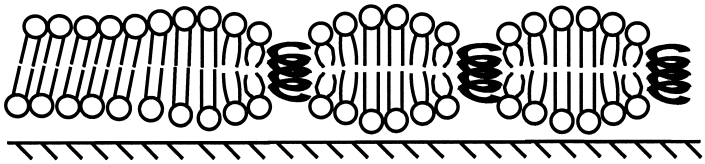

FIGURE 3.5 Proposed model for the molecular organization in the striated domains. The tilted packing of saturated PC in the gel phase (left) is disturbed by the presence of the peptides, depicted as coiled springs. This results in disorder and in a decrease in tilt of the lipids in between the peptide arrays, hence they appear higher, and have a higher compressibility than the bulk gel-state bilayer.

3.4.3 The pattern of the striated domains

We have compared the striking pattern of the domains with resembling patterns described in the literature, in order to gain more insight in why the lipids and peptides would form such ordered stripes.
Binary systems undergoing spinodal decomposition (Cahn, 1968), also form a pattern of alternating lines. Such systems are thermodynamically unstable. It could be that in the striated domains the lipids and peptides are on their way to phase separation. During this process the width of the lines would continuously increase. However, because the domains still exhibit the same pattern after two days (data not shown), and the bilayers which were cooled down very slowly (10°C per hour) exhibited striated domains with the same periodicity (data not shown), we regard it unlikely that the pattern we see in the striated domains originates from a mixture of peptides and lipids undergoing spinodal decomposition.
Seul and Andelman (1995) give an analysis of domain shapes and striped (or bubbled) patterns, referred to as modulated phases. These patterns occur in various thermodynamically stable systems, and are the result of a compromise between competing interactions in these systems. From their overview (Seul and Andelman, 1995) it follows that striated patterns induced in membranes, vesicles and bilayers find their origin in curvature and molecular tilt, but this applies to pure phospholipid systems. The period of the described

systems can be tuned by varying involved parameters, like temperature, concentration and the length of the phospholipid tails. For example, the period of ripples in phospholipid systems in the P_{β}' phase is determined by the acyl chain length of the lipids present. In our case, the period remains constant when the length of the lipid acyl chains or peptides is varied (except for WALP16). So, even though the morphology of the ripple phase resembles the pattern of the striated domains in the three-fold symmetry of the ripples and lines, we exclude the possibility that the striated domains we observe are bilayer areas in the P_{β}' phase.

Recently it was found by Vlot and van der Eerden (1998), using Monte Carlo computer simulations, that in binary systems of enantiomers, striated phases were formed when steric hindrance was introduced, denoted as spaghetti solid or spaghetti liquid. When the optimum distance, or, steric hindrance between the two components increased, the system became more liquid, being expressed as lines which are more curved, while the width of the lines remained the same. Thus, geometrical factors influenced only the line stiffness. WALP19, 23 and 27 are estimated to be longer than the hydrophobic thickness of fluid DPPC (Table 3.1 and 3.2), so when the peptide length increases from 19 to 27 amino acids, the hydrophobic mismatch between the peptides and their supposedly neighboring phospholipids would also increase. Also, going from WALP19 to WALP27, the lines in the striated domains get less straight and the angles at which the lines curve get less sharp (Fig. 3.3 *B*, *C*). Analogous to the spaghetti phases, an increase in mismatch may decrease the line stiffness, while the width of the lines remains constant. However, in our systems also specific interactions, like the preference of tryptophans to anchor at the headgroup-tail interface of the bilayer, could be involved in the striated pattern formation. Therefore the spaghetti phase should not be considered as an accurate model for our system, but merely as an indication that geometrical factors could be involved in the pattern formation.

The results we obtained in this study have some striking similarities with the study of Mou et al. (1996) on Gramicidin (GA) in saturated PC bilayers. GA is a β-helical peptide, which spans the bilayer as a dimer. Also this hydrophobic peptide induces line-type depressions in gel-state PC bilayers, and at higher concentration (2 mol%) domains are observed. Along the line-type depressions higher areas appear and the domains are higher than the surrounding bilayer. The pattern of the domains observed in the presence of GA consists of point-like depressions surrounded by percolating line-type depressions. As in our systems, the line-type depressions in the domains tend to curve at angles of 120°. It was suggested that this is reflecting the arrangement of the peptide in the depressions, which is thought to be as hexamers (Mou et al., 1996; Spisni et al., 1983). However, there are no indications that the WALP peptides used in the current study would form hexamers, and yet, defined angles of 120° are observed. Since in these two studies different peptides (GA and WALPs) are used,

we deduce that the observed hexagonality is either directed by the lipids, or by general geometrical packing properties of the system.
Also notable is that the distance between the line-type depressions within the domains induced by both peptides is similar (for WALP19-27 ± 4 nm and for GA 4.6 nm). It may seem counterintuitive that the length scale of the bilayer deformations is independent of the chemistry and the geometry of the inclusions. However, according to a theoretical study of Nielsen et al. (1998), it is the rigidity of the bilayer that largely influences this length scale.
From the above, we conclude that most likely general geometrical factors of both lipids and peptides, and elastic properties of the lipid bilayer are involved in the formation of the striated domain pattern.
Computer simulations of peptides or proteins in lipid bilayers usually show the formation of clusters or aggregates of the proteins (Gil et al., 1998; Sperotto and Mouritsen, 1991). The peptides or proteins may be ordered within the aggregate, forming 2-D crystals (Sabra et al., 1998) however, to our knowledge, line-type aggregates, forming an ordered pattern within the lipid phase have never been observed, also not in simulations concerning proteins in gel-state bilayers (Sperotto and Mouritsen, 1991). AFM images as presented in this study provide small-scale experimental pictures, potentially guiding theoreticians doing computational studies on peptide-lipid aggregation.

3.5 CONCLUSIONS

We have found that transmembrane α-helical peptides in gel-state DPPC bilayers form line-type aggregates, and that these aggregates cluster together in striated domains, which in most cases are unexpectedly, highly ordered. This ability to form highly ordered structures might have implications for the organization in biological membranes. In future work, we will investigate the role of the tryptophans in the formation of the domains, by varying the flanking residues.

CHAPTER 4

Domain formation in phosphatidylcholine bilayers containing transmembrane peptides: Specific effects of anchoring residues.

(Biophysical Journal, submitted)

ABSTRACT

Lateral segregation in biomembranes would lead to the formation of domains, which are thought to be biologically functional. We have studied the lateral segregation of various model peptides in supported dipalmitoylphosphatidylcholine (DPPC) bilayers, using Atomic Force Microscopy. The model peptides are derivatives of the Ac-GWWL(AL)$_n$WWA-Etn peptides (the so-called WALP peptides) and have instead of tryptophans, other flanking residues. In a previous study we found that WALP peptides induce the formation of extremely ordered, striated domains in supported DPPC bilayers. In this study we show that WALP analogs with other uncharged residues (tyrosine, phenylalanine or histidine at pH 9) can also induce the formation of striated domains, albeit in some cases with a slightly different pattern. The WALP analogs with positively charged residues (lysine or histidine at low pH) cannot induce striated domains and give rise to a completely different morphology: they induce irregularly shaped depressions in DPPC bilayers. It is concluded that the positively charged peptides repel each other and hence cannot form striated domains in which they would have to be in close vicinity. They reside in disordered, fluid-like lipid domains, which appear below the level of the ordered gel-state lipid domains, accounting for the irregularly shaped depressions.

4.1 INTRODUCTION

Interactions between lipids and membrane proteins are generally known to have a major effect on the structure and function of biological membranes. An important aspect in the function and biogenesis of membrane proteins are the interactions between the amino acids flanking the hydrophobic transmembrane domain, and the hydrophobic-hydrophilic interfaces in the membrane.

It has been found that in integral membrane proteins with single- or multiple spanning transmembrane helices, the interfacial region is enriched in aromatic residues (Landolt-Marticorena et al., 1993; Reithmeier, 1995; von Heijne, 1994). Especially tryptophans and tyrosines are abundant in the interface, and they are generally thought to have an anchoring (Braun and von Heijne, 1999; de Planque et al., 1999) and stabilizing (Woolf, 1997; Ridder et al., 2000) function. Moreover, it has been suggested that aromatic residues are essential for the proper folding and assembly (Schiffer et al., 1992), and functioning of integral membrane proteins (Becker et al., 1991; Hu and Cross, 1995). Tryptophan residues were found to be located at the hydrophobic side of the interfacial region, near the carbonyl/glycerol groups of the surrounding phospholipids (Yau et al., 1998; de Planque et al., 1999).

The positively charged residues lysine and arginine are enriched at the hydrophilic side of the interfacial region of transmembrane domains (Landolt-Marticorena et al., 1993; Ridder et al., 2000) and in the segments flanking transmembrane α-helices (Reithmeier, 1995; von Heijne, 1994). Following the positive inside rule, they are preferentially located on the *cis*-side of membranes, (von Heijne, 1986), where they associate with anionic phospholipids (van Klompenburg et al., 1997), fulfilling a topology-determining role (von Heijne, 1989). When flanking a hydrophobic α-helix in transmembrane model peptides, lysines showed a distinct preference for the hydrophilic side of the interfacial region, close to the phosphate groups of the surrounding lipid bilayer (de Planque et al., 1999).

In order to gain more insight in these interfacial interactions, model peptides have been used (Wimley and White, 1996; de Planque et al., 1999; Mall et al., 2000). An example of synthetic model peptides, are the so-called WALP peptides (Killian et al., 1996). These peptides consist of an alternating alanine-leucine stretch, forming a hydrophobic α-helix, which is flanked on both sides by two tryptophans.

Recently we have studied supported DPPC gel-state bilayers containing WALP peptides with Atomic Force Microscopy (AFM; Binnig et al., 1986) (Rinia et al., 2000). AFM offers the possibility to image supported bilayers under aqueous conditions with a high resolution (Czajkowsky et al., 1999; Shao et al., 1996; Müller et al., 1999). We found that the majority of the peptides segregated, together with some lipids, forming extremely ordered striated

domains, in an otherwise predominantly flat bilayer. Overall, the length of the peptides and/or lipids did not influence this peculiar behavior. Previously, Mou and co-workers (Mou et al., 1996) found comparable results on Gramicidine A (GA), which also clustered together with some lipids in ordered domains. Like WALP peptides, GA has tryptophan residues located at the hydrophobic-hydrophilic interface of the surrounding lipid bilayer.

In order to determine whether the formation of ordered striated domains is a general property of transmembrane peptides, or whether it is unique for peptides containing tryptophans as flanking residues, we have studied DPPC bilayers containing the WALP analogs YALP, FALP, KALP and HALP. These peptides also consist of an alanine-leucine stretch, but are flanked by tyrosines, phenylalanines, lysines, or histidines, respectively, instead of tryptophans. Those amino acids are known to have different preferences for the hydrophobic-hydrophilic interface in membranes (Wimley and White, 1996). Since these peptides share the same hydrophobic alanine-leucine segment, solely the effect of different flanking residues on the aggregation behavior of transmembrane peptides in DPPC bilayers could be determined.

We studied these systems with AFM and found that the peptides containing uncharged flanking residues were able to induce the formation of striated domains in supported DPPC bilayers, whereas the peptides containing positively charged residues induced homogeneously distributed, irregularly shaped depressions in the bilayer, and never striated domains. In order to explain this difference in morphology, Circular Dichroism (CD) and Differential Scanning Calorimetry (DSC) measurements were done on several systems containing WALP analogs. To rule out that interactions between the bilayer and the substrate cause the observed morphology, freeze-fracture Electron Microscopy (EM) was performed on large multilamellar vesicles containing WALP or KALP. EM images of such vesicles showed bilayers with a morphology comparable to the supported bilayer systems.

Pulmonary surfactant protein C (SPC) is a small (4 kD), extremely hydrophobic protein, which takes part in maintaining the desired surface pressure of the air-water interface in the lung alveoli during breathing. A large part of the protein consists of a valine-rich hydrophobic stretch forming a surprisingly stable and rigid α-helix, which is able to span a DPPC bilayer (Morrow, 1993). At the *N*-terminus side of the α-helix, three positively charged residues are present. Monolayers containing SPC have been studied extensively by Amrein et al. (1997). When incorporated in DPPC bilayers, SPC enables us to study a naturally occurring protein in a biologically relevant environment, since 40-60% of the pulmonary lipids consists of DPPC (Brouwers et al., 1998; Yu et al., 1993) and compare it directly to the results we obtained on the model peptides. We found that SPC induced essentially the same morphology in supported DPPC bilayers, as the positively charged peptides.

4.2 MATERIALS AND METHODS

4.2.1 Materials

1,2–Dipalmitoyl-*sn*-glycero-3-phosphocholine (DPPC) was purchased from Avanti Polar Lipids (Alabaster, AL) and used without any further purification. WALP21, YALP21 and FALP21 consist of 21 amino acids in total. They contain a hydrophobic alanine-leucine stretch of 15 amino acids flanked on each side by two tryptophans, tyrosines or phenylalanines respectively. WALP23, KALP23, and HALP23 peptides consist of 23 amino acids, containing a hydrophobic alanine-leucine stretch of 17 amino acids flanked on each side by either tryptophans, lysines or histidines. Table 1 shows the amino acid sequences of the different peptides we used. The N-terminus and C-terminus are blocked with an acetyl group and an ethanolamine or amide group respectively.

Table 4.1 Amino acid sequences of the model peptides and of porcine SPC.

Peptide	Amino acid sequence
WALP21	Ac-GWWL$(AL)_8$WWA-etn
YALP21	Ac-GYYL$(AL)_7$YYA-amide
FALP21	Ac-GFFL$(AL)_7$FFA-amide
WALP23	Ac-GWWL$(AL)_8$WWA-etn
KALP23	Ac-GKKL$(AL)_8$KKA-amide
HALP23	Ac-GHHL$(AL)_8$HHA-amide
Porcine SPC[a]	*N*-LRIPCCPVDLKRLL$(V)_7$L$(V)_4$IVGALLMGL-*C*

[a] *N-terminal cysteines are palmitoylated, postitively charged residues are denoted in bold and the hydrophobic α-helical segment is underlined (from Curstedt et al., 1990).*

All peptides were synthesized essentially as described, (de Planque et al., 1999) and were >95% pure, as checked with HPLC. Porcine surfactant protein C consisting of 35 amino acids (sequence listed in Table 4.1), was isolated from lung lavage (Oosterlaken-Dijksterhuis et al., 1991) and was a kind gift of dr. E. J. A. Veldhuizen. 2,2,2-Trifluoroethanol (TFE) was from Sigma (St. Louis, MO). For all experiments MilliQ water was used.

4.2.2 Vesicle preparation

The peptides were dissolved in either TFE or in a mixture of chloroform and methanol (3:1; v/v), both yielding similar results, and added to DPPC dissolved in a chloroform/methanol (3:1; v/v) mixture. The obtained peptide/lipid mixtures contained 1, 2 or 5 mol% peptide in lipid. These mixtures were dried in a rotary evaporator followed by overnight storage under high vacuum. To the dried mixed films, 1.25 ml of 20 mM NaCl solution was added. In the case of the HALP23 peptides, a 10 mM Tris buffer with 20 mM NaCl, pH 9, or a 10 mM HAc buffer with 20 mM NaCl, pH 5 was used. For oriented CD measurements, pure MilliQ water was added. The hydrated film was shortly heated to 50°C and vortexed, to promote vesicle formation. After ten cycles of freeze-thawing (thawing at 50°C), large multilamellar vesicles (MLV's) were obtained. Small unilamellar vesicles (SUV's) were made by sonicating a suspension of MLV's in a bath sonicator (Branson, Danburry, Connecticut) at maximum power for at least 30 minutes, at 50°C. Possible remaining large vesicles were spun down at 20800 g for 1 hr, at 4°C. The supernatant containing SUV's was used for the preparation of supported bilayers.

4.2.3 Preparation of supported bilayers

The supported bilayers were prepared as described (Rinia et al., 2000) using the vesicle fusion method. Briefly, 75 µl of SUV suspension with a lipid concentration of ± 0.5 mM was applied onto freshly cleaved mica (∅ 10 mm). The vesicles were allowed to adsorb to the mica for at least 10 hrs at 4°C, as described (Mou et al., 1996). After rinsing (10 times with 75 µl of buffer), the sample was heated to 60°C for 60 minutes and afterwards, the sample was left to cool down to room temperature at ambient conditions and subsequently rinsed again. In this way bilayers were obtained, usually containing defects and with some unopened vesicles on top. Differences in lipid concentration in the SUV suspensions lead to different substrate coverages, which was optimized by prolonged or shortened adsorption times or additional heating and rinsing of the sample. This did not affect the observed morphology of the bilayers, but merely promoted the formation of large areas of bilayer without too many defects or unopened vesicles. The latter two yield features in the images, which disturb image

processing with the AFM software. Supported bilayers of DPPC with 2 mol% SPC incorporated were prepared following the above protocol, however, in this case the SUV suspension had to be diluted 4 times before it was applied to mica, to obtain a bilayer without too many unopened vesicles on top. All samples were scanned a few hours after preparation.

4.2.4 Atomic Force Microscopy

The sample was mounted on an E-scanner, which was calibrated on a standard grid, of a Nanoscope III (Digital Instruments, Santa Barbara, CA). A quartz flow cell was used without the O-ring. All samples were scanned with oxide-sharpened tips with a spring constant of 0.06 N/m, as estimated by the manufacturer (Digital Instruments, Santa Barbara, CA). Scans were recorded with a scan speed of 6 lines/s and at a minimal force where the image was stable and clear, which was usually smaller than 500 pN. All images shown are flattened raw data. All bilayers were imaged at room temperature.

4.2.5 Oriented Circular Dichroism

CD measurements on oriented lipid bilayers containing either WALP23 or KALP23 were performed following the procedure of de Jongh et al. (1994). SUV's with a lipid concentration of ~5 mM with 2 mol% peptide in lipid, in MilliQ water were prepared as described above. On a CD quartz cuvet, 60 µl of water was applied and subsequently heated to 60°C. To the warm droplet, 20-80 µl vesicle suspension was added and kept at 60°C under humid conditions for 20 minutes. Then the sample was left at 60°C to dry, and after cooling down, CD spectra were recorded on a Jasco J-600 spectropolarimeter with a scan speed of 20 nm/min, with 0.2 nm resolution, 1 nm bandwidth and 1 s response time.

4.2.6 Differential Scanning Calorimetry

For DSC measurements, MLV's with a lipid concentration of 5.0 mM, prepared as described above were used. The samples were degassed prior to use. 500 µl vesicles were injected in the sample cell of a MCS (Microcal Inc., Northampton, MA). Thermograms were recorded between 15 °C and 70 °C at a scan rate of 60 °C/hr (upscan) and 45 °C/hr (downscan).

4.2.7 Freeze-fracture Electron Microscopy

Samples of MLV's with a lipid concentration of 10 mM with 2 mol% peptide in lipid were sandwiched between two hat-shaped copper holders and rapidly frozen in propane cooled in liquid nitrogen using a KF80 plunge freezing device (Reichert Jung, Vienna, Austria). After fracturing, platinum/carbon replicas were made in a BAF400 (Bal-tec, Baltzers, Liechtenstein). Replicas were observed with a CM10 Electron Microscope (Philips, Eindhoven, the Netherlands) operated at 80 kV.

4.3 RESULTS

4.3.1 Morphology of supported bilayers containing uncharged peptides

WALP peptides induce striated domains in supported DPPC bilayers (Rinia et al., 2000), and this was found for peptides with a length of 19, 23 and 27 amino acids (WALP19, WALP23 and WALP27). An example of such a domain in a DPPC bilayer with 2 mol% WALP23 is given in Fig. 4.1 *A*, showing that the striated domains consist of ordered high (light) and low (dark) lines, with a repeat distance (i.e. the width of a low and a high line) of 7.5±0.4 nm, which curve at angles of 120°.

Fig. 4.1 *B* depicts an image of a supported DPPC bilayer with 2 mol% WALP21 incorporated, also showing striated domains. The domains appear 2-3 Å above the level of the bilayer and consist of lines with a repeat distance of 7.6±0.6 nm. In the gel-state bilayer outside the striated domains, line-type depressions can be seen, which were also observed for the WALP with other lengths. They are thought to consist of disordered, fluid-like lipids and peptides being excluded from the solidified DPPC domains (Rinia et al., 2000).

In order to determine whether these striated domains are only induced by peptides with a hydrophobic segment flanked by tryptophans, peptides containing other aromatic flanking residues were incorporated in DPPC bilayers and imaged by AFM. In YALP21, the flanking residues consist of tyrosines. In supported DPPC bilayers, containing 2 mol% YALP21, striated domains can be seen (Fig. 4.1 *C*). The lines in these domains have a repeat distance of 7.6±0.4 nm, they are straight and seem to curve at defined angles (usually 120°). Incorporation of FALP21, which has phenylalanines as flanking residues, also led to the formation of striated domains (Fig. 4.1 *D*), with a repeat distance of of 8.2±1.0 nm. The lines in these striated domains are curled and do not curve at defined angles.

Occasionally areas were observed, appearing below the level of the bilayer. An example is given in Fig. 4.1 *E*, which shows a DPPC bilayer with 2 mol% YALP21. These lower areas sometimes appeared as flat roundish domains in the bilayer (Fig. 4.1 *E*), as thick lines, situated in the gel-state bilayer outside the striated domains (Fig. 4.1 *E*), and in the case of YALP21, also within the striated domains (not shown). Fig. 4.1 *F* shows the profile of this bilayer at the line drawn in Fig. 4.1 *E*. This height profile shows that these areas are approximately 2 nm below the surface of the bilayer. We assume that these lower areas consist of peptide and fluid-like lipids, which would indeed appear about 2 nm below the level of a gel-state bilayer.

In conclusion it can be said that apparently not only WALP peptides containing tryptophans as flanking residues, but also WALP analogs, containing other aromatic residues have the ability to induce the formation of striated domains.

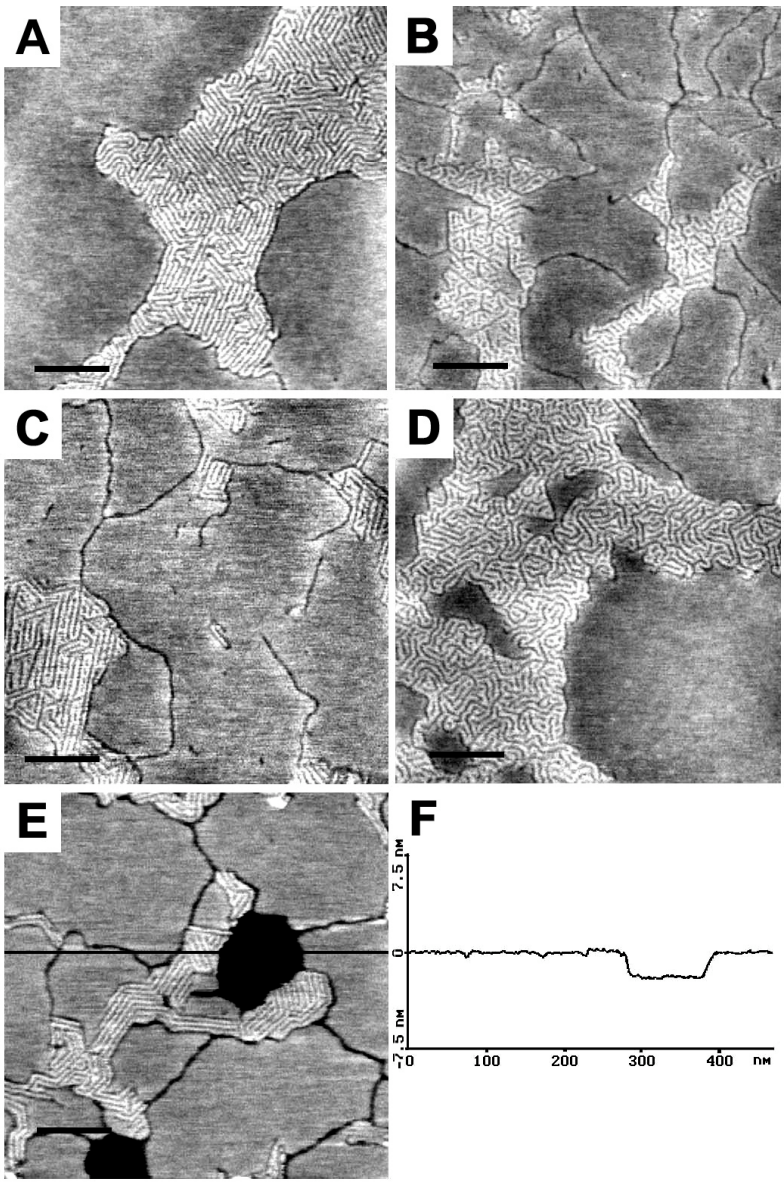

FIGURE 4.1 AFM images of striated domains induced in supported DPPC bilayers by uncharged model peptides. (A) DPPC with 2 mol% WALP23; (B) DPPC with 2 mol% WALP21; (C) DPPC with 2 mol% YALP21; (D) DPPC with 2 mol% FALP21. (E) Occasionally lower areas were seen, as shown here for DPPC with 2 mol%YALP21. (F) Cross-section of the line drawn in E. All bilayers are scanned in 20 mM NaCl. All scale bars are 100 nm.

4.3.2 Morphology of supported bilayers containing positively charged peptides

Another class of amino acids with the ability to anchor transmembrane segments, are the positively charged lysines. KALP23 peptides consist of 23 amino acids in total, with the hydrophobic segment flanked by lysines. KALP23 has been shown to behave as if it has a hydrophobic length comparable to the shorter peptide WALP21, to the extent that they have the same mismatch dependent destabilizing effect on the lamellar phase of fluid PC's (de Planque et al., 1999). We found however that in DPPC bilayers, KALP23 peptides induce a completely different morphology than WALP peptides, and striated domains were never seen.

In DPPC bilayers with 2 mol% KALP23 incorporated, homogeneously distributed areas, appearing below the level of the bilayer, can be seen in the form of irregularly shaped small areas, meandering lines, and points. In Fig. 4.2 *A*, a 1x1 μm area of such a bilayer is depicted, and Fig. 4.2 *E* shows the height profile of the line drawn in the image of Fig. 4.2 *A*. The depth of the depressions depended on the width of these depressions: the wider the holes, the deeper they were. The small holes and the point- and line-type depressions had a maximum depth of 1- 2 nm. The largest holes had a depth of 6 nm, which corresponds to the thickness of a bilayer with a water layer that is generally assumed to reside between the bilayer and the substrate (Shao et al., 1996). This indicates that at least in some cases the depressions pierce the bilayer.

When 1 mol% KALP23 was incorporated, again homogeneously distributed, irregular lower lines, small areas and points were present, but the fraction of area appearing below the level of the bilayer was smaller (Fig. 4.2 *B*), compared to the bilayers with 2 mol% KALP23 (Fig. 4.2 *A*). In bilayers with 5 mol% KALP23, more irregular shaped lower areas were seen (data not shown) than in the bilayers with 2 mol% KALP23, thus the fraction of lower area is dependent on the concentration of the peptide. Since the height differences between the bilayer and the lower areas were small, it was not possible to quantify the amounts of lower area with the existing AFM software.

The morphology of bilayers containing peptides with lysines as flanking residues differs distinctly from the morphology of bilayers containing peptides with aromatic flanking residues (Fig. 4.1). It could be that the observed difference is due to specific properties of lysines, or that positively charged residues in general induce the described morphology. In order to distinguish between these two possibilities, we studied HALP23. In these peptides the flanking residues are histidines, which are protonated at low pH and deprotonated at high pH. They offer the possibility to image bilayers with positively charged peptides (HALP at low pH) and bilayers with the same peptide, but uncharged (HALP at high pH).

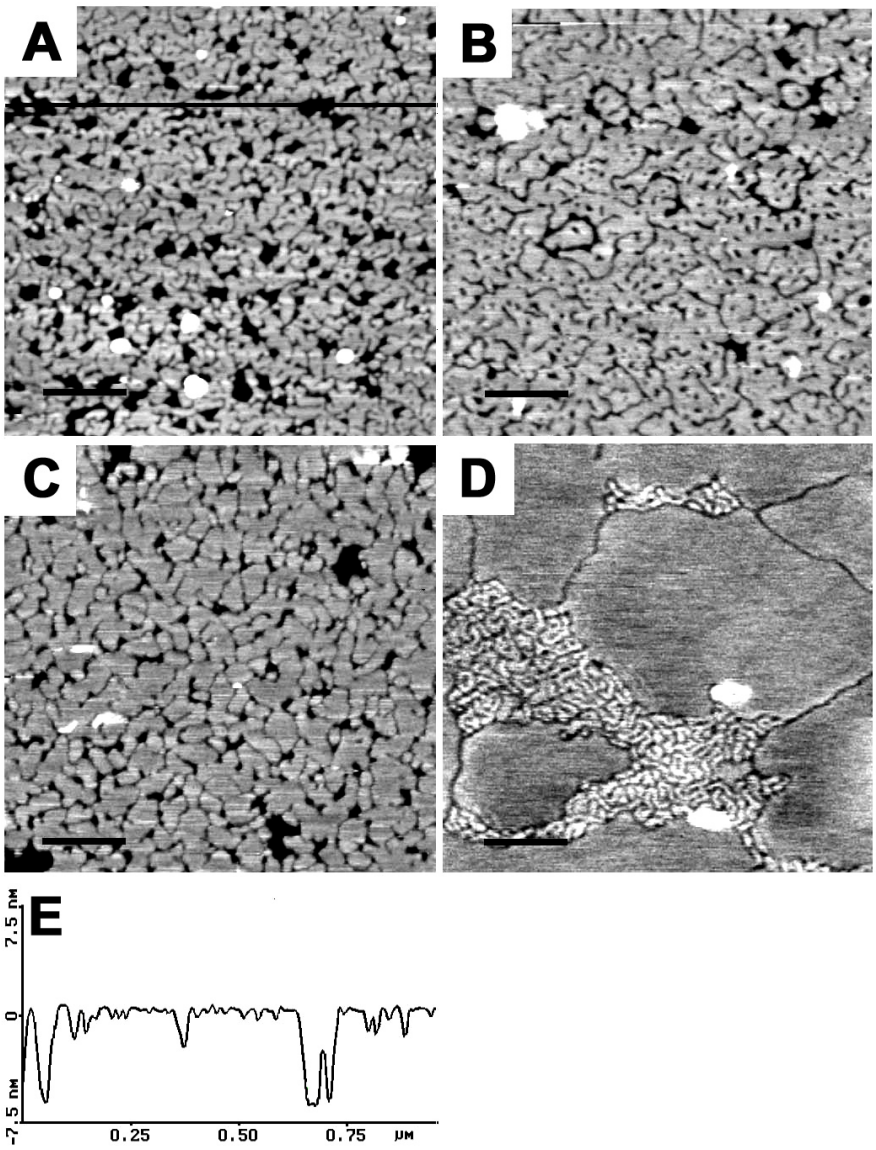

FIGURE 4.2 AFM images of supported DPPC bilayers with model peptides incorporated. (A) DPPC with 2 mol% KALP23, scanned in 20 mM NaCl, scale bar 200 nm; (B) DPPC with 1 mol% KALP23, scanned in 20 mM NaCl, scale bar 200 nm; (C) DPPC with 2 mol% HALP23, scanned in 10 mM HAc, 20 mM NaCl, pH=5, scale bar 200 nm; (D) DPPC with 2 mol% HALP23, scanned in 10 mM Tris, 20 mM NaCl, pH=9, scale bar 100 nm; (E) Cross-section of the line drawn in A.

In Fig. 4.2 *C*, a DPPC bilayer with 2 mol% HALP23 is shown, made and imaged at pH 5 (in HAc buffer). Under these circumstances the HALP23 peptides are positively charged. Small irregularly shaped areas and lines, and occasional points appeared below the level of the bilayer, yielding a morphology comparable to bilayers containing KALP23 peptides (Fig. 4.2 *A*).

Fig. 4.2 *D* depicts an image of a DPPC bilayer with 2 mol% HALP23, made and imaged at pH 9 (in Tris buffer). Uncharged HALP23 peptides give essentially the same results as the WALP23 peptides, in that line-type depressions are formed along with striated domains. The repeat distance of the lines in the striated domains is 8.5±1.3 nm, which is comparable to the repeat distance of the lines in the domains induced by WALP23. However, as in the case of FALP21 (Fig. 4.1 *D*), the pattern formed by the lines in the striated domains induced by HALP23 is not as ordered as in the WALP23 domains (Fig. 4.1 *A*), and the lines seem more curled.

Bilayers containing WALP23 peptides, or KALP23 peptides made and scanned in the presence of the Tris buffer (pH 9) or HAc buffer (pH 5), always gave the same results compared to the ones obtained in the presence of 20 mM NaCl (Figs. 4.1 *A* and 4.2 *A*). Thus, the observed difference in morphology of HALP23 containing bilayers at different pH's is not induced by the components of the buffers used.

In additional experiments, vesicles with 2 mol% HALP23 at pH 5, had been left to adsorb to mica, and subsequently the protocol was changed by rinsing the sample with Tris buffer (pH 9). After heating, rinsing and scanning in Tris buffer pH 9, striated domains were observed (data not shown). These domains were however smaller and more connected and homogeneously distributed than the ones observed in bilayers completely made and imaged at pH 9. When vesicles, made and left to adsorb at pH 9 were subsequently treated with HAc buffer (pH 5), irregular cracks were observed in the bilayer surface, comparable to Fig. 4.2 *C*, occasionally together with large flat areas appearing 1-2 nm below the surface of the bilayer (data not shown). Apparently the formation of the striated domains could be manipulated by changing the pH, i. e. the charge of the HALP23 peptides, when the pH is changed before heating the adsorbed vesicles. When the pH was changed after the adsorbed vesicles had been heated, the bilayers became unstable, making it impossible to obtain clear and reproducible images.

The morphology induced by KALP23 is not unique for lysine flanked peptides, but is also induced by HALP23, when the histidine residues are positively charged. Preliminary results on bilayers containing peptides flanked by another positively charged residue, arginine, gave comparable results (data not shown). Thus we conclude that this morphology is typical for supported DPPC bilayers containing positively charged WALP analogs.

Since peptides with uncharged histidines as flanking residues can also induce the formation of striated domains, we propose that the induction of striated domain formation is typical for uncharged WALP analogs.

4.3.3 Orientation of peptides in the bilayer

WALP23 and KALP23 are known to adopt a transmembrane orientation in DMPC bilayers in the fluid phase (at 34°C) (de Planque et al., 1999), however this is not necessarily the case in DPPC bilayers in the gel phase. In order to determine whether the observed difference in morphology induced by the uncharged and the charged peptides is due to a different orientation of the peptides in the bilayer (Janshoff et al., 1999), we performed CD measurements on oriented bilayers with WALP23 or KALP23 incorporated.

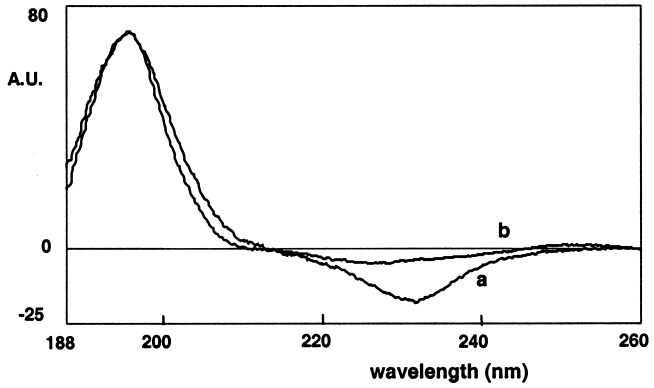

FIGURE 4.3 Circular Dichroism spectra of 2 mol% WALP23 (a) and 2 mol% KALP23 (b) in oriented DPPC gel-state bilayers.

In Fig. 4.3, CD spectra are shown of oriented lipid layers, with a peptide concentration of 2 mol%. The spectra of both WALP23 (curve a) and KALP23 (curve b) show a maximum at 195 nm, while the cross over point is at 213 nm and 210 nm respectively. This is characteristic for α-helices, oriented parallel to the beam of incoming light and, in this case, perpendicular to the bilayer plane (de Jongh et al., 1994). In agreement with previous experiments with WALP23 and KALP23 incorporated in DMPC, the line-shape of the spectrum of WALP23 in oriented bilayers deviates somewhat from the spectrum of KALP23 in the 220-240 nm region, which is attributed to the tryptophan side-chain chromophores in WALP peptides (de Planque et al., 1999).

According to our CD measurements, both WALP23 and KALP23 form an α-helix with a transmembrane orientation, in planar DPPC gel-state bilayers. Thus, the observed difference

in morphology between supported DPPC bilayers with uncharged and positively charged peptides is not due to a different orientation of the peptides in the bilayer.

4.3.4 Influence of peptides on the lipid thermotropic phase behavior

In order to understand how uncharged and charged peptides can induce such different morphology in DPPC bilayers, even though they both form a transmembrane α-helix, we aimed to obtain more insight in the peptide-lipid interactions of the different systems. Therefore the effects of WALP23, KALP23 and HALP23 on the thermotropic phase behavior of DPPC, were studied using Differential Scanning Calorimetry (DSC) (McElhaney, 1986).
In Fig. 4.4, the thermograms of DPPC vesicles containing 2 mol% WALP23, KALP23, or HALP23, at pH 9 and 5, are depicted, together with the thermogram of DPPC vesicles containing no peptide.

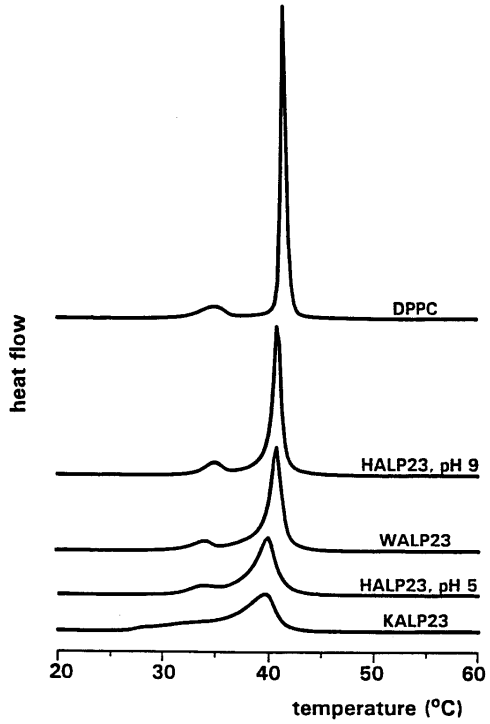

FIGURE 4.4 DSC heating curves of vesicles of: (from top to bottom) pure DPPC in 20 mM NaCl; DPPC with 2 mol% HALP23 in 10 mM Tris, 20 mM NaCl, pH=9; DPPC with 2 mol% WALP23 in 20 mM NaCl; DPPC with 2 mol% HALP23 in 10 mM HAc, 20 mM NaCl, pH=5; DPPC with 2 mol% KALP23 in 20 mM NaCl.

The quantification of the thermodynamic parameters of these peptide/lipid and pure lipid systems are listed in Table 4.2.
The thermogram of pure DPPC shows a small, broad endothermic peak with a maximum at 35.1°C, ascribed to the pre-transition, from the tilted solid to the ripple phase, and a large, narrow endothermic peak, with a maximum at 41.5°C, ascribed to the main, ripple-to-fluid transition. This is characteristic for the phase behavior of DPPC (Lewis et al., 1987).
Thermograms of DPPC with uncharged peptides (WALP23 and HALP23 at pH 9) incorporated, show a small downward shift of the main transition temperature, of less than 1°C and a small increase in width of the main endothermic peak ($\Delta T_{1/2}$). The relative enthalpy has decreased about 10%, compared to the pure lipids. These effects on the thermodynamic parameters are typical for the so-called type 3 proteins (Papahadjopoulos et al., 1975), indicating that the peptides mainly interact with the hydrophobic part of the lipid bilayer.

Table 4.2 Thermodynamic parameters of pure DPPC and DPPC with 2 mol% incorporated model peptides, as measured with DSC.

	no peptide	WALP23	HALP23 pH 9	KALP23	HALP23 pH 5
T_{tr} main (°C)	41.5	40.7	40.8	39.8	39.8
T_{tr} pre (°C)	35.1	33.9	34.7	–	33.8
$\Delta T_{1/2}$ main (°C)	0.6	1.7	0.8	4.0	2.5
Enthalpy (%)	100	91	92	91	87

Thermograms of DPPC with positively charged peptides (KALP23 and HALP23 at pH 5) incorporated, show a slightly larger downward shift of 1.7°C and a significant increase in width of the main endothermic peak, compared to the uncharged peptides. The pre-transition peak of DPPC with HALP23 at pH 5 is also shifted to a lower temperature, while the pre-transition peak of DPPC with KALP23 incorporated has almost disappeared. As in the case of uncharged peptides, the relative enthalpy has decreased with about 10%. This behavior is more like the behavior described for type 2 proteins ((Papahadjopoulos et al., 1975), which indicates that the positively charged peptides also interact with the hydrophilic lipid headgroup region. The results we obtained on the positively charged peptides are

comparable to the ones obtained by the group of McElhaney on similar peptides in saturated diacyl-PC's (Zhang et al., 1995).
In conclusion, the DSC data indicate that the positively charged peptides disturb DPPC bilayers more than the uncharged peptides do.

4.3.5 Morphology of vesicles containing peptides

The morphologies shown thus far have been observed in supported planar bilayers. In order to examine the possible influence of the solid support on the observed morphologies, we studied multilamellar vesicles containing 2 mol% WALP23 or KALP23. These vesicles were quenched from room temperature (below the main phase transition temperature), freeze-fractured and imaged by Electron Microscopy (EM). Pure DPPC vesicles, as observed by freeze fracture EM, showed smooth featureless planes (data not shown).

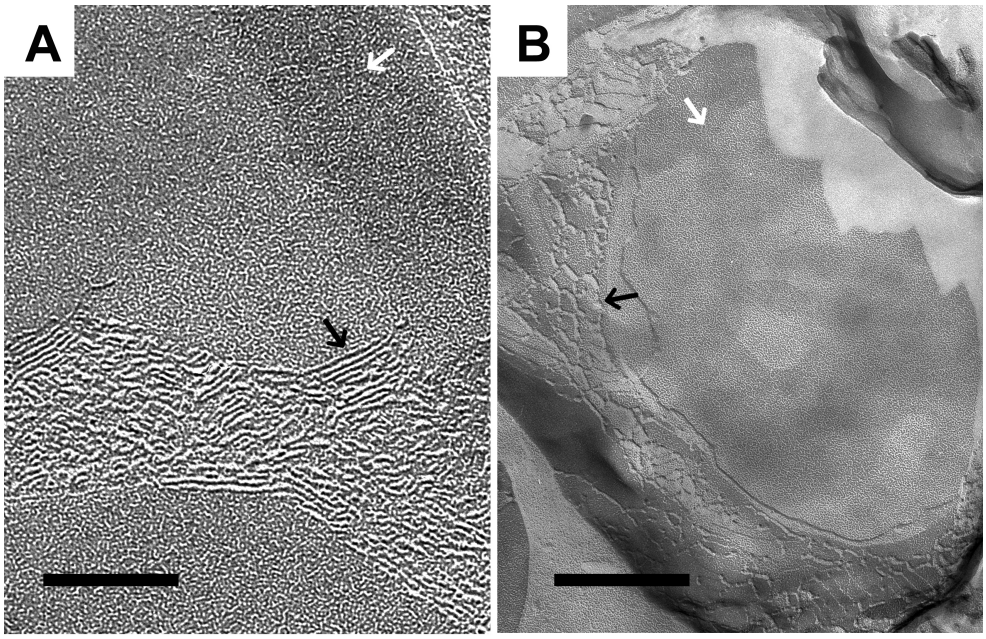

FIGURE 4.5 Electron Microscopy images of Freeze-Fractured vesicles of (A) gel-state DPPC with 2 mol% WALP23, in 20 mM NaCl. Scale bar 125 nm; (B) gel-state DPPC with 2 mol% KALP23, in 20 mM NaCl. Scale bar 250 nm.

In the fracture plane of vesicles of DPPC with WALP23 incorporated, smooth featureless areas can be seen (denoted with a white arrow in Fig. 4.5 *A*), which are thought to be DPPC domains. In between these smooth areas, rough domains were observed. In some cases, in the

structure of these domains, ordered lines were visible as shown in Fig. 4.5 *A* (denoted with a black arrow). The repeat distance of these lines were found to be 7.1±0.8 nm, which is in excellent agreement with the repeat distance of the lines found in the striated domains in the supported bilayers. Hence it can be said that the formation of ordered striated domains is a characteristic feature of these peptide lipid systems and is not induced by the substrate onto which the supported bilayers were deposited.

Fig. 4.5 *B* depicts a fracture plane of a DPPC vesicle with 2 mol% KALP23 incorporated. In such vesicles, lines with a width of about 10 nm could be seen, with the same irregular pattern as observed for the supported bilayers containing 2 mol% KALP23 (Fig. 4.2 *A*), although the distance between the lines is larger. Furthermore, the lines are not homogeneously distributed through the bilayer, but clustered in large domains (denoted with a black arrow in Fig. 4.5 *B*). Outside these domains, smooth surfaces are visible (denoted with a white arrow in Fig. 4.5 *B*), presumably consisting of pure lipid domains. Domains as seen in the vesicles with WALP23 were never observed. Note that the scale bar in Fig. 4.5 *A* is 125 nm, and in Fig 4.5 *B*, 250 nm.

4.3.6 Supported bilayers with SPC

To compare the effects of model peptides to those of a naturally occurring protein, we also used AFM to study supported DPPC bilayers containing pulmonary surfactant protein C (SPC). This small hydrophobic, predominantly α-helical protein contains several positively charged residues (Table I).

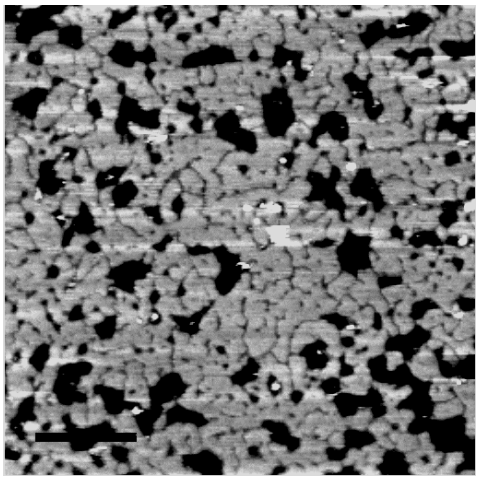

FIGURE 4.6 AFM image of a supported DPPC bilayer with 2 mol% SPC incorporated, scanned in 20 mM NaCl. Scale bar 200 nm.

Supported DPPC bilayers with 2 mol% SPC incorporated, contained many irregularly shaped defects (see Fig. 4.6), of which the largest could be determined to pierce through the whole bilayer. In the surface of the bilayer itself, randomly distributed small cracks could be seen, with a width and a depth of 11.8±3.8 nm and 0.6±0.2 nm respectively. Striated domains were never observed. Overall, the morphology of bilayers containing SPC resembles the morphology of bilayers containing positively charged model peptides (Figs. 4.2 *A* and *C*).

4.4 DISCUSSION

4.4.1 Morphology of bilayers containing uncharged peptides

In a previous study we showed that WALP peptides induce line-type depressions and striated domains in supported DPPC bilayers, and that the size and amount of the striated domains were dependent on the concentration of the peptide (Rinia et al., 2000). In that study we proposed a model of the molecular organization of both line-type depressions and the striated domains. Upon cooling the bilayer during the vesicle fusion protocol, from above to below the phase transition temperature of DPPC, the lipids probably start to solidify at different "nucleation-sites" in the bilayer. This implies the formation of different lipid patches, and in one patch, the lipids could be tilted in a different direction than in another. The peptides would be expelled from these rigidly packed, gel-state DPPC domains and end up in the boundaries between the patches, possibly with some disordered, fluid-like lipids. This would account for the line-type depressions. Excess peptide is thought to be accommodated in the striated domains, which would exist of arrays of peptide, flanked by disordered fluid-like lipids, forming the dark (low) lines in the striated domains in Fig. 4.1 *A*. These lines are thought to be separated by lipids whose interaction with the peptides tends to straighten their acyl chains and to orient them parallel to the peptides. Therefore the lipids appear above the level of the bilayer, forming the light (high) lines in the striated domains in Fig. 4.1 *A*. Fig. 4.7 *A* shows a cartoon of a cross-section of this proposed model of the molecular organization in the striated domains (on the right) next to a gel-state lipid patch (left). Fig. 4.7 *B* depicts a top-view of this model. The results of the oriented CD measurements, indicate that WALP23 peptides are indeed in a perpendicular orientation with respect to the plane of the membrane (Fig. 4.3, line a). The finding with freeze-fracture EM, that in unsupported DPPC systems containing WALP23, also striated domains are present (Fig. 4.5 *A*), with a repeat distance of 7.1±0.8 nm, shows that the striated domains are not induced by the support onto which the bilayers are deposited. This also is in agreement with the proposed model.

The proposed model involves the preference of the peptides to be surrounded by lipid, while the lipids, due to their tight packing in the gel phase, prefer to stay together. The resulting compromise is the formation of lines, clustered together in striated domains. The mechanism underlying this model implies that the formation of the striated domains is a-specific for the peptide. This is supported by the finding of Mou et al. (1996) that Gramicidin A (GA) also induces the formation of ordered domains. However, since both GA and WALP peptides contain tryptophans as flanking residues, the possibility exists that line formation is induced by stacking-interactions between tryptophans of neighboring peptides. However, peptides with other uncharged flanking residues (tyrosine, phenylalanine and histidine (at high pH), Fig. 4.1 *C* and *D* and Fig. 4.2 *D*), also induce the formation of striated domains, indicating that no such stacking interactions are involved, and illustrating the a-specificity of the underlying mechanism. We propose that the molecular organization of both line-type depressions and the striated domains, present in bilayers containing YALP21, FALP21 and HALP23 (high pH), as depicted in Fig. 4.1 *C* and *D* and Fig. 4.2 *D*, is the same as in bilayers containing WALP peptides (see also Fig 4.7 *A*, *B*).

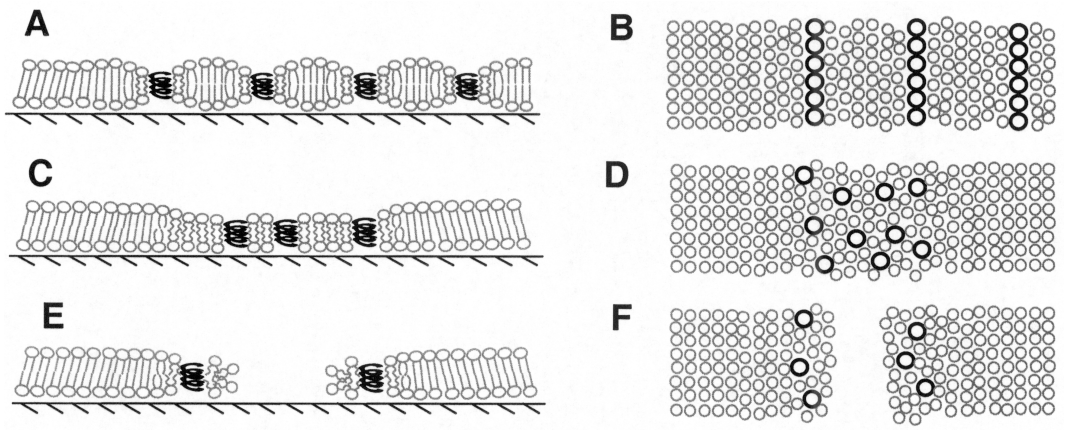

FIGURE 4.7 Proposed models for the molecular organization of bilayers with model peptides incorporated. The tilted packing of DPPC is disturbed by the presence of the peptides, depicted as black coiled springs. Uncharged peptides segregate, together with some lipids in striated domains in which peptide arrays flanked by fluid-like lipids appear as low lines, separated by less-tilted lipids, appearing as high lines. A cross-section is depicted in (A) and (B) shows a top-view. In the top views lipids are depicted as gray circles, and peptides as black circles. Charged peptides repel each other and thus cannot be forced in arrays. They either segregate with fluid-like lipids between the small gel-state patches (C: cross-section and D: top-view) or are accommodated in the disordered lipids, bordering holes that pierce the whole bilayer (E: cross-section and F: top-view).

The pattern of the striated domains induced by WALP21, WALP23 and YALP21 resembles the ripple phase in that it consists of ripples and exhibits three-fold symmetry. However, since the repeat distance remained constant upon changing the length of the peptides or lipids, it was concluded in the previous chapter (Rinia et al., 2000) that the striated domains do not correspond to the ripple phase. Moreover, on some samples a second bilayer on top of the first bilayer was observed, showing a ripple phase structure, with different repeat distances and morphology compared to the striated domains (Rinia et al., unpublished observations). Second bilayers have been found more often to exhibit ripple phase structures (Mou et al., 1996; Fang and Yang, 1996).

The pattern varies for peptides with different flanking residues. WALP21, WALP23 and YALP21 form domains with straight lines, curving at defined angles (Fig. 4.1 *A-C*). The flanking residues of these peptides, i.e. tryptophan and tyrosine are known to preferentially locate at a specific position in the membrane interface (Killian and von Heijne, 2000), and have a "strong" anchoring potency (de Planque, 2000). Striated domains containing FALP21 and HALP23 (at high pH) consist of curled lines, curving at less defined angles (Fig. 4.1 *D* and 4.2 *D*). The flanking residues of these peptides, e.g. phenylalanine and histidine were found to anchor less strongly compared to tryptophan and tyrosine (de Planque, 2000). Although the exact mechanism is not understood, we suggest that there is a correlation between the anchoring function of the flanking residues of the peptides, and the order in the pattern of the striated domains induced by these peptides. The effect of the geometry of the involved molecules and the difference in tilt between the peptides and the lipids, on the formation of striated phases will be investigated in the near future by using Monte Carlo computer simulations (van der Eerden et al., submitted).

4.4.2 Morphology of bilayers containing positively charged peptides

Supported DPPC bilayers with KALP23 or HALP23 (at low pH) give rise to a completely different morphology compared to bilayers with uncharged peptides. Striated domains were never seen. Since both KALP23 and HALP23 (at low pH) are positively charged, and since HALP23 at high pH, when it is uncharged, did induce the formation of striated domains, we propose that the different morphology as seen for KALP23 and HALP23 at low pH, is due to the positive charges of the flanking residues. These charges would cause the peptides to repel each other and therefore the peptides cannot form striated domains in which they would have to be in close vicinity.

DPPC bilayers containing 2 mol% KALP23, show point-like and irregularly shaped line-type depressions along with irregularly shaped lower areas, all homogeneously distributed over the bilayer (Fig. 4.2 *A*). In bilayers with 1 mol% KALP23 (Fig. 4.2 *B*) and 5 mol% KALP23

(data not shown), also point-like and line-type depressions and lower areas can be seen, but less and more respectively, compared to bilayers with 2 mol% KALP23. Apparently the amount of depressions is dependent on the concentration of the peptide. According to the CD measurements, the peptides are present, in a perpendicular orientation with respect to the plane of the bilayer, (Fig. 4.3, line b). Since both KALP23 and HALP23 (3.6 nm) are shorter than the thickness of a DPPC gel-state bilayer (4.7 nm (Marsh, 1990)), logically they would appear below the level of the bilayer. From this we deduce that the KALP23 and HALP23 are located in or at the edges of the depressions.

We could not determine the depth of the points, lines and lower areas unambiguously, since the depth seemed to vary with the width of the depressions, most probably because the tip is not sharp enough to completely reach "the bottom" of narrow holes. This means that all the depressions could be as deep as the whole bilayer, as seen for the large depressions (Fig. 4.2 *E*). On the other hand, it could also be that the depths of the point-like and line-type depressions are indeed merely 1- 2 nm deep.

In the case that the point-like and irregular line-type depressions are about 1- 2 nm deep, then these lines most probably consist of disordered fluid-like lipids, in which the peptides are dissolved. The positively charged peptides are separated by the fluid-like lipids. This organization is depicted as a cross-section in Fig. 4.7 *C*, and as a top-view in Fig. 4.7 *D*.

In the case that all the lower areas pierce the entire bilayer, the charged peptides would be situated in the edges of the bilayer, bordering the aqueous phase in the hole through the bilayer. These edges are assumed to consist of lipids oriented such that the hydrophilic headgroups shield the hydrophobic acyl chains from the aqueous phase, as depicted in Fig. 4.7 *E* (Grandbois et al., 1998; Rinia et al., 1999). In order to make this curve, the lipids cannot be in the tightly packed gel state, but have to be disordered. It should be the most favorable for the peptides to reside in these disordered sites (Fig. 4.7 *E*). A top-view of this organization is depicted in Fig. 4.7 *F*.

In both cases, the bilayer is fragmented in small domains of gel-state lipids. This would decrease the cooperativity of a phase transition of such a bilayer, and this is reflected in the large $\Delta T_{1/2}$ of the phase transition of DPPC vesicles containing positively charged peptides.

Freeze-fracture EM of vesicles containing 2 mol% KALP23 revealed meandering lines and occasionally points in the bilayer. If these lines and points correspond to the line-type and point-like depressions as seen in the AFM images, it is most likely that in these lines and points peptides are/were residing. This suggests that the molecular organization of the point-like and line-type depressions in bilayers containing positively charged peptides, is most likely as depicted in Fig. 4.7 *C*.

Although the EM images of DPPC vesicles with WALP23 incorporated, closely resemble the AFM images of the same systems on mica, the EM results on DPPC vesicles containing KALP23 differ from the AFM images of supported DPPC bilayers with KALP23. In the vesicles containing KALP23 (Fig. 4.5 *B*), the lines are present in domains outside smooth areas of, most likely, pure lipid, whereas in the supported systems, the irregular line-type depressions are homogeneously distributed over the bilayer (Fig. 4.2 *A*). We suspect that the negative charges of the substrate cause this distribution of the positively charged peptides. However, since shielding of the charges, by preparing and scanning supported bilayers with incorporated KALP23 in the presence of 10 mM Mg^{2+}, did not yield bilayers with domains (data not shown), the exact cause of this observed difference remains unclear.
The pulmonary surfactant protein SPC is a small protein involved in lowering the surface tension in the lungs during breathing. DPPC is an abundant lipid in the lungs. Thus bilayers of DPPC containing SPC are biologically relevant systems. SPC contains a hydrophobic α-helix, and two arginines and a lysine, making it positively charged. The images we obtained on supported DPPC bilayers with 2 mol% SPC have a morphology comparable to bilayers containing positively charged model peptides (Fig. 4.6). This means that by studying model peptides in lipid bilayers, one can make predictions about the morphology of bilayers with incorporated biologically relevant small proteins.

4.5 CONCLUSIONS

We have imaged supported DPPC bilayers with incorporated model peptides containing various flanking residues. It was found that the uncharged peptides induce ordered, striated domains in which the peptides are thought to reside with some disordered lipids. The positively charged peptides induced irregularly shaped depressions. These morphologies were also seen with EM in unsupported systems. DSC data confirm that WALP analogs with positively charged residues disturb DPPC bilayers more than WALP analogs with uncharged residues. The difference in morphologies was found to be not induced by a different orientation of the uncharged and positively charged peptides, because oriented CD measurements showed that both WALP23 and KALP23 form transmembrane α-helices in DPPC bilayers. DPPC with a naturally occurring, positively charged, α-helical protein (SPC) gave similar results to bilayers with positively charged model peptides.

CHAPTER 5

Visualizing detergent resistant domains in model membranes with Atomic Force Microscopy

(FEBS Letters, 2001, 501:92-96)

ABSTRACT

Evidence is accumulating that in cell membranes microdomains, also referred to as rafts or detergent resistant membranes (DRM's), do exist. In this study, Atomic Force Microscopy (AFM) is used to study supported lipid bilayers, consisting of a fluid phosphatidylcholine (PC), sphingomyeline (SpM) and cholesterol. Domains were visualized, of which the morphology and size depended on the cholesterol concentration. The presence of cholesterol was found to induce bilayer coupling. At 30 mol% cholesterol, a change in percolation phase was observed, and at 50 mol%, when both fluid lipids and solid lipids are saturated with cholesterol, phase separation was still observed. In addition, we were able to directly visualize the resistance of domains against non-ionic detergent.

5.1 INTRODUCTION

Since biological membranes consist of many different lipids and proteins, and thus form heterogeneous mixtures, it has been speculated that lateral domains can form in biomembranes (Welti and Glaser, 1994; Mouritsen and Bloom, 1984). Especially domains that would consist of sphingolipids and cholesterol have received much attention lately (London and Brown, 2000; Harder and Simons, 1997; Jacobson and Dietrich, 1999). Such domains are usually referred to as rafts (Simons and Ikonen, 1997) and they are believed to correspond to parts of biological membranes that are resistant to non-ionic detergent in the cold (Brown and London, 1998). Detergent resistant membranes (DRM's) (Yu et al., 1973; Brown and Rose, 1992) have indeed been found to be enriched in sphingolipids and cholesterol.

Eukaryotic plasma membranes consist of glycerophospholipids, sphingolipids and sterols. The glycerophospholipids usually have a low melting temperature (T_m) while sphingolipids in biomembranes usually have a high T_m. Cholesterol, the sterol present in mammalian cells, is able to induce the liquid ordered phase (Recktenwald and McConnell, 1981; Sankaram and Thompson, 1990). In this phase, lipid acyl chains are extended and tightly packed, as in the solid phase, but the lateral diffusion is almost as high as in the fluid phase (Almeida et al., 1992; Dietrich et al., 2001). The basis of the idea that rafts exist in cell membranes is that, because sphingolipids and cholesterol preferentially interact (Demel et al., 1977; Ferraretto et al., 1997), they phase-separate from glycerophospholipids in the fluid phase, and form domains, which are in the liquid ordered phase, and insoluble in non-ionic detergents, like Triton X-100, in the cold.

Liquid ordered phases have been studied in model systems with different techniques like fluorescence quenching (Ahmed et al., 1997; Xu and London, 2000), fluorescence polarization (Xu and London, 2000; Schroeder et al., 1994), electron spin resonance (Sankaram and Thompson, 1990) and fluorescence microscopy (Dietrich et al., 2001). Atomic Force Microscopy (AFM) can image biological samples under aqueous conditions with high resolution in three dimensions without the use of any probes. AFM has been successfully used to image isolated DRM's (Giocondi et al., 2000), phase separated bilayers (Mou et al., 1995; Dufrêne and Lee, 2000) and peptide-lipid domains in supported bilayers (Mou et al., 1996; Rinia et al., 2000). Also monolayers containing glycospingolipids and cholesterol have been imaged (Yuan and Johnston, 2000), but so far membrane mimicking bilayers consisting of phospholipids, sphingolipids and cholesterol have not been investigated by AFM. We have, for the first time, used AFM to image bilayers consisting of a fluid glycerophospholipid, sphingomyelin and varying amounts of cholesterol and directly visualized domains and their

resistance against cold non-ionic detergent extraction. In addition we report on some novel findings concerning these systems.

5.2 MATERIALS AND METHODS

5.2.1 Materials

1,2–Dioleoyl-*sn*-glycero-3-phosphocholine (DOPC) and egg Sphingomyelin (SpM) were purchased from Avanti Polar Lipids (Alabaster, AL). Egg SpM consist for 84% of sphingosines with $C_{16:0}$ acyl chains. Cholesterol was from Merck (Darmstadt, Germany). For all experiments MilliQ water was used.

5.2.2 Vesicle preparation

All lipids were dissolved in chloroform/methanol (3:1; v/v), and subsequently mixed at predetermined ratios. The ratio of SpM and DOPC was always 1:1 (moles/moles) and cholesterol concentrations varied between 0 and 50 mol% of the total amount of lipid. The lipid mixtures were dried in a rotary evaporator followed by overnight storage under high vacuum. To the dried mixed films, 1 ml of 20 mM NaCl solution was added, which resulted in a lipid concentration of 1 mM. The hydrated film was freeze-thawed and sonicated in a bath sonicator (Branson, Danburry, Connecticut) at maximum power for at least 30 minutes, to obtain small unilamellar vesicles (SUV's). Possible remaining large vesicles were spun down at 20800 g for 1 hr, at 4°C. The supernatant containing SUV's was used for the preparation of supported bilayers.

5.2.3 Preparation of supported bilayers

The supported bilayers were prepared using the vesicle fusion method. 75 µl of SUV suspension was applied onto freshly cleaved mica (∅ 10 mm). The vesicles were allowed to adsorb and fuse on the mica while the sample was heated to 60°C for 60 minutes. Afterwards, the sample was left to cool down to room temperature at ambient conditions and subsequently rinsed. In this way bilayers were obtained, suitable for scanning with AFM.
Bilayers made of vesicles that were not heated, but left to adsorb for 5 hrs at room temperature, had the same morphology as the heated bilayers. The same holds true for bilayers made of unsonicated, multi lamellar vesicles (MLV's), but in this case the quality of the AFM images was bad, most likely due to the fact that multiple bilayers were present underneath the scanned bilayer.

5.2.4 AFM measurements

The sample was mounted on an E-scanner, which was calibrated on a standard grid, of a Nanoscope III (Digital Instruments, Santa Barbara, CA). A quartz flow cell was used without the O-ring. All samples were scanned with oxide-sharpened tips with a spring constant of 0.06 N/m, as estimated by the manufacturer (Digital Instruments, Santa Barbara, CA). Scans were recorded with a scan speed of 6 lines/s and at a minimal force where the image was stable and clear, which was usually smaller than 500 pN. All images shown are flattened raw data. All bilayers were imaged at room temperature. With the Nanoscope software it is possible to study cross-sections and height distributions of AFM images. We used the cross-sections to determine the height of the observed domains and the height distributions to quantify the amount of area occupied by domains.

5.2.5 Detergent extraction

Samples of DOPC/SpM (1:1) with 0, 10 or 25 mol% cholesterol were, after scanning, left to cool down in the refrigerator to 4°C for one hour. Subsequently 50 µl of the solution on the bilayer was replaced by cold 10% Triton X-100, and the sample was left to incubate for 1 min. After rinsing with 10 times 75 µl cold 20 mM NaCl solution, the sample was left to warm up to room temperature and scanned again with AFM. The exact same area that was scanned before Triton extraction could be found again by using an electron microscopy grid, glued under the mica.

5.2.6 Differential Scanning Calorimetry and Thin Layer Chromatography

DSC measurements were done on MLV's of pure SpM and of SpM/DOPC (1:1), with a SpM concentration of 5 mM, in a MCS (Microcal Inc., Northampton, MA) with a scan-rate of 60ºC/hr. TLC was performed on silica plates (Merck, Darmstadt, Germany) with an eluent of chloroform/methanol/water (65:25:4). Lipids were stained with iodine and with short heating after spraying with 10% H_2SO_4.

5.3 RESULTS AND DISCUSSION

We have prepared supported bilayers consisting of DOPC and SpM (1:1), with increasing concentrations of cholesterol, from 0 to 50 mol% of the total amount of lipid. Of each system, several samples were made and scanned, and we show here the most representative AFM images. Occasionally, in all bilayers, small pinholes were seen, indicating that a bilayer was indeed present, but they were always too narrow to measure the bilayer thickness (Shao et al., 1996)

5.3.1 Bilayers of sphingomyelin and DOPC

Fig. 5.1 *A* depicts an AFM image of a DOPC/SpM (1:1) bilayer, without cholesterol. This bilayer is expected to show phase separation because Egg SpM has a T_m of 38°C, as measured with DSC (data not shown) and thus is in the solid phase at room temperature. DOPC has a T_m of -15°C (Demel et al., 1977) and thus is in the fluid phase at room temperature. Since bilayers in the solid phase are thicker than bilayers in the fluid phase, higher domains consisting of SpM can be seen in Fig. 5.1 *A*. The size of the solid domains was in the order of 10 to 100 nm.

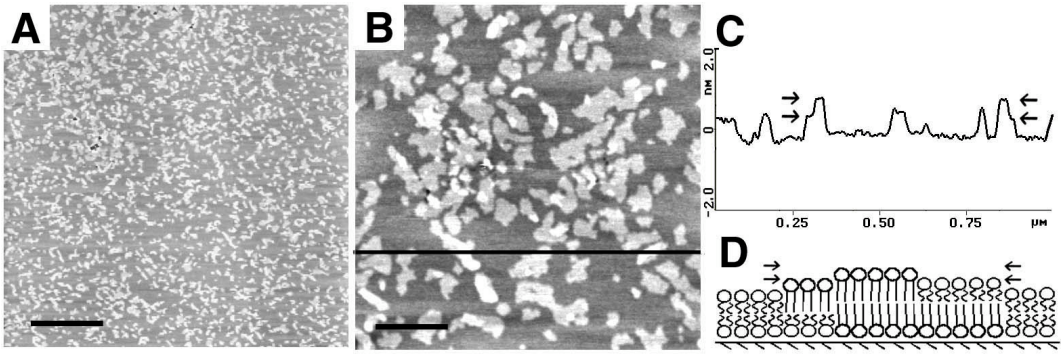

FIGURE 5.1 Bilayer of DOPC/SpM (1:1). (A) AFM image showing phase separation, image size 5x5 mm, scale bar is 1 mm and z-scale is 10 nm. (B) DOPC/SpM (1:1) bilayer at larger magnification. The domains appear in two different heights, visible as white and light gray. The dark gray represents the level of the fluid bilayer. Image is 1x1 mm, scale bar is 200 nm and z-scale is 5 nm. (C) Cross-section of line drawn in B. The two different height levels of the domains are denoted with arrows. (D) Molecular model of the domains showing the two height levels. It is not known whether in the domains of intermediate thickness, the ordered molecules face the support or not.

In Table 5.1, the height differences between the domains and the surrounding bilayer, and the areas of the domains, as percentages of the total amount of area, are listed for all bilayers.
The average amount of area occupied by domains, was 21% of the total area, which is relatively small compared to the amount of SpM present. However, in a DOPC/SpM mixture, the T_m of SpM decreases (Demel et al., 1977). The thermogram the DSC scan of mixed DOPC and SpM showed a broad phase transition peak of SpM, starting at 10°C and finishing at 30°C (data not shown), indicating that at room temperature only a fraction of SpM is in the solid phase. It is this fraction that is seen as higher domains in AFM images of such bilayers (Fig. 5.1 *A*), while the remaining part of the SpM is in the fluid phase, present in the surrounding bilayer, probably dissolved in DOPC.

The average height difference between the solid domains and the fluid bilayer is 1 nm, which is in agreement with other results obtained with AFM on phase-separated fluid-solid bilayers (Mou et al., 1995). Occasionally some intermediate levels, appearing 0.6 nm above the level of the fluid bilayer were seen. This is illustrated in Fig. 5.1 *B* which shows an image of a DOPC/SpM (1:1) bilayer at higher magnification. Fig. 5.1 *C* depicts the cross-section of the line drawn in Fig. 5.1 *B*. This indicates that some parts of the domains are asymmetric in their monolayer composition. Apparently not in all domains, both monolayers are made up by solid lipid, but some also by fluid lipid. This is clarified in Fig. 5.1 *D*.
The chain length asymmetry in SpM has been found to cause monolayer coupling, for SpM with a difference in chain length of 11 carbons (Schmidt et al., 1978). Chain length differences of 5 carbons were not sufficient to induce this effect. In our system, where the SpM chain length difference is even smaller, namely 3 carbons, monolayer coupling should not occur, which is supported by our data (Fig. 5.1 *B-D*).

Table 5.1 Amount of area occupied by domains and height differences between the domains and surrounding bilayer in DOPC/SpM bilayers containing different amounts of cholesterol.

Cholesterol concentration (mol%)	Area domains (% of total area)	Height difference domains and bilayer (nm)
0	21±11 (n=7)	1.0±0.1 (n=8)
2	25±6 (n=3)	0.9±0.3 (n=3)
5	24±9 (n=6)	0.8±0.2 (n=6)
10	28±5 (n=4)	0.8±0.1 (n=3)
15	21±10 (n=5)	0.9±0.2 (n=5)
25	41±7 (n=21)	0.8±0.2 (n=20)
30	58±2 (n=3)	0.6±0.2 (n=3)
50		0.4±0.1 (n=4)

5.3.2 Bilayers of sphingomyelin, DOPC and cholesterol

Bilayers of DOPC/SpM (1:1) with 2, 5, 10 or 15 mol% cholesterol had an appearance comparable to the bilayers without cholesterol, except that the domains were slightly larger. Also, some large domains (500 nm) were present that seemed to consist of coalesced smaller domains. In Fig. 5.2 *A*, a bilayer containing 10 mol% cholesterol is shown with arrows denoting such "clusters" of domains.

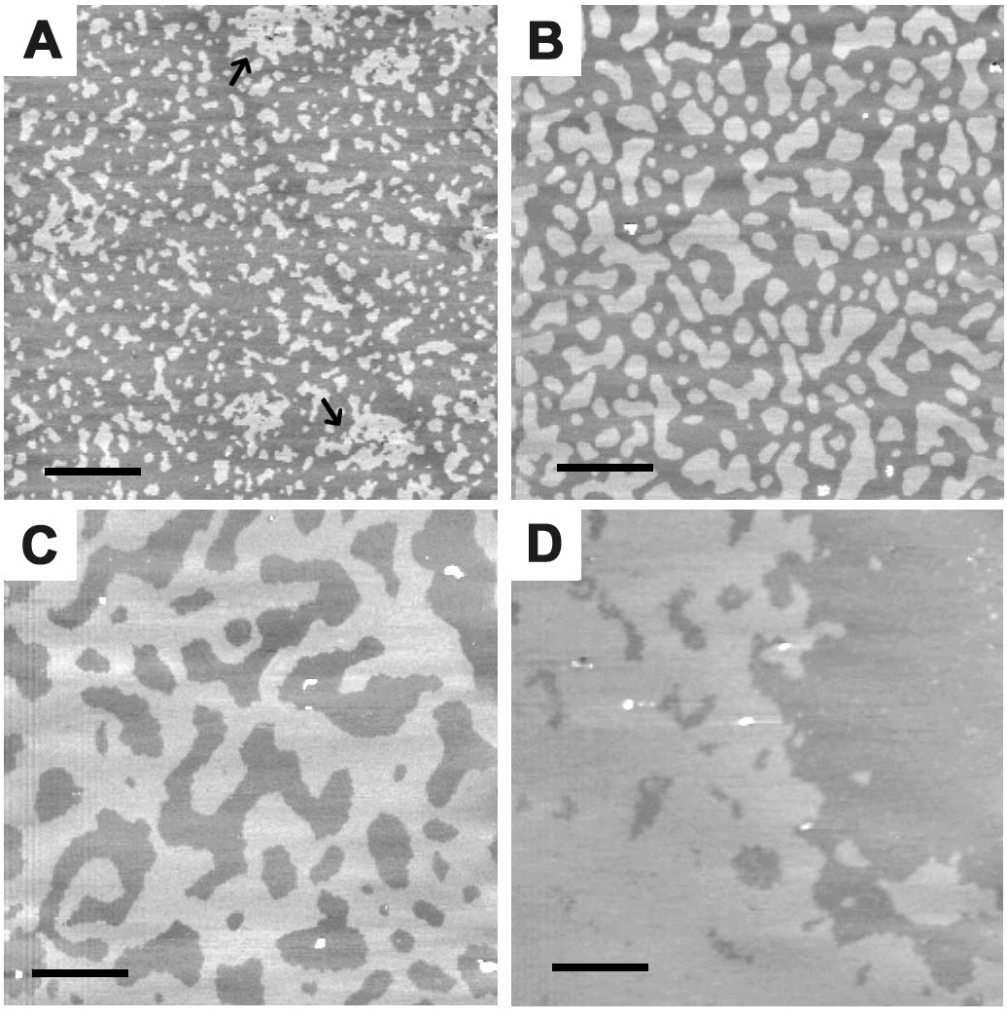

FIGURE 5.2 AFM images showing domains in DOPC/SpM (1:1) bilayers with (A) 10 mol% cholesterol; (B) 25 mol% cholesterol; (C) 30 mol% cholesterol, and (D) 50 mol% cholesterol. All images are 5x5 mm, scale bars are 1 mm, z-scales are 10 nm.

The average height difference between the domains and the surrounding fluid bilayer is slightly lower than for domains without cholesterol, while the average amount of area occupied by domains is slightly higher (Table 5.1). For all bilayers containing 5 mol% cholesterol or more, the intermediate levels described for the system without cholesterol (Fig. 5.1) were never observed. This implies that cholesterol has the ability to couple monolayers in membranes, at least in the presence of SpM. Previous observations have suggested that in cell membranes, the rafts in the outer leaflet are coupled to the cytoplasmic leaflet, although the latter is sphingolipid-poor (Brown and London, 2000). Our findings indicate that cholesterol may play a role in this leaflet coupling.

Fig. 5.2 *B* shows a bilayer of DOPC/SpM (1:1) with 25 mol% cholesterol. Domains formed in such bilayers are larger in size (up to 1 μm) and less irregular in shape than the domains formed at lower cholesterol concentrations. The height of the domains is comparable to the height of the other domains containing cholesterol (Table 5.1). The average amount of area occupied by these domains is significantly higher, namely 41% of the total area. Possibly all SpM molecules in the solid phase are saturated with cholesterol, and now also SpM, originally dissolved in DOPC in the fluid phase, is incorporated in the higher domains.

At 30 mol% cholesterol (Fig. 5.2 *C*), the amount of higher area has increased further (Table 5.1). The average height difference between high and low areas decreased slightly, to 0.6 nm. At this point, the higher phase is in the majority and apparently the percolation threshold has been passed, since the higher phase is now the percolating phase. A change in percolating phase has been proposed to be biological functional (Vaz, 1994) and this is the first time such a change is visualized directly in bilayers of phospholipids, sphingolipids and cholesterol.

The maximum concentration of cholesterol in lipid bilayers is 50 mol%. At this concentration bilayers showed large phase-separated areas with sizes of more than 10 μm. The amount of high area could not be quantified reliably, but by eye it seemed to be about 50% of the total area. The average height difference between the two phases was found to be merely 0.4 nm. In these systems SpM as well as DOPC are saturated with cholesterol. Yet, still two phases can be distinguished in these systems (Fig. 5.2 *D*), one consisting of SpM and cholesterol, and the other of DOPC with cholesterol which appears as the lower areas. This implies that in biomembranes, rich in cholesterol, like myelin, phase-separation, and thus domain formation, can occur.

Cholesterol is known to thicken fluid bilayers (Levine and Wilkins, 1971) which explains the decrease in height difference between the two phases to 0.4 nm. Since the height difference at low cholesterol concentrations was 0.8 nm, this means that cholesterol thickened the fluid bilayer with 0.4 nm. This is in agreement with other studies, which found cholesterol to cause an increase in bilayer thickness of 0.41 nm (Nezil and Bloom, 1992).

5.3.3 Detergent resistance of the domains

To test whether the domains shown in this study are resistant to non-ionic detergent extraction in the cold, we treated several samples with Triton X-100 at 4°C. An example is presented in Fig. 5.3.

A DOPC/SpM (1:1) bilayer with 25 mol% cholesterol is depicted in Fig. 5.3 *A* (compare to Fig. 5.2 *B*), before detergent extraction. Fig. 5.3 *B* shows the cross-section of the line drawn in Fig. 5.3 *A*, showing the height difference between the domains and the surrounding bilayer. Fig. 5.3 *C* depicts an image of the same area after detergent extraction, and Fig. 5.3 *D* shows the cross-section of the line drawn in Fig. 5.3 *C*. It is clear that after detergent extraction, the fluid phase has disappeared, revealing the underlying mica substrate, and that the domains are still present. The height difference between the domains and the mica was found to be 5-6 nm. This corresponds to the thickness of a solid bilayer and a layer of water between the mica and the lipid layer (Shao et al., 1996).

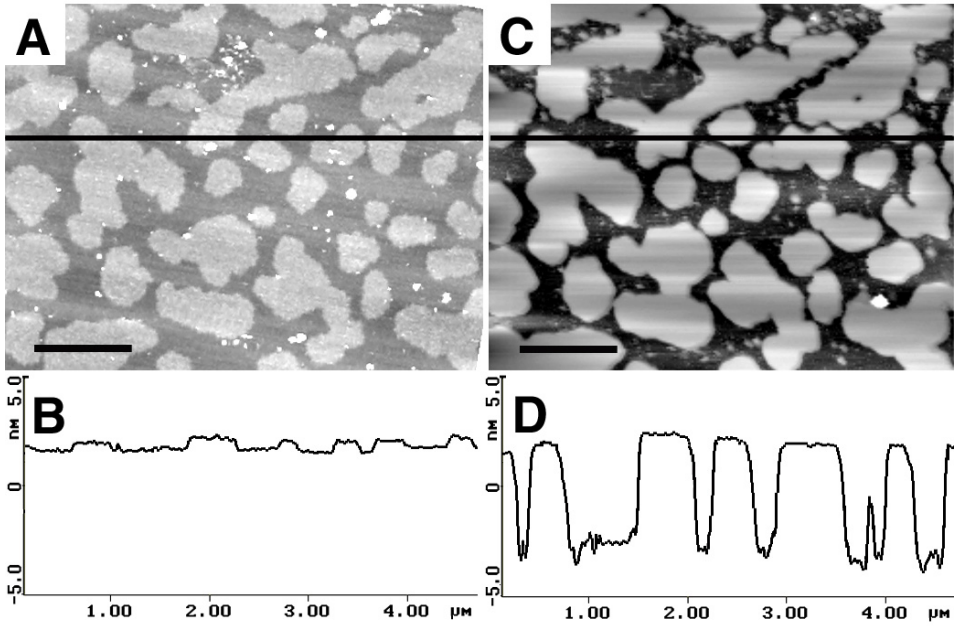

FIGURE 5.3 Visualization of the resistance to Triton X-100. (A) DOPC/SpM (1:1) bilayer containing 25 mol% cholesterol. (B) Cross-section of line drawn in A showing the height difference between liquid ordered domains and surrounding bilayer is less than 1 nm. (C) The same bilayer as in A, after treatment with Triton X-100 at 4°C. The domains are still present, but the surrounding bilayer is dissolved. (D) Cross-section of line drawn in C. The height difference between the domains and the underlying mica is 5.5 nm. Both images are 5x5 mm, scale bars 1 mm, z-scales 10 nm.

When the detergent extraction was performed at room temperature, nearly the whole bilayer had disappeared (data not shown). Domains formed in bilayers with a concentration of 10 mol% cholesterol, were also found to be resistant to detergent extraction in the cold, while the surrounding fluid bilayer was not (data not shown). The same was found for bilayers without cholesterol, illustrating that indeed also domains in the solid phase are detergent resistant (Ribeiro and Dennis, 1973; Schroeder et al., 1994) Detergent treated bilayers with varying amounts of cholesterol were collected and their lipid composition was checked with TLC. This showed that indeed the domains were depleted from DOPC.

It has been postulated that DRM's isolated from cell membranes by detergent extraction in the cold may have been formed during cooling or by the detergent extraction itself (London and Brown, 2000). The domains in our system, after the detergent extraction (Fig. 3 *C*) are merely slightly larger than before the detergent extraction, possibly either due to the cooling, or due to the fact that the lateral support of the surrounding bilayer has disappeared, causing the domains to sag. This increase in size has caused some domains to coalesce. However, altogether the domains still have roughly the same size and shape. This means that detergent treatment in the cold hardly influences cholesterol/SpM domains present in our model membranes and that any domain found after the treatment was already present before the treatment. Extrapolating this to biological membranes, domains found after detergent treatment of mammalian cell membranes were present as such within the membranes before the treatment.

5.4 CONCLUDING REMARKS

This study shows that it is possible to directly visualize SpM/cholesterol domains and their resistance to detergent using AFM, illustrating the usefulness of this technique in raft studies. Also our results promise the possibility to directly visualize rafts in cell membranes in the near future.

CHAPTER 6

Summarizing Discussion

Biological membranes consist of many different protein and lipid species. Thus, membranes are heterogeneous mixtures, in which lateral segregation could occur, leading to the formation of domains. AFM can image biological samples under aqueous conditions with a high resolution and hence is a suitable tool to study domains in bilayers. This thesis deals with heterogeneities in supported model membranes, imaged with AFM. It describes studies on trans bilayer asymmetry, on the formation of peptide-lipid domains and on the formation of raft-mimicking domains in supported lipid bilayers.

In Chapter 2 the preparation and imaging of asymmetric phospholipid bilayers is described. The first leaflet of these bilayers consisted of DPPC or DMPE, both zwitterionic, uncharged phospholipids in the solid phase. The second leaflet consisted of anionic, negatively charged phospholipids. For most of these systems it was found that the defects, present in the bilayers, were surrounded by elevations of about 2 nm high. These elevations were found to reversibly disappear in the presence of divalent cations. It was concluded that, around the defects in supported phospholipid bilayers, the two leaflets are in contact and lipid exchange takes place. In the case of a second leaflet of anionic phospholipids, this means that negatively charged lipids end up in the first leaflet, facing the negatively charged surface. Due to electrostatic interactions, the bilayer edges around the defects are repelled and appear as elevations. Since these elevations were found to expand in time and detach the bilayer from the solid support, their formation was called bilayer blistering.
The presence of defects in solid-state bilayers had been observed previously, but the molecular organization of the bilayer bordering these defects was not discussed. Grandbois et al. (1998) had published a model in which the lipids facing the aqueous phase in the defects forming a convex curvature such that their headgroups shield the acyl chains from the aqueous surrounding. They had based this model on their findings of phospholipase A_2, which started to degrade DPPC bilayers at the edges of the defects. Our study supports this model but we also concluded that if the two leaflets are indeed in contact, then lipids from the

first leaflet can diffuse to the second leaflet and visa versa. Until then, it was, as far as I know, generally assumed that there is no exchange between two leaflets in supported bilayers, regarding lipids as well as surface pressure. The finding that bilayer blistering occurred in our systems suggests that due to lipid exchange, asymmetric supported bilayers loose their asymmetry in bilayer composition, and possibly the asymmetry in surface pressure is not maintained either.

Another striking effect was the influence of the lipids present in the first leaflet on the shape of the defects. DPPC yielded irregularly shaped defects, while DMPE gave rise to round defects. It was suggested that because PE headgroups form intermolecular hydrogen bridges, it is energetically more favorable for them to reduce the amount of bilayer-water interface around the defects and the best way to do this is to form round defects. Also the fact that they are able to form round defects points at a relatively high mobility of the DMPE lipids. This was supported by the observation that a triangle, cut in a bilayer with a first leaflet of DMPE (Chapter 2, Fig. 2.5), changed to a rounder shape within an hour. A square tip-induced defect in a bilayer with a first leaflet of DPPC merely had slightly rounded corners after 12 hours (data not shown). The proposed higher mobility of DMPE compared to DPPC also implies that bilayers with a first leaflet of DMPE loose their asymmetry quicker than bilayers with a first leaflet of DPPC. This would explain why the elevations are further expanded than in the systems with DPPC as the first leaflet.

Chapter 3 and 4 describe the aggregation of synthetic model peptides in PC bilayers. The idea to image such systems was based on a previous study done on Gramicidin A (GA) by Shao and co-workers (Mou et al., 1996). This small channel forming protein, spans bilayers as a dimer, one monomer in each leaflet, oriented perpendicular to the plane of the membrane. It was incorporated in PC bilayers with saturated acyl chains of varying length. In DPPC bilayers with 1 mol% GA, line-type depressions were present, and at 2 mol%, higher domains were formed, in which point-like and line-type depressions were present, forming a distinct polygonal pattern. At 5 mol% GA, the whole bilayer was covered by point-like depressions and interconnected line-type depressions forming a similar pattern.

At 1 mol%, WALP23 was found to induce line-type depressions, as described for the GA containing bilayers, but in this case, also small higher domains were present already at this low concentration. Upon increasing the peptide concentration, these domains increased in amount and size, and it could be clearly seen that the line-type depressions in the domains formed an extremely ordered pattern exhibiting a three-fold symmetry (Chapter 3, Figs. 3.1 and 3.2). These domains were referred to as striated domains. At 10 mol%, the whole bilayer seemed to consist of lines forming this pattern. The repeat distance of these lines, i.e. the

width of a low and a high line, was found to be 8 nm. This is nearly the same value as Mou and coworkers found for the width of the depressions and the shortest distance between two depressions (3.7 nm, and 4.6 nm respectively, together 8.3 nm).

Since both peptides yield such similar results, and since GA also contains tryptophans, which are, as in the case for WALP peptides, located at the hydrophobic-hydrophilic interface of bilayers, it was investigated if the tryptophans were involved in the domain formation. In Chapter 4 it is shown that this was not the case since peptides with tyrosines (YALP) or phenylalanines (FALP) as flanking residues instead of tryptophans, were also found to be able to induce striated domains in DPPC bilayers. However, peptides flanked by positively charged residues like lysine (KALP) and arginine (RALP) gave rise to a completely different morphology. They induced line type depressions and irregularly shaped lower areas, both increasing with increasing peptide concentration. Peptides with histidines (HALP) as flanking residues offered the possibility to see if this change in morphology is due to the presence of positive charges. Histidines are uncharged at high pH and positively charged at low pH. Indeed, at high pH HALP peptides induced striated domains and at low pH they induced a morphology comparable to the one induced by KALP peptides. This suggested that uncharged peptides are able to induce striated domains in DPPC bilayers, while positively charged peptides are not.

DPPC bilayers with incorporated peptides containing positively charged residues resemble DPPC bilayers with bound α-helical amphipathic peptides and these peptides are suggested to orient parallel to the bilayer (Janshoff et al., 1999). Therefore CD measurements were performed on oriented DPPC bilayers with incorporated KALP peptides, and they were found to adopt an α-helical conformation, oriented not parallel, but perpendicular to the plane of the bilayer. This was also confirmed for WALP peptides.

The morphology of these bilayers was explained by assuming that the solid-state DPPC lipids form rigidly packed domains in which the lipids are known to be tilted, and from which the peptides would be excluded. The excluded peptide would be, possibly together with some fluid-like lipids, present in the line-type depressions, bordering these lipid domains. In the case of uncharged peptides, excess peptide is accommodated in the striated domains. In these domains the peptides are present as 1-dimensional aggregates, probably flanked by fluid-like lipids. In the case of positively charged peptides, the packing in 1-dimensional aggregates is prevented due to the electrostatic repulsion between the peptides. Hence they form, together with fluid-like lipids, irregularly shaped depressions distributed over the bilayer, breaking up the bilayer in small solid DPPC domains. The proposed fluidizing effect of the peptides on the lipids was supported by DSC data.

The fact why the striated domains have such striking ordered patterns remains unclear. They do not follow the behavior of the well-known striated phases described in the literature. Since the repeat distance of the striated domains did not change when the systems where cooled down at different rates, we could exclude the possibility that they were formed due to spinodal decomposition. Also, in systems with longer (WALP27) or shorter (WALP19) peptides, or longer lipids (DSPC), the repeat distance of the pattern remained the same. Thus, the striated domains do not reflect a ripple phase or any other modulated phase. There is a possibility that the three-fold symmetry in the pattern stems from the underlying mica, which is also hexagonally ordered. However, if this were the case then peptides like FALP and HALP should also induce striated domains with an ordered pattern (Chapter 4, Figs. 4.1 and 4.2). The fact that this is not the case also makes one wonder about the proposed involvement of the hexagonal order of the DPPC acyl chains. It seems more likely that the geometry of the involved molecules play a role, as described for the so-called spaghetti phases, found with Monte-Carlo computer simulations (Vlot and van der Eerden, 1998). According to this theory, increase in mismatch between the peptides and the hydrophobic thickness of the bilayer would fluidize the striated domains, making the pattern less ordered (Chapter 3, Figs. 3.1 and 3.2). Phenylalanine and histidine were found to anchor less effective than tryptophan and tyrosine (de Planque et al., 2000). Possibly also the anchoring potency of the flanking residues affects the order in the pattern of the striated domains. Strong anchoring would induce ordered domains, while weak anchoring would render the domains more fluid, explaining why FALP and HALP induce striated domains with less ordered patterns than WALP and YALP. Recently, differences in tilt between the peptides and the lipids were found to be involved in the formation of striated patterns (van der Eerden et al., submitted).

The red line through the first three chapters, is a pattern in DPPC containing bilayers, consisting of polygonal lines, resembling cracks in dry ground. They were present as elevated lines in DPPC/DPPG bilayers, and as line-type depressions in DPPC/DMPG (DMPG in the fluid phase) bilayers, DPPC/DOPG bilayers and in DPPC bilayers with peptides incorporated. In all cases they stem from grain-boundaries, separating different solid DPPC domains. The size of these domains was decreased by the presence of positively charged peptides (KALP, HALP, RALP and SPC). The most well known location of DPPC in mammals is in the alveoli of the lungs, where it helps in maintaining the desired surface pressure during breathing. The pulmonary surfactant proteins SPB and SPC ensure reversible collapse of this alveolar monolayer. Recently it was suggested that the presence of multiple DPPC domains facilitates this reversible collapse (Krol et al., 2000). The collapse of many small domains renders the adaptation to changes in surface pressure much more flexible and dynamic, compared to the

collapse of one large domain. DPPC readily forms solid domains within one lipid layer, even in the absence of proteins or peptides, and maybe herein lies an explanation why Nature has chosen DPPC as the most abundant lipid in pulmonary surfactant, apart from its ability to dramatically increase the surface pressure.

In Chapter 5 fluid-liquid ordered phase separation is visualized. This phase separation is of particular interest since it is suspected to give rise to biologically functional domains in biological membranes (Brown and London, 2000). Such domains are also referred to as rafts (Simons and Ikonen, 1997) or as detergent resistant membranes (DRM's, Brown and London, 1998) because they are insoluble in non-ionic detergent in the cold. They have been found to be enriched in sphingolipids and cholesterol. In Chapter 5, bilayers consisting of DOPC and sphingomyelin in a 1:1 ratio, and varying amounts of cholesterol were imaged. Domains were seen which increased with increasing cholesterol concentration. One of the big issues in research on rafts, is the size of these domains. In a recent paper, the observation of domains with Fluorescence Microscopy has been described, (Dietrich et al., 2001). These authors found that the size of the sphingolipid-cholesterol domains is probably depending on the preparation of the bilayers, which is in agreement with our findings.
At high cholesterol concentrations, (> 25 mol%), a change in percolating phase was observed, and at 50 mol% cholesterol, both DOPC and SpM were saturated with cholesterol, and still phase separation was observed. By measuring height differences between several phases, it could be deduced that cholesterol thickens DOPC bilayers with 0.4 nm, and decreases the thickness of SpM bilayers with 0.2 nm. Differences in morphology between pure SpM domains and SpM domains containing cholesterol gave a hint that cholesterol is able to induce bilayer coupling.
Furthermore, the resistance to non-ionic detergent in the cold could be visualized directly. Bilayers containing 25 mol% cholesterol were imaged before and after treatment with Triton X-100 at 4°C. The same domains that were present before the extraction were still seen after the extraction, but the surrounding DOPC bilayer had disappeared. Bilayers, collected after treatment with Triton X-100 were indeed found to be depleted from DOPC, as checked with TLC. Dietrich et al. (2001) had performed similar experiments and visualized supported detergent extracted domains, but we were able to image the exact same area before and after treatment with Triton X-100. This showed that the domains had nearly the same size and shape after the treatment, indicating that extraction with non-ionic detergents in the cold does not induce the formation of DRM's, as had been suggested (Brown and London, 1998).
This last study illustrates that AFM can be a useful tool in raft-studies. It can directly measure height differences induced by cholesterol and visualize sphingolipid-cholesterol domains.

Interesting possibilities are visualization of such domains in bilayers with reconstituted GPI-anchored proteins. The preference of these proteins for different lipid phases could be imaged. Moreover, by varying the amount of cholesterol, the size of the domains can be regulated such that the domains are saturated with protein, and possibly patches of 2-D protein crystals would form.
Another possibility would be to image supported bilayers made of isolated eukaryotic outer membranes and see directly whether in these systems higher domains are present. This could give the proof that rafts do or do not exist in biological membranes.

References

Ahmed, S. H., D, A. Brown, and E. London. 1997. On the origin of sphingolipid/cholesterol-rich detergent-insoluble cell membranes: physiological concentrations of cholesterol and sphingolipid induce formation of a detergent-insoluble, liquid-ordered lipid phase in model membranes. *Biochemistry* 36:10944-10953.

Almeida, P. F. F., W. L. C. Vaz, and T. E. Thompson. 1992. Lateral diffusion in the liquid phases of dimyristoylphosphatidylcholine/cholesterol lipid bilayers: a free volume analysis. *Biochemistry* 31:6739-6747.

Amrein, M., A. von Nahmen, and M. Sieber. 1997. A scanning force- and fluorescence light microscope study of the structure and function of a model pulmonary surfactant. *Eur. Biophys. J.* 26:349-357.

Bassereau, P., and F. Pincet. 1997. Quantitative analysis of holes in supported bilayers providing the adsorption energy of surfactants on solid substrates. *Langmuir* 13:7003-7007.

Becker, M. D., D. V. Greathouse, R. E. Koeppe II, and O. S. Andersen. 1991. Amino acid sequence modulation of gramicidin channel function: Effects of tryptophan-to-phenylalanine substitutions on the single-channel conductance and duration. *Biochemistry* 30:8830-8839.

Beckmann, M., P. Nollert, and H.-A. Kolb. 1998. Manipulation and molecular resolution of a phosphatidylcholine-supported planar bilayer by atomic force microscopy. *J. Membrane Biol.* 161:227-233.

Binnig, G., C. F. Quate, and Ch. Gerber. 1986. Atomic Force Microscope. *Phys. Rev. Lett.* 56:930-933.

Blodgett, K. B. 1935. Films built by depositing successive monomolecular layers on a solid surface. *J. Am. Chem. Soc.* 57:1007-1022.

Bloom, M. and I. C. P. Smith. 1985. Manifestation of lipid-protein interactions in deuterium NMR, in Progress in Protein-Lipid Interactions, eds. Watts, A. and De Pont, *J. J. H. H. M.* Elsevier, Amsterdam, pp. 61-88.

Braun, P. and G. von Heijne. 1999. The aromatic residues Trp and Phe have different effects on the positioning of a transmembrane helix in the microsomal membrane. *Biochemistry* 38:9778-9782.

Breukink, E., R. A. Demel, G. de Korte-Kool, and B. de Kruijff. 1992. SecA insertion into phospholipids in stimulated by negatively charged lipids and inhibited by ATP: A monolayer study. *Biochemistry* 31:1119-1124.

Brian, A. A., and H. M. McConnell. 1984. Allogeneic stimulation of cytotoxic T cells by supported planar membranes. *Proc. Natl. Acad. Sci.* USA. 81:6159-6163.

Brouwers, J. F., B. M. Gadella, L. M. G. van Golde, and A. G. Tielens. 1998. Quantitative analysis of phosphatidylcholine molecular species using HPLC and light scattering detection. *J. Lipid. Res.* 39:344-353.

Brown, D. A. and J. K. Rose 1992. Sorting of GPI-anchored proteins to glycolipid-enriched membrane subdomains during transport to the apical cell surface. *Cell* 68:533-544.

Brown, D. A. and E. London. 1998. Structure and origin of ordered lipid domains in biological membranes. *J. Membr. Biol.* 164:103-144.

Brown, D. A. and E. London. 2000. Structure and function of sphingolipid- and cholesterol-rich membrane rafts. *J. Biol. Chem*. 275:17221-17224.

Bustamante, C., D. A. Erie, and D. Keller. 1994. Biochemical and structural applications of scanning force microscopy. *Curr. Opin. Struct. Biol.* 4:750-760.

Butt, H-J. 1991a. Electrostatic interaction in atomic force microscopy. *Biophys. J.* 60:777-785.

Butt, H-J. 1991b. Measuring electrostatic, van der Waals, and hydration forces in eletcrolyte solutions with an atomic force microscope. *Biophys. J.* 60:1438-1444.

Cahn, J. W. 1968. Spinodal decomposition. *Transactions Metallurgical Society AIME*. 242:166-180.

Cullis, P. R. and B. de Kruijff. 1979. Lipid polymorphism and the functional roles of lipids in biological membranes. *Biochim. Biophys. Acta* 559:399-420.

Curstedt, T., J. Johansson, P. Persson, A. Eklund, B. Robertson, B. Löwenadler, and H. Jörnvall. 1990. Hydrophobic surfactant-associated polypeptides: SP-C is a lipopeptide with two palmitoylated cysteine residues, whereas SP-B lacks covalently linked fatty acyl groups. *Proc. Natl. Acad. Sci. USA* 87:2985-2989.

Czajkowsky, D. M., C. Huang, and Z. Shao. 1995. Ripple phase in asymmetric unilamellar bilayers with saturated and unsaturated phospholipids. *Biochemistry* 34:12501-12505.

Czajkowsky, D. M., and Z. Shao. 1998. Submolecular resolution of single macromolecules with atomic force microscopy. *FEBS Lett.* 430:51-54.

Czajkowsky, D. M., S. Sheng, and Z. Shao. 1998. Staphylococcal alpha-hemolysin can form hexamers in phospholipid bilayers. *J. Mol. Biol.* 276:325-330.

Czajkowsky, D. M., H. Iwamoto, T. L. Cover, and Z. Shao. 1999. The vacuolating toxin from Helicobacter pylori forms hexameric pores in lipid bilayers at low pH. *Proc. Natl. Acad. Sci. USA* 96:2001-2006.

Dan, N. and S. A. Safran. 1998. Effect of lipid characteristics on the structure of transmembrane proteins. *Biophys. J.* 75:1410-1414.

Demel, R. A. 1994. Monomolecular layers in the study of biomembranes. *Subcellular Biochemistry* 23:83-120.

Demel, R. A., J. W. C. M. Jansen, P. W. M. van Dijck, and L. L. M. van Deenen. 1977. The preferential interaction of cholesterol with different classes of phospholipids. *Biochim. Biophys. Acta* 465:1-10.

De Jongh, H. H. J., E. Goormaghtigh, and J. A. Killian. 1994. Analysis of circular dichroism spectra of oriented protein-lipid complexes: toward a general application. *Biochemistry* 33:14521-14528.

de Kruijff, B. and E. J. J. van Zoelen. 1978. Effect of the phase transition on the transbilayer movement of dimyristoyl phosphatidylcholine in unilamellar vesicles. *Biochim. et Biophys. Acta* 511:105-115.

De Planque, M. R. R., D. V. Greathouse, R. E. Koeppe II, H. Schäfer, D. Marsh, and J. A. Killian. 1998. Influence of lipid/peptide hydrophobic mismatch on the thickness of diacylphosphatidylcholine bilayers. A 2H NMR and ESR study using designed transmembrane α-helical peptides and Gramicidin *A. Biochemistry* 37:9333-9345.

De Planque, M. R. R., J. A. W. Kruijtzer, R. M. J. Liskamp, D. Marsh, D. V. Greathouse, R. E. Koeppe, II, B. de Kruijff, and J. A. Killian. 1999. Different membrane anchoring positions of tryptophan and lysine in synthetic transmembrane α-helical peptides. *J. Biol. Chem.* 274:20839-20846.

De Planque, M. R. R. 2000. thesis.

Dietrich, C., L. A. Bagatolli, Z. N. Volovyk, N. L. Thompson, M. Levi, K. Jacobson, and E. Gratton 2001. Lipid rafts reconstituted in model membranes. *Biophys. J.* 80, 1417-1428.

Dufrene, Y. F., and G. U. Lee. 2000. *Biochim. Biophys. Acta* 1509, 14-41.

Dumas, F., M. M. Sperotto, M.-C. Lebrun, J.-F. Tocanne, and O. G. Mouritsen. 1997. Molecular sorting of lipids by bacteriorhodopsin in dilauroylphosphatidylcholine/ distearoylphosphatidylcholine lipid bilayers. *Biophys. J.* 73:1940-53.

Dumas, F., M. C. Lebrun, and J.-F. Tocanne. 1999. Is the protein/lipid hydrophobic matching principle relevant to membrane organization and functions? *FEBS Letters* 458:271-277.

Egger, M., F. Ohnesorge, A. L. Weisenhorn, S.P. Heyn, B. Drake, C. B. Prater, S. A. C. Gould, P. K. Hansma, and H. E. Gaub. 1990. Wet lipid-protein membranes imaged at submolecular resolution by atomic force microscopy. *J. Struct. Biol.* 103:89-94.

Engel, A. 1991. Biological applications of scanning probe microscopes. *Annu. Rev. Biophys. Biophys. Chem.* 20:79-108.

Engel, A., C.-A. Schoenenberger, and D. J. Müller. 1997. High resolution imaging of native biological sample surfaces using scanning probe microscopy. *Curr. Opin. in Struct. Biol*. 7:279-284.

Fang, Y. and J. Yang. 1996. Role of the bilayer-bilayer interaction on the ripple structure of supported bilayers in solution. *J. Phys. Chem.* 100:15614-15619.

Fang, Y. and J. Yang. 1997. The growth of bilayer defects and the induction of interdigitated domains in the lipid-loss process of supported phospholipid bilayers. *Biochim. et Biophys. Acta* 1324:309-319.

Ferraretto, A., M. Pitto, P. Palestini, and M. Masserini. 1997. Lipid domains in the membrane: thermotropic properties of sphingomyelin vesicles containing GM1 ganglioside and cholesterol. *Biochemistry* 36:9232-9236.

Fotiadis, D., P. Jeno, T. Mini, S. Wirtz, S. A. Müller, L. Fraysse, P. Kjellbom, and A. Engel. 2001. Structural characterization of two aquaporins isolated from native spinach leaf plasma membranes. *J. Biol. Chem.* 276:1707-1714.

Gennis, R. B. 1989. Biomembranes. Molecular structure and function. Ed Cantor, C. R. Springer-Verlag, New York, Berlin, Heidelberg.

Gil, T., J. H. Ipsen, O. G. Mouritsen, M. C. Sabra, M. M. Sperotto, and M. J. Zuckermann. 1998. Theoretical analysis of protein organization in lipid membranes. *Biochim. et Biophys. Acta* 1376:245-266.

Giocondi, M.C., V. Vie, E. Lesniewska, J. P. Goudonnet, and C. Le Grimellec. 2000. In situ imaging of detergent-resistant membranes by atomic force microscopy. *J. Struct. Biol.* 131: 38-43.

Grandbois, M., H. Clausen-Schaumann, and H. Gaub. 1998. Atomic force microscope imaging of phospholipid bilayer degradation by phospholipase A_2. *Biophys. J.* 74:2398-2404.

Hansma H. G., R. L. Sinsheimer, J. Groppe, T. C. Bruice, V. Elings, G. Gurley, M. Bezanilla, I. A. Mastrangelo, P. V. Hough, and P. K. Hansma. 1993. Recent advantages in atomic force microscopy of DNA. *Scanning* 15:296-299.

Hansma, H. G. and J. H. Hoh. 1994. Biomolecular imaging with the atomic force microscope. *Annu. Rev. Biophys. Biomol. Struct.* 23:115-139.

Harder, T. and K. Simons. 1997. Caveolae, DIGs, and the dynamics of sphingolipid-cholesterol microdomains. *Curr. Opin. Cell Biol*. 9:534-542.

Hauser, H., I. Pascher, R. H. Pearson, and S. Sundell. 1981. Preferred conformation and molecular packing of phosphatidylethanolamine and phosphatidylcholine. *Biochim. et Biophys. Acta* 650:21-51.

Haverstick, D. M. and M. Glaser. 1987. Visualization of Ca2+-induced phospholipid domains. *Proc. Natl. Acad. Sci. USA* 84:4475-4479.

Hoh, J. H., R. Lal, S. A. John, J-P. Revel, and M. F. Arnsdorf. 1991. Atomic force microscopy and dissections of gap-junctions. *Science* 253:1405-1408.

Hoh, J. H., G. E. Sosinsky, J.-P. Revel, and P. K. Hansma. 1993. Structure of the extracellular surface of the gap junction by atomic force microscopy. *Biophys. J.* 65:149-163.

Hoh J. H. and C. A. Schoenenberger. 1994. Surface morphology and mechanical properties of MDCK monolayers by atomic force microscopy. *J. Cell. Sci.* 107:1105-1114.

Hollars, C. W. and R. C. Dunn. 1998. Submicron structure in L-α-dipalmitoyl-phosphatidylcholine monolayers and bilayers probed with confocal, atomic force, and near-field microscopy. *Biophys. J.* 75:342-353.

Hu, W. and T. A. Cross. 1995. Tryptophan hydrogen bonding and electric dipole moments: Functional roles in the gramicidin channel and implications for membrane proteins. *Biochemistry* 34:14147-14155.

Hui, S. W., R. Viswanathan, J. A. Zasadzinski, and J. N. Israelachvili. 1995. The structure and stability of phospholipid bilayers by atomic force microscopy, *Biophys. J.* 68:171-178.

Israelachvili, J. N. 1985. Intermolecular and surface forces with applications to colloidal and biological systems. Academic Press, London.

Jacobson, K. and C. Dietrich. 1999. Looking at lipid rafts? *Trends Cell Biol*. 9:87-91.

Janshoff, A., D. T. Bong, C. Steinem, J. E. Johnson, and M. R. Ghadiri. 1999. An animal virus-derived peptide switches membrane morphology: possible relevance to nodaviral transfection processes. *Biochemistry* 38:5328-5336.

Jones, M. N. and D. Chapman. 1995. Micelles, monolayers and biomembranes. Wiley-Liss, New York, Chinchester, Brisbane, Toronto, Singapore.

Karrasch, S., R. Hegerl, J. H. Hoh, W. Baumeister, and A. Engel. 1994. Atomic force microscopy produces faithful high-resolution images on protein surfaces in an aqueous environment. *Proc. Natl. Acad. Sci. USA* 91:836-838.

Kasas, S., N. H. Thompson, B. L. Smith, H. G. Hansma, X. Zhu, M. Guthold, C. Bustamante, E. T. Kool, M. Kashlev and P. K. Hansma. 1997. Escherischia coli RNA polymerase activity using atomic force microscopy. *Biochemistry* 36:461-468.

Killian, J. A., I. Salemink, M. R. R. de Planque, G. Lindblom, R. E. Koeppe II, and D. V. Greathouse. 1996. Induction of nonbilayer structures in diacylphosphatidylcholine model membranes by transmembrane α-helical peptides: Importance of hydrophobic mismatch and proposed role of tryptophans. *Biochemistry* 35:1037-1045.

Killian, J. A. 1998. Hydrophobic mismatch between proteins and lipids in membranes. *Biochim. et Biophys. Acta*. 1376:401-416.

Killian, J. A., and G. von Heijne. 2000. How proteins adapt to a membrane-water interface. *Trends in Biochem. Sci*. 25:429-434.

Krol, S., M. Ross, M. Sieber, S. Künneke, H-J. Galla, and A. Janshoff. 2000. Formation of three-dimensional protein-lipid aggregates in monolayer films induced by surfactant protein B. *Biophys. J*. 79:904-918.

Lal, R., H. Kim., M. Garavito, and M. F. Arnsdorf. 1993. Imaging of reconstituted biological channels at molecular resolution by atomic force microscopy. *Am J Physiol.* 265:C851-856.

Lal, R. and S. A. John. 1994. Biological applications of atomic force microscopy. *Am. J. Physiol*. 266 (Cell Physiol.) 35:C1-C21.

Landolt-Marticorena, C., K. A. Williams, C. M. Deber, and R. A. F. Reithmeier. 1993. Non-random distribution of amino acids in the transmembrane segments of human type I single span membrane proteins. *J. Mol. Biol*. 229:602-608.

Levine, Y. K. and Wilkins, M. H. 1971. Structure of oriented lipid bilayers. *Nat. New Biol*. 230:69-72.

Lewis, B. A. and D. M. Engelman. 1983. Lipid bilayer thickness varies linearly with acyl chain length in fluid phosphatidylcholine vesicles. *J. Mol. Biol*. 166:211-217.

Lewis, R. N. A. H., N. Mak, and R. N. McElhaney. 1987. A differential scanning calorimetric study of the thermotropic phase behavior of model membranes composed of phosphatidylcholines containing linear saturated fatty acyl chains. *Biochemistry* 26:6118-6126.

London, E. and D. A. Brown. 2000. Insolubility of lipids in triton X-100: physical origin and relationship to sphingolipid/cholesterol membrane domains (rafts). *Biochim. Biophys. Acta* 1508:182-195.

Luna, E. J., and H. M. McConnell. 1978. Multiple phase equilibria in binary mixtures of phospholipids. *Biochim. Biophys. Acta* 509:462-473.

Mall, S., R. Broadbridge, R. P. Sharma, A. G. Lee, and J. M. East. 2000. Effects of aromatic residues at the ends of transmembrane α-helices on helix interactions with lipid bilayers. *Biochemistry* 39:2071-2078.

Marsh, D. 1990. Handbook of Lipid Bilayers, (CRC, Boca Raton).

McElhaney, R. N. 1986. Differential scanning calorimetric studies of lipid-protein interactions in model membrane systems. *Biochim. Biophys. Acta* 864:361-421.

Meyer, E. and H. Heinzelmann. 1992. Scanning Force Microscopy, in Scanning Tunneling Microscopy II, eds. Wiesendanger, R, and Güntherodt, H-J., Springer Verlag, Berlin, Heidelberg, New York.

Morrow, M. R., S. Taneva, G. A. Simatos, L. A. Allwood, and K. M. W. Keough. 1993. ^{2}H NMR studies of the effect of pulmonary surfactant SP-C on the 1,2-dipalmitolyl-*sn*-3-phosphocholine headgroup: a model for transbilayer peptides in surfactant and biological membranes. *Biochemistry* 32:11338-11344.

Mou, J., J. Yang, and Z. Shao. 1994a. Tris(hydroxymethyl)aminomethane (C4H11NO3) induced a ripple phase in supported unilamellar phospholipid bilayers, *Biochemistry* 33:4439-4443.

Mou, J., J. Yang, C. Huang, and Z. Shao. 1994b. Alcohol induces interdigitated domains in unilamellar phosphatidylcholine bilayers. *Biochemistry* 33:9981-9985.

Mou, J., J. Yang, and Z. Shao. 1995. Atomic force microscopy of cholera toxin B-oligomers bound to bilayers of biologically relevant lipids. *J. Mol. Biol*. 248:507-512.

Mou, J., D. M. Czajkowsky, and Z. Shao. 1996. Gramicidin A aggregation in supported gel state phosphatidylcholine bilayers. *Biochemistry* 35:3222-3226.

Mouritsen, O. G. and M. Bloom. 1984. Mattress model of lipid-protein interactions in membranes. *Biophys. J.* 46:141-153.

Mouritsen, O. G. and R. L. Biltonen. 1993. in Protein-Lipid Interactions, ed. Watts, A., Elsevier, Amsterdam. pp. 1-39.

Müller, D. J., F. A. Schabert, G. Büldt, and A. Engel. 1995. Imaging purple membranes in aqueous solutions at sub-nanometer resolution by atomic force microscopy. *Biophys. J.* 68:1681-1686.

Müller, D. J., W. Baumeister, and A. Engel. 1996. Conformational change of the hexagonally packed intermediate layer of deinococcus radiodurans monitored by atomic force microscopy. *J. Bacteriol*. 178:3025-3030.

Müller, D. J., M. Amrein, and A. Engel. 1997a. Adorption of biological molecules to a solid support for scanning probe microscopy. *J. Struct. Biol.* 119:172-188.

Müller, D. J., C. A. Schoenenberger, F. Schabert, and A. Engel. 1997b. Structural changes in native membrane proteins monitored at subnanometer resolution with the atomic force microscope: a review. *J. Struct. Biol.* 119:149-157.

Müller, D. J. and A. Engel. 1997. The height of biomolecules measured with the atomic force microscope depends on electrostatic interactions. *Biophys. J.* 73:1633-1644.

Müller, D. J., D. Fotiadis, S. Scheuring, S. A. Müller, and A. Engel. 1999. Electrostatically balanced subnanometer imaging of biological specimens by Atomic Force Microscopy. *Biophys. J.* 76:1101-1111.

Müller, D. J., J. B. Heymann, F. Oesterhelt, C. Moller, H. E. Gaub, G. Buldt and A. Engel. 2000. Atomic force microscopy of native purple membrane. *Biochim. Biophys. Acta* 1460:27-38.

Nezil, F. A. and M. Bloom. 1992. Combined influence of cholesterol and synthetic amphiphillic peptides upon bilayer thickness in model membranes. *Biophys. J.* 61:1176-1183.

Nielsen, C., M. Goulian, and O. S. Andersen. 1998. Energetics of inclusion-induced bilayer deformations. *Biophys. J.* 74:1966-1983.

O'Leary, T. J, and I. W. Levin. 1984. Raman spectroscopic study of an interdigitated lipid bilayer dipalmitoylphosphatidylcholine dispersed in glycerol. *Biochim. Biophys. Acta* 776:185-189.

Oosterlaken-Dijksterhuis, M. A., H. P. Haagsman, L. M. G. van Golde and R. A. Demel. 1991. Characterization of lipid insertion into monomolecular layers mediated by lung surfactant proteins SP-B and SP-C. *Biochemistry* 30:10965-10971.

Op den Kamp, J. A. F. 1979. Lipid asymmetry in membranes. *Ann. Rev. Biochem.* 48, 47-71.

Papahadjopoulos, D., M. Moscarello, E. H. Eylar, and T. Isac. 1975. Effects of proteins on thermotropic phase transitions of phospholipid membranes. *Biochim. Biophys. Acta* 401:317-335.

Rädler, J., M. Radmacher, and H. E. Gaub. 1994. Velocity-dependent forces in atomic force microscopy imaging of lipid films. *Langmuir* 10:3111-3115.

Recktenwald, D. J. and H. M. McConnell. 1981. Phase equilibria in binary mixtures of phosphatidylcholine and cholesterol. *Biochemistry* 15:4505-4510.

Reithmeier, R. A. F. 1995. Characterization and modeling of membrane proteins using sequence analysis. *Curr. Opp. Struct. Biol*. 5:491-500.

Reviakine, I., W. Bergsma-Schutter, and A. Brisson. 1998. Growth of 2-D crystals on supported planar lipid bilayers imaged in situ by AFM. *J. Struct. Biol.* 121:356-361.

Reviakine, I. and A. Brisson. 2000a. Formation of supported phospholipid bilayers from unilamellar vesicles investigated by atomic force microscopy. *Langmuir* 16:1806-1815.

Revakine, I., W. Bergsma-Schutter, C. Mazeres-Dubut, N. Govorhukina, and A. Brisson. 2000b. Surface topography of the p3 and p6 annexin V crystal forms determined by atomic force microscopy. *J. Struct. Biol.* 131:234-239.

Ribeiro, A. A. and E. A. Dennis. 1973. Effect of thermotropic phase transitions of dipalmitoyl-phosphatidylcholine on the formation of mixed micelles with Triton X-100. *Biochim. Biophys. Acta* 33226-35.

Ridder, A. N. J. A., S. Morein, J. G. Stam, A. Kuhn, B. de Kruijff, and J. A. Killian. 2000. Analysis of the role of interfacial tryptophan residues in controlling the topology of membrane proteins. *Biochemistry* 39:6521-6528.

Rinia, H. A., R. A. Demel, J. P. J. M. van der Eerden, and B. de Kruijff. 1999. Blistering of Langmuir-Blodgett bilayers containing anionic phospholipids as observed by atomic force microscopy. *Biophys. J.* 77:1683-1693.

Rinia, H. A., R. A. Kik, R. A. Demel, M. M. E. Snel, J. A. Killian, J. P. J. M. van der Eerden, and B. de Kruijff. 2000. Visualization of highly ordered striated domains induced by transmembrane peptides in supported phosphatidylcholine bilayers. *Biochemistry* 39:5852-5858.

Roberts, G. 1990. Langmuir-Blodgett films. Plenum Press, New York and London.

Sabra, M. C., J. C. M. Uitdehaag, and A. Watts. 1998. General model for lipid-mediated two-dimensional array formation of membrane proteins: application to bacteriorhodopsin. *Biophys. J.* 75:1180-1188.

Sankaram, M. B. and T. E. Thompson. 1990. Interaction of cholesterol with various glycerophospholipids and sphingomyelin. *Biochemistry* 29:10670-10675.

Schabert, F. A., C. Henn, and A. Engel. 1995. Native Escherichia coli OmpF porin surfaces probed by atomic force microscopy. *Science* 268:92-94.

Scheuring, S., P. Ringler, M. Borgnia, H. Stahlberg, D. J. Müller, P. Agre, and A. Engel. 1999a. High resolution AFM topographs of the Escherichia coli water chanel aquaporin Z. *Embo J.* 18:4981-4987.

Scheuring, S., D. J. Müller, P. Ringler, B. Heymann, and A. Engel. 1999b. Imaging streptavidin 2D crystals on biotinylated lipid monolayers at high resolution with the atomic force microscope. *J. Microsc.* 193:28-35.

Scheuring, S., P. Tittmann, H. Stahlberg, P. Ringler, M. Borgnia, P. Agre, H. Gross and A. Engel. The aquaporin sidedness revisited. *J. Mol. Biol.* 299:1271-1278.

Schiffer, M., C.-H. Chang, and F. J. Stevens. 1992. The functions of tryptophan residues in membrane proteins. *Prot. Eng.* 5:213-214.

Schmidt, C. F., Y. Barenholz, C. Huang, and T. E. Thompson. 1978. Monolayer coupling in sphingomyelin bilayer systems. *Nature* 271:775-777.

Schroeder, R., E. London, and D. Brown. 1994. Interactions between saturated acyl chains confer detergent resistance on lipids and glycosylphosphatidylinositol (GPI)-anchored proteins: GPI-

anchored proteins in liposomes and cells show similar behavior. *Proc. Natl. Acad. Sci. USA* 91:12130-12134.

Seelert, H., A. Poetsch, N. A. Dencher, A. Engel, H. Stahlberg, and D. J. Müller. 2000. Structural biology. Proton-powered turbine of a plant motor. *Nature* 405:418-419.

Seul, M., and D. Andelman. 1995. Domain shapes and patterns: the phenomenology of modulated phases. *Science* 267:476-483.

Shao, Z., J. Mou, D. M. Czajkowsky, J. Yang, and J.-Y. Yuan. 1996. Biological atomic force microscopy: what is achieved and what is needed. *Adv. in Phys*. 45:1-86.

Sheng, S., D. M. Czajkowsky, and Z. Shao. 1999. AFM tips: how sharp are they? *J. Microsc.* 196:1-5

Simons, K. and E. Ikonen. Functional rafts in cel membranes. 1997. *Nature* 387:569-572.

Simons, S. A. and T. J. McIntosh. 1984. Interdigitated hydrocarbon chain packing causes the biphasic transition behavior in lipid/alcohol suspensions. *Biochim. Biophys. Acta* 773:169-172.

Sommer, F., S. Alexandre, N. Dubreuil, D. Lair, Tran-minh Duc, and J. M. Valleton. 1997. Contribution of lateral force and "tapping mode" microscopies to the study of mixed protein Langmuir-Blodgett films. *Langmuir* 13:791-795.

Sperotto, M. M. and O. G. Mouritsen. 1991. Mean-field and Monte Carlo simulation studies of the lateral distribution of proteins in membranes. *Eur. Biophys. J*. 19:157-168.

Sperotto, M. M. and O. G. Mouritsen. 1993. Lipid enrichment and selectivity of integral membrane proteins in two-component lipid bilayers. *Eur. Biophys. J*. 22:323-328.

Spisni, A., I. Pasquali-Ronchetti, E. Casali, L. Lindner, P. Cavatorta, L. Masotti, and D. W. Urry. 1983. Supramolecular organization of lysophosphatidylcholine-packaged Gramicidin A. *Biochim. et Biophys. Acta* 732:58-68.

Tamm, L. K. and Z. Shao. 1998. The Application of AFM to biomembranes, in Biomembrane Structures, eds. Harris, P. I., and Chapman, D., IOS Press, Amsterdam pp. 169-185.

Ten Grotenhuis, E., J. C. van Miltenburg, and J. P. van der Eerden. 1995. Monolayer formation on silica and mica surfaces from *n*-alkanol melts studied by scanning force microscopy. *Coll. and Surf. A.* 105:309-318.

Van der Eerden, J. P. J. M., M. M. E. Snel, J. Makkinje, A. D. J. van Dijk, and H. A. Rinia. Striped phases in thin layers: observation and simulation. *J. Cryst. Growth.* submitted.

Van Klompenburg, W., I. Nilsson, G. von Heijne, and B. de Kruijff. 1997. Anionic phospholipids are determinants of membrane protein topology. *EMBO J.* 16:4261-4166.

Van Mau, N., V. Vie, L. Chaloin, E. Lesniewska, F. Heitz, and C. Le Grimellec. 1999. Lipid-induced organization of a primary amphipathic peptide: a coupled AFM-monolayer study. *J. of Membrane Biol.* 167:241-249.

Vaz, W. L. C. 1994. Diffusion and chemical reactions in phase-separated membranes. *Biophys. Chem*. 50:139-145.

Verkleij, A. J. 1989. in Electron Microscopy of Subcellular Dynamics, ed. Plattner, H., CRC, Boca Raton. pp. 75-94.

Verkleij, A. J. and P. H. J. Th. Ververgaert. 1975. The architecture of biological and artificial membranes as visualized by freeze etching. *Ann. Rev. Rhys. Chem.* 26:101-122.

Verwey, E. J. W. and J. Th. G. Overbeek. 1948. Theory of the stability of lyophobic colloids. Elsevier Publishing Company, Inc., New York.

von Heijne, G. 1986. The distribution of positively charged residues in bacterial inner membrane proteins correlates with the trans-membrane topology. *EMBO J*. 5:3021-3027.

von Heijne, G. 1989. Control of topology and mode of assembly of a polytopic membrane protein by positively charged residues. *Nature* 341:456-458.

von Heijne, G. 1994. Membrane proteins: from sequence to structure. *Annu. Rev. Biophys. Biomol. Struct.* 23:167-192.

von Nahmen, A., M. Schenk, M. Sieber, and M. Amrein. 1997. The structure of a model pulmonary surfactant as revealed by scanning probe microscopy. *Biophys. J*. 72:463-469.

Vlot, M. J. and J. P. J. M. van der Eerden. 1998. Symmetric Lennard-Jones mixtures in two dimensions. *J. Chem. Phys*. 109:6043-6050.

Walz, T., P. Tittmann, K. H. Fuchs, D. J. Müller, B. L. Smith, P. Agre, H. Gross, and A. Engel. 1996. Surface topographies at subnanometer-resolution reveal asymmetry and sidedness of aquaporin-1. *J. Mol. Biol.* 264:907-918.

Weisenhorn, A. L., M. Egger, F. Ohnesorge, S. A. C. Gould, S.-P. Heyn, H. G. Hansma, R. L.

Sinsheimer, H. E. Gaub, and P. K. Hansma. 1991. Molecular-resolution images of Langmuir-Blodgett films and DNA by atomic force microscopy. *Langmuir* 7:8-12.

Welti, R. and M. Glaser. 1994. Lipid domains in model and biological membranes. *Chem. Phys. Lipids.* 73:121-137.

Wertzer, B., D. Pum, and U. B. Sleytr. 1997. S-Layer stabilized solid supported lipid bilayers. *J. Struct. Biol.* 119:123-128.

Wiegrabe, W., M. Nonnemacher, R. Gückenberger, and O. Wolter. 1991. Atomic force microscopy of a hydrated bacterial surface protein. *J. Microsc*. 163:79-84.

Wimley, W. C. and S. H. White. 1996. Experimentally determined hydrophobicity scale for proteins at membrane interfaces. *Nat. Struct. Biol.* 3:842-848.

Woolf, T. B. 1997. Molecular dynamics of individual α-helices of bacteriorhodopsin in dimyristoyl phosphatidylcholine. I. Structure and dynamics. *Biophys. J.* 73:2376-2392.

Xu, X. and E. London. 2000. The effect of sterol structure on membrane lipid domains reveals how cholesterol can induce lipid domain formation. *Biochemistry* 39:843-849.

Yang, J., L. K. Tamm, A. P. Somlyo, and Z. Shao. 1993. Promises and problems of biological atomic force microscopy. *J. Microsc*. 171:183-198.

Yang, J., L. K. Tamm, T. W. Tillack, and Z. Shao. 1993. New approach for atomic force microscopy of membrane proteins, the imaging of cholera toxin. *J. Mol. Biol.* 229:286-290.

Yau, W.-M., W. C. Wimley, K. Gawrisch, and S. H. White. 1998. The preference of tryptophans for membrane interfaces. *Biochemistry* 37:14713-14718.

Yu, J., D. A. Fischman, and T. L. Steck. 1973. Selective solubilization of proteins and phospholipids from red blood cell membranes by nonionic detergents. *J. Supramol. Struct.* 3, 233-248.

Yu, S., P. G. Harding, N. Smith, and F. Possmayer. 1983. Bovine pulmonary surfactant: chemical composition and physical properties. *Lipids* 18:522-529.

Yuan, C. and L. J. Johnston. 2000. Distribution of ganglioside GM1 in L-α-dipalmitoylphosphatidylcholine/cholesterol monolayers: a model for lipid rafts. *Biophys. J.* 79:2768-2781.

Zasadzinski, J. A. N., C. A. Helm, M. L. Longo, A. L. Weisenhorn, S. A. C. Gould, and P. K. Hansma. 1991. Atomic force microscopy of hydrated phosphatidylethanolamine bilayers. *Biophys. J.* 59:755-760.

Zhang, Y.-P., R. N. A H. Lewis, R. S. Hodges, and R. N. McElhaney. 1995. Peptide models of helical hydrophobic transmembrane segments of membrane proteins. 2. Differential scanning calorimetric and FTIR spectroscopic studies of the interaction of Ac-K_2-$(LA)_{12}$-K_2-amide with phosphatidylcholine bilayers. *Biochemistry* 34:2362-2371.

Samenvatting

Deze samenvatting is bedoeld voor niet-ingewijden, opdat zij een idee krijgen van waar ik tijdens mijn promotie mee bezig ben geweest.

Ik heb vijf jaar lang modelmembranen bekeken met een geavanceerd soort microscoop. Om te snappen waarom iemand als ik zich überhaupt zo lang met modelmembranen bezig kan houden, is het handig om wat meer te weten over biologische membranen, waar mijn membranen model voor stonden. Biologische membranen zijn een soort vliesjes die om (en in) levende cellen zitten. Zij vormen een barrière tussen wat binnen en wat buiten de cel zit. Membranen bestaan uit lipiden en eiwitten. De lipiden vormen een dubbellaag waarin de eiwitten zitten (zie Fig. I). De eiwitten zorgen er onder andere voor dat er transport door de lipide laag mogelijk is, van bijvoorbeeld voedingsstoffen die de cel in moeten, of afval stoffen die de cel uit moeten. Ook signalen worden via eiwitten door de membraan doorgegeven, zoals bijvoorbeeld signalen van je hersenen naar je spieren.
Het is belangrijk dat membranen goed functioneren, en dat de transport routes goed werken, anders gaat een cel dood. Er zijn dan ook erg veel ziektes die te wijten zijn aan het feit dat er ergens in het lichaam membranen niet goed werken.

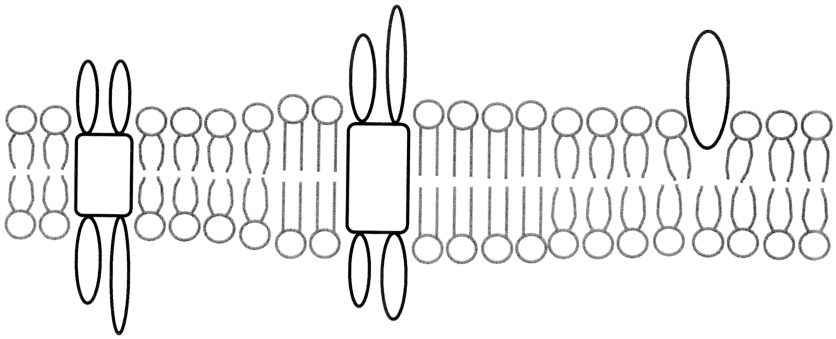

FIGUUR I Schematische tekening van een membraan, bestaande uit een dubbellaag van lipiden (grijs) met daarin eiwitten (zwart). De kopgroepen van de lipiden (afgebeeld als bolletjes) zijn wateroplosbaar (hydrofiel). De staarten van de lipiden (afgebeeld als streepjes, twee per kopgroep) zijn niet wateroplosbaar (hydrofoob). Omdat membranen in een waterige omgeving zitten, is het 't voordeligst voor de lipiden om met de hydrofobe staarten naar elkaar toe te zitten, zodat ze allemaal grenzen aan andere staarten, en zijn afgeschermd van het water door de hydrofiele kopgroepen. Het gedeelte van de membraaneiwitten dat in contact staat met de staarten, is ook relatief hydrofoob.

De laatste tijd denken steeds meer wetenschappers dat niet alleen de eiwitten, maar ook de lipiden van belang zijn bij het transport door de membraan. Lipiden zouden zich met dat transport kunnen bemoeien doordat bepaalde lipide soorten in de membraan bij elkaar gaan zitten en zo clusters (domeinen) kunnen vormen. Hoe dit precies werkt is nog niet helemaal duidelijk. Wat wel duidelijk is, is dat de structuur van membranen erg belangrijk is voor het goed functioneren van die membranen.

Het doel van mijn onderzoek was enerzijds het verkrijgen van know-how op het gebied van het maken van modelmembranen die geschikt zijn om met Atomic Force Microscopie (AFM) te bekijken, en het daadwerkelijke bekijken van die lagen met AFM. Met deze techniek wordt een oppervlak (in dit geval het oppervlak van mijn zelfgemaakte modelmembraan) met een hele scherpe tip afgetast, vergelijkbaar met een grammofoon. Deze tip voelt hoogteverschillen in het oppervlak en uiteindelijk krijg je een profiel van je oppervlak op je beeldscherm te zien. Deze techniek is zo gevoelig en nauwkeurig dat je er individuele moleculen mee zichtbaar kunt maken. Anderzijds was het de bedoeling om eiwitten in die lagen in te bedden en meer informatie over de structuur van die membraaneiwitten te verkrijgen. Aan de eerste vraag is beantwoord. Het is gelukt om zulke modelmembranen op plaatjes te maken en ze zonder al te veel geknoei onder die AFM te krijgen en te bekijken. Het tweede doel bleek iets moeilijker, en uiteindelijk ben ik, zoals zovele andere promovendi, een andere weg ingeslagen.
Als eerste heb ik modelmembranen bekeken waarvan de onderste laag uit ongeladen lipiden bestond, en de bovenste laag uit negatief geladen lipiden. Negatief geladen lipiden zijn van belang voor de werking van verschillende membraaneiwitten. Op deze lagen bleken vreemde verhogingen te zitten (Figuren in Hoofstuk 2), die in het begin veel verwarring zaaiden, maar uiteindelijk bleken te zijn ontstaan doordat de lipide dubbellagen op bepaalde plekken omhoog kwamen van het plaatje waar ik ze op had gezet. Hierdoor zijn we meer te weten gekomen over hoe lipide dubbellagen zich op een plaatje gedragen, onder andere dat lipiden uit de bovenste laag naar de onderste laag kunnen bewegen (en vice versa). In ons geval waren dat negatief geladen lipiden die uit de bovenste laag naar de onderste laag waren verhuisd, maar daar werden afgestoten door het onderliggende plaatje, dat ook negatief geladen is.
Naast pure lipide lagen heb ik ook membranen bekeken waar ik kleine model eiwitjes in heb gestopt en daarin werden domeinen gevormd met een extreem geordend streepjes patroon (Figuren in Hoofdstuk 3 en 4, met name 3.2 A). Dit wil niet zeggen dat in de echte membranen ook zulke streepjes zitten, maar het is wel vreemd dat er in dit soort systemen zo'n ordening plaatsvindt. We hebben een vermoeden dat deze ordening niet wordt

veroorzaakt door speciale interacties tussen eiwitten en lipiden, maar dat waarschijnlijk algemenere factoren, zoals de vorm van de moleculen, een rol spelen.
Verder heb ik in lipidelagen, bestaande uit drie verschillende lipiden, lipide domeinen kunnen zien (Hoofdstuk 5, Figuren 5.2 en 5.3) die ervan verdacht worden invloed te hebben op het transport door membranen. Dit is wederom geen sluitend bewijs dat er in membranen om levende cellen ook zulke domeinen zitten, maar het geeft wel aanwijzingen dat dit toch best wel eens het geval zou kunnen zijn. Bovendien is de stap naar echte celmembranen onder de microscoop te leggen nu makkelijker gemaakt. Als blijkt dat daarin inderdaad ook zulke domeinen te zien zijn, zou dat het beeld dat iedereen vanaf 1972 over membranen heeft, drastisch kunnen veranderen.

Thanx……

En dan nu, het dankwoord. Dat wat iedereen leest, en waar ik, ondanks mijn goede voornemens toch net iets te weinig tijd voor heb. Maar jullie hebben mazzel, ik ben in een goeie bui vanavond.

Allereerst, duizendmaal dank aan mijn promotoren, Ben de Kruijff en Jan van der Eerden. Jullie bekeken mijn resultaten allebei op jullie eigen manier. Ben met een, mijn leven lange ervaring op het gebied van lipiden, en Jan op een modelmatige manier die alle ingewikkelde systemen reduceert tot bolletjes die wel of niet graag bij elkaar zitten. Met beide manieren heb ik mijn voordeel kunnen doen. Maar allebei bekeken jullie mijn resultaten met enthousiasme, hetgeen bijzonder aangenaam voor mij was aangezien ik er zelf nooit zo over te spreken was. Bedankt voor jullie steun, hulp en ideeën. En Ben, bedankt voor de vijf jaar durende, geruststellende achtergrondgedachte, dat (zelfs al leek het niet goed te gaan) jij er wel voor zou zorgen dat het wél goed zou komen.

Daarnaast wil ik mijn begeleiders, Rudy Demel en Margot Snel bedanken. Rudy voor het mij wegwijs maken in de wondere wereld der monolagen en Margot voor haar altijd voelbare steun in de rug. Verder hebben mijn collegae van beide vakgroepen mij geholpen met talloze grote en kleine klussen, variërend van kristalgroeitheorie tot soniceren, van fosfaatbepaling tot fasendiagrammen, en van printproblemen tot pdf-files. Hiervoor wil ik met name Edzer, Jan Huinink, Eefjan, Rutger, Laura, Jeroen Makkinje en Antoinette bedanken en natuurlijk (van WALP tot KALP) Maurits, Jeroen en Matthijs.
I would like to thank Zhifeng Shao and Daniel Müller for their helpful replies to my “Hilde needs help” e-mails. Denise Greathouse and Roger Koeppe II are acknowledged for providing the WALP and KALP peptides. En hierbij wil ik ook graag Dirk Rijkers bedanken voor het synthetiseren van, voor elke vraag, een passende XALP. Richard heeft zijn credits verdiend toen hij als student bij mij het vesicle-fusie protocol heeft uitgevogeld en een jaar lang met dubbellagen met WALPs en KALPs in de weer is geweest, terwijl ik daar toen geen heil inzag, maar wat uiteindelijk toch tot twee hoofdstukken in mijn proefschrift heeft geleid.
Qua technische begeleiding ben ik bijgestaan door Dick, die voor elke monolagen klus de juiste Langmuir trog kan maken, en met name door Gerrit, die niet alleen technische hoogstandjes en magnetische-metalen-plaatjes-met-een-laagje-siliconen-maar-niet-in-het-midden-want-daar-moet-het-mica-geplakt-en-wel-met-de-juiste-diameters kan fabriceren, maar ook meedenkt en helpt.
De Audiovisuele Dienst van Jan de Boesterd & Co wil ik bedanken voor hun plezante hulp bij het maken van mijn figuren, posters, pdf files, bit-maps en de voorkant van dit proefschrift. Waarbij ik Ronald niet mag vergeten, die een heel arsenaal aan droge grond foto's voor mij heeft gemaakt, waaronder die op de voorkant.

Ik wil nogmaals Edzer bedanken, maar nu voor zijn uitermate scabreuze, grove grappen die het leven op een Universiteit zoveel aangenamer maken. En Rutger nog een keer, voor vijf jaar lang goeie middagpauzes.
Andere belangrijke personen, binnen en buiten het Kruytgebouw, zijn Gerrit en Carien. Gerrit, samen gestudeerd, samen gepromoveerd en nu allebei poost-dokken in Deutschland. Ik vind je de coolste wetenschapper aller tijden. Met Carien, van collega tot vriendin, heb ik jarenlang promotielief en -leed gedeeld. Tige tank foar de serieuse gesprekken, mar ek de lol en ik wit al net wat.
En natuurlijk de belangrijkste persoon in het Kruytgebouw: Liesbeth, de beste en liefste kamergenote ter wereld.

Margot, bedankt voor alle lunch-, winkel- en kopjes-koffie-in-kroeg plezier, en voor de goeie discussies over streepjes fasen. Maar bovenal bedankt voor de harten onder de riem in de eerste jaren. Jij kan, als ik het over een probleem heb, een analoge ervaring vertellen, hetgeen mij op de een of andere manier altijd een opgelucht en goed gevoel geeft.
José, ik heb veel lol en steun gehad aan onze promotie-klaag-gesprekken in bijvoorbeeld East of Eden. Door jouw verhalen ben ik erachter gekomen dat ik inderdaad best geluk heb met Ben en Jan als mijn promotors, en dat ik bijvoorbeeld niet de enige ben die het gek vindt dat Duitsers met hun knokkels op tafel kloppen in plaats van te applaudisseren. Verder vind ik je gewoon vreselijk leuk.
Margot en José, bedankt dat jullie mijn paranimfen willen zijn.

Dan zijn er nog een aantal mensen die wetenschappelijk gezien weinig tot geen inbreng hebben gehad, maar die mij morele steun hebben verleend, variërend van esoterisch advies tot een luisterend oor. Daar zijn, de vrienden die ik in Utrecht heb gemaakt, die tevens, elk op hun eigen manier, mijn goeroes zijn: Lydia, Monique en John. En Stefan, bedankt dat je, tijdens onze studie al, er altijd zonder twijfel vanuit gaat dat het mij wel lukt.
Vervolgens, ook heel belangrijk, Machiel, Marjolijn, René, Michiel en Regi, en Nico, Angelo, Alies en wederom Lydia, die het thuiskomen en thuiszijn tot een uitermate plezierige bezigheid hebben gemaakt en die altijd geduldig naar mijn onderzoeksgeneuzel hebben geluisterd.
Rest mij nog het bedanken van mijn familie, en met name Jocé, voor het vervaardigen van mijn promotie-outfit. Met speciale dank aan mijn zus Anneke, en Michel voor het, tot de juiste proporties terugbrengen van het belang dat mijn onderzoek naar mijn idee heeft, alleen al door voor mijn ogen nieuw leven op deze wereld te zetten, in de vorm van Mick.
Pa en Ma, bedankt dat jullie er altijd voor mij zijn, maar bovenal, dàt jullie er zijn.

En dan natuurlijk mijn rots in de branding,
mijn Lief,
mijn Pierre.

Curriculum Vitae

Hilde Rinia werd op 9 juni 1971 geboren te Franeker. Na het behalen van haar VWO diploma aan de R.S.G. Simon Vestdijk te Harlingen in 1989, is zij in datzelfde jaar aan haar studie Moleculaire Wetenschappen aan de toenmalige Landbouw Universiteit Wageningen begonnen. Na een afstudeervak bij de vakgroep Fysische en Colloïd Chemie, een bijvak bij de vakgroep Microbiologie en een stage bij het onderzoeksinstituut de CSIRO in Melbourne, Australië, is ze in 1995 afgestudeerd. In 1996 trad zij in dienst als Onderzoeker in Opleiding bij de vakgroep Biochemie van Membranen in samenwerking met de vakgroep Grensvlakken. Het aldaar verrichte onderzoek, onder leiding van prof. dr. Ben de Kruijff en prof. dr. Jan van der Eerden staat in dit proefschrift beschreven. Per september 2001 is zij, gefinancierd door een Madame Curie beurs van de Europese Unie, werkzaam als postdoctoraal onderzoeker aan de vakgroep Angewandte Physik van de Ludwig-Maximilians-Universität in München, onder leiding van prof. dr. Herman Gaub.

Hilde's Publications

Maste, M. C. L., H. A. Rinia, C. M. J. Brands, M. R. Egmond and W. Norde. 1995. Inactivation of a subtilisin in colloidal systems. *Biochim. Biophys. Acta*. 1252:261-268.

Caruso, F., H. A. Rinia and D. N. Furlong. 1996. Gravimetric monitoring of nonionic surfactant adsorption from nonaqueous media onto Quartz Crystal Microbalance electrodes and colloidal silica. *Langmuir*. 12:2145-2152.

Oude Elferink, S. J. W. H., H. A. Rinia, M. E. Bruins, W. M. de Vos and A. J. M. Stams. 1997. Detection and quantification of *Desulforhabdus amnigenus* in anaerobic granular sludge by dot blot hybridization and PCR amplification. *J. Appl. Microbiol*. 83:102-110.

Rinia, H. A., R. A. Demel, J. P. J. M. van der Eerden and B. de Kruijff. 1999. Blistering of Langmuir-Blodgett bilayers containing anionic phospholipids as observed by Atomic Force Microscopy. *Biophys. J.* 77:1683-1693.

Rinia, H. A., R. A. Kik, R. A. Demel, M. M. E. Snel, J. A. Killian, J. P. J. M. van der Eerden and B. de Kruijff. 2000. Visualization of highly ordered striated domains induced by transmembrane peptides in supported phosphatidylcholine bilayer. *Biochemistry*. 39:5852-5858.

Rinia, H. A., J. W. Boots, R. A. Kik, M. M. E. Snel, R. A. Demel, J. A. Killian, J. P. J. M. van der Eerden and B. de Kruijff. Domain formation in gel-state bilayers containing transmembrane peptides: Specific effects of anchoring residues. *Biophys. J.* Submitted.

Rinia, H. A., M. M. E. Snel, J. P. J. M. van der Eerden and B. de Kruijff. 2001. Visualizing detergent resistant domains in model membranes with Atomic Force Microscopy. *FEBS Letters.* 501:92-96.

van der Eerden, J. P. J. M., M. M. E. Snel, J. Makkinje, A. D. J. van Dijk and H. A. Rinia. Striped phases: observation and simulation. *J. Cryst. Growth*. Submitted.

Rinia, H. A., and B. de Kruijff. Imaging domains in model membranes with Atomic Force Microscopy. *FEBS Letters.* Submitted.

Abbreviations

2-D	2-Dimensional
AFM	Atomic Force Microscopy
CD	Circular Dichroism
CM	Contact Mode
DMPE	Dimyristoylphosphatidylethanolamine
DMPG	Dimyristoylphosphatidylglycerol
DMPS	Dimyristoylphosphatidylserine
DOPC	Dioleoylphosphatidylcholine
DOPG	Dioleoylphosphatidylglycerol
DPPC	Dipalmitoylphosphatidylcholine
DPPE	Dipalmitoylphosphatidylethanolamine
DPPG	Dipalmitoylphosphatidylglycerol
DPPS	Dipalmitoylphosphatidylserine
DRM	Detergent Resistant Membrane
DSC	Differential Scanning Calorimetry
DSPC	distearoylphosphatidylcholine
EM	Electron Microscopy
FALP	Ac-GFFL(AL)$_n$FFA-amide
GA	Gramicidin A
HAc	Acetic acid
HALP	Ac-GHHL(AL)$_n$HHA-amide
H_{II}-phase	hexagonal phase
HOPG	Highly Orientated Pyrolitic Graphite
HPI-layer	Hexagonally Packed Intermediate layer
KALP	Ac-GKKL(AL)$_n$KKA-amide
LB	Langmuir-Blodgett
LS	Langmuir-Schaeffer
L_α phase	fluid phase
L_β phase	gel phase
MLV	Multi Lamellar Vesicle
PA	Phosphatidic Acid
PBS	Phosphate buffered saline

PC	Phosphatidylcholine
PE	Phosphatidylethanolamine
PG	Phosphatidylglycerol
PI	Phosphatidylinositol
POPC	Palmitoyl-oleoylphosphatidylcholine
PS	Phosphatidylserine
SPC	Surfactant Protein C
SPB	Surfactant Protein B
SpM	Sphingomyeline
SUV	Small Unilamellar Vesicle
TFE	tri-Fluorethane
TLC	Thin Layer Chromatography
T_m	melting temperature
TM	Tapping Mode
TMD	transmembrane domain
Tris	Trishydroxymethylaminomethane ($C_4H_{11}NO_3$)
T_{tr}	phase transition temperature
WALP	Ac-GWWL(AL)$_n$WWA-etn
YALP	Ac-GYYL(AL)$_n$YYA-amid